UNIVERSITY OF CRETE

FORTH

Foundation for Research & Technology - Hellas

University of Crete

School of Science and Engineering

Department of Materials Science and Technology

and

FORTH-Institute of Electronic Structure and Laser

Diploma Thesis

Spin Valley Polarization measurements on two dimensional semiconducting WSe_2

Michalis Gavalas

Supervisor: Prof. George Kioseoglou

March 2020

Contents

Abstract

Acknowledgments

Contents

Abstract

Transition Metal Dichalcogenides (TMDs), MX2 (M = Mo, W and X = S, Se) is an extensively-studied class of materials. They are weakly bonded layered structures that can be reduced to single monolayer two-dimensional semiconductor crystals. Unlike their three-dimensional counterparts that are indirect gap semiconductors, and unlike graphene which has a zero bandgap, single layers of MX2 have a direct-gap at the K-point of the Brillouin zone with a range of bandgaps in the visible spectrum, making them suitable for optoelectronic applications from light emitting diodes to light harvesting and sensors.

In the present work, we study two-dimensional monolayers of WSe2 after mechanical exfoliation from the bulk crystal. Several spectroscopic techniques such as Raman, photoluminescence and reflection, are used to study the excitonic properties of this material. Also, using circular polarized light, we study the polarization of the emitted light as function of temperature in the range from 78K to 300K.

Acknowledgements

It is very important to have trusted people around you, when you pass through a big challenge. Such a big challenge was not only the accomplishment of that diploma thesis, but also all the academic years of studying for the achievement of a university diploma. For that reason, some people make this progress even more special, throughout my academic adventure.

The first gratitude cannot be held by other than my professor and supervisor, George Kioseoglou, for his extreme inspiration and the guidance he gave me with his large experience of scientific staff, the whole time of my thesis. Through him, I was introduced to the Ultrafast Laser Micro and Nano Processing Laboratory which located in the Foundation of Research and Technology Hellas (FORTH), where I met a lot of highly educated, interesting and hard-working people. Second gratitude must be taken by the doctoral student George Kourmoulakis. Although his huge load of tasks that he had during his Ph.D period, he didn't hesitate to pause his work, even sometimes for a few seconds, just to help me, give me advises about making my work better, more efficient and also to accompany me with my experimental processes. His contribution and help was really decisive for the achievement of the goals of my thesis. It is truly something that a few people in my life, have done for me. That is really invaluable.

Also special thanks that must be given furthermore, to my close friend and colleague Ioannis Makris. Not only for his support who show me during my years of study, but also for the endless and useful talks that we had, while we were usually hanging out. I should also give my thanks to many other friends that they were close to me on hard studying times.

A huge "thank you", should be given to the security team of the University campus and FORTH, for times when our study-load was too big, they gave me and my colleagues the permission to stay inside the campus for long night study sessions, something that happened several times in my academic years.

I. Introduction

Since the beginning of the TMDs studies, the scientific community has mostly focused on bulk 3D structures of these materials. The next natural step was to change the structure but not the composition of the material. In that case the scientific community on 2D monolayers. Common examples are monolayers of MoS_2, WS_2, $MoSe_2$, WSe_2 and many more. With the discovery of graphene, from the two noble prize scientists Geim and Novoselov [1], the most interest of TMDs falls on the 2D structures, but not with the same, fluent success, as before.

The first attempts, since the beginning of 2D studies, were dealing with problems related to isolating few layers of material from the bulk crystal. The initial efforts were focused on the determination of the number of layers and their characterization after the isolation. Mechanical exfoliation [1] was among the first methods that gave acceptable results. Raman, x-ray and photoluminescence spectroscopy gave also insight on the nature of these materials.

The big challenges that lie within the studies of the 2D structures make them even more interesting each passing year. Big promises about possible applications on optoelectronic and valleytronic devices, keep the scientific interest to the highest level.

1. 2D Transition Metal Dichalcogenides (TMDs)

1.1 Overview

As the need for better and more advanced technology based on TMDs, on the last decade, the scientific community mostly focuses on the new world of 2D structures. This sector of research started even before the first isolation of thin pieces of TMDs structures. The first attempts started with carbon films [2] and its properties since 2004. These films where finally recognized as a 2D material, due to their tiny size compare to the well-known bulk graphite structure.

The well-known acceptable and also successful creation of a 2D structure came up with the unexpected idea of isolation layers of materials from its bulk origin. As the globally famous, Nobel laureates, A.K. Geim and K.S. Novoselov once tried to isolate a single layer of graphite in 2004, the new discovery of graphene [1] set immediately a new sector of scientific interest. Graphene was the actual first 2D structure that recognized as a "monolayer", the first periodic structure of the crystalloid material. Thus several years later now, the 2D materials studies are fully expanded, not only in experimental but also in theoretical level and have shown tremendous results, considering their variety of properties and their applications in optoelectronics, mechanical applications, optics, advanced chemistry, medical purposes and much more.

Graphene is a one atom thick layer of carbon structure order arranged in hexagonal lattice. It behaves as a metal despite the complete absent of metallic compound in its structure. From the early experiments was found out that graphene has high electrical conductivity and optical transparency. Although the graphite, many layers bulk form can be recognized as a semiconductor, the graphene appears, on the other hand, almost zero electronic band gap [1], between the electronic bands, something that confirms the limitation of application it has in opto- and micro-electronics. So the main interest of optoelectronics explores other choices of 2D materials, such as the TMDs, that have a decent energy band gap.

Compounds like the MoS_2, WS_2, $MoSe_2$, WSe_2, of group IV, are widely common 2D materials and have been part of countless experiments globally the last few years. These materials have also been studied extensively in their bulk form. After mechanical exfoliation, it is verified now that few layers, even monolayers of these materials can be exfoliated and be tested for their optoelectronic and vibrational

properties pretty quickly. As easy as it seems to be, it's the exact opposite. Mechanical isolation isn't always successful and most of times it is really hard to produce an isolated monolayer from the bulk material. The most interesting thing about TMDs, and yet most useful, it is the electronic band structure that depends on their number of layers. As you approach the single layer limit, the system undergoes a transition from indirect to direct band-gap semiconductor [3]. That unique property makes this class of materials perfect for micro and optoelectronics applications. The direct gap of the monolayer (1L) is clearly representative on optical response spectroscopy [4] like the PL spectroscopy and Differential reflectivity, compared to the indirect gap of the bulk form. Undoubtedly, the PL intensity from the bulk is much weaker than the corresponding one from the monolayer.

Although it is often difficult, the mechanical isolation of a monolayer is possible, due to the weak interaction (van der Waals bonding) between two adjacent layers. The van der Waals interactions are weak enough to break, while a force is applied to the two layers. In that way small pieces of material are isolated from the bulk form by using a transition medium. Hetero-structures can be made with this technique also by mixing the isolating layers together in order to create a new artificial structure. Since the achievement of the isolated monolayers, they have been proved useful enough in a big range of applications in many fields of science, engineering and medicine[45].

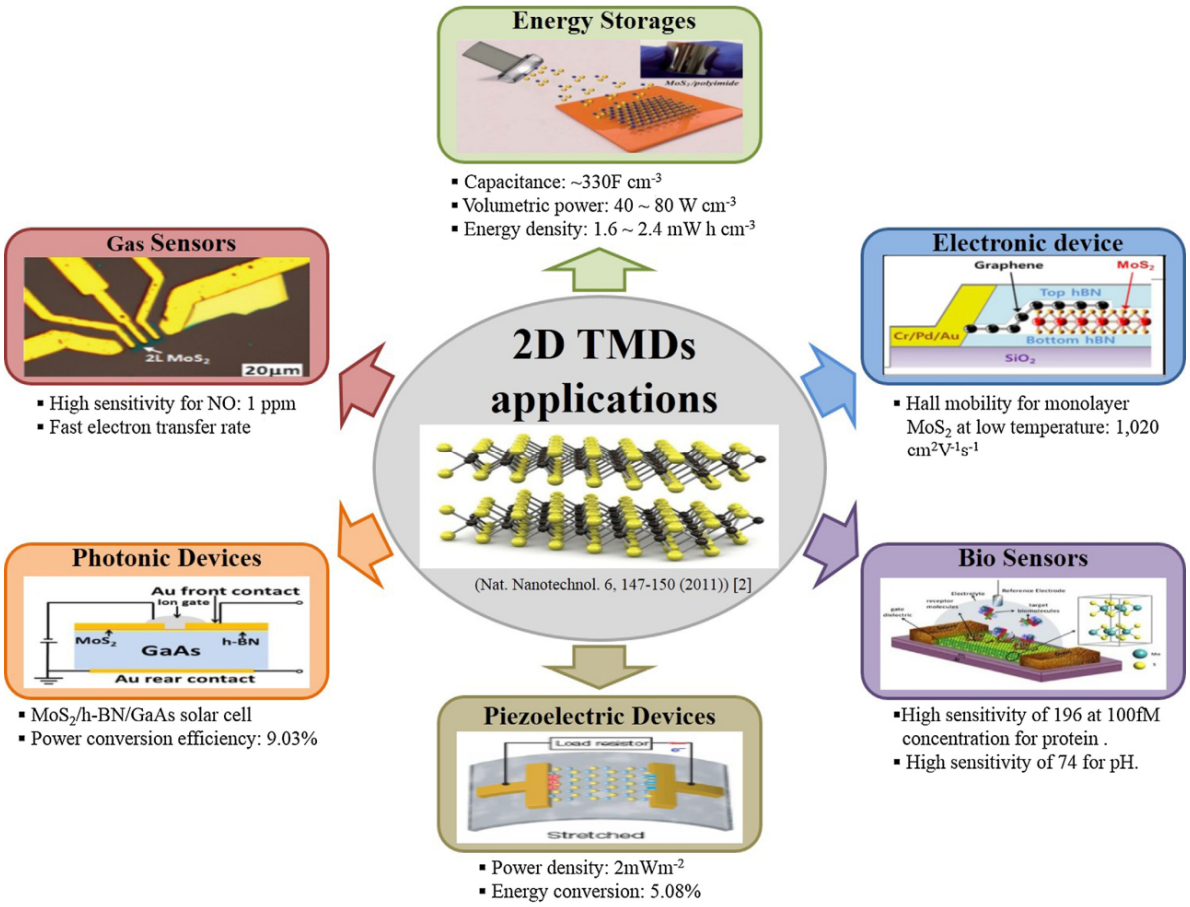

Figure.1.1. Application network of 2D TMDs materials [45].

Most recent notable applications are emphasized on the microelectronics and optoelectronics like the creation of tunnel effect transistors, promising good gate control and high electric conductivity with only a hint of induced voltage and a sub threshold swing smaller than 60 mV/decade [46]. Another spotted highlight is the biomedical application since the introduction of super capacitors electrodes, which uses a hybrid compound by 2D TMDs, like the MoS_2 and the Graphene oxide, with organic materials to store high amount of charge and electrical energy than the usual industrial rate [47,48]. By this case it can be measured the electrical pulses of a decent brain and the frequency rate for neurological diagnosis. Last but not least the whole range of 2D TMDs have shown plenty of physical and chemical properties and their prospect to various and advanced applications.

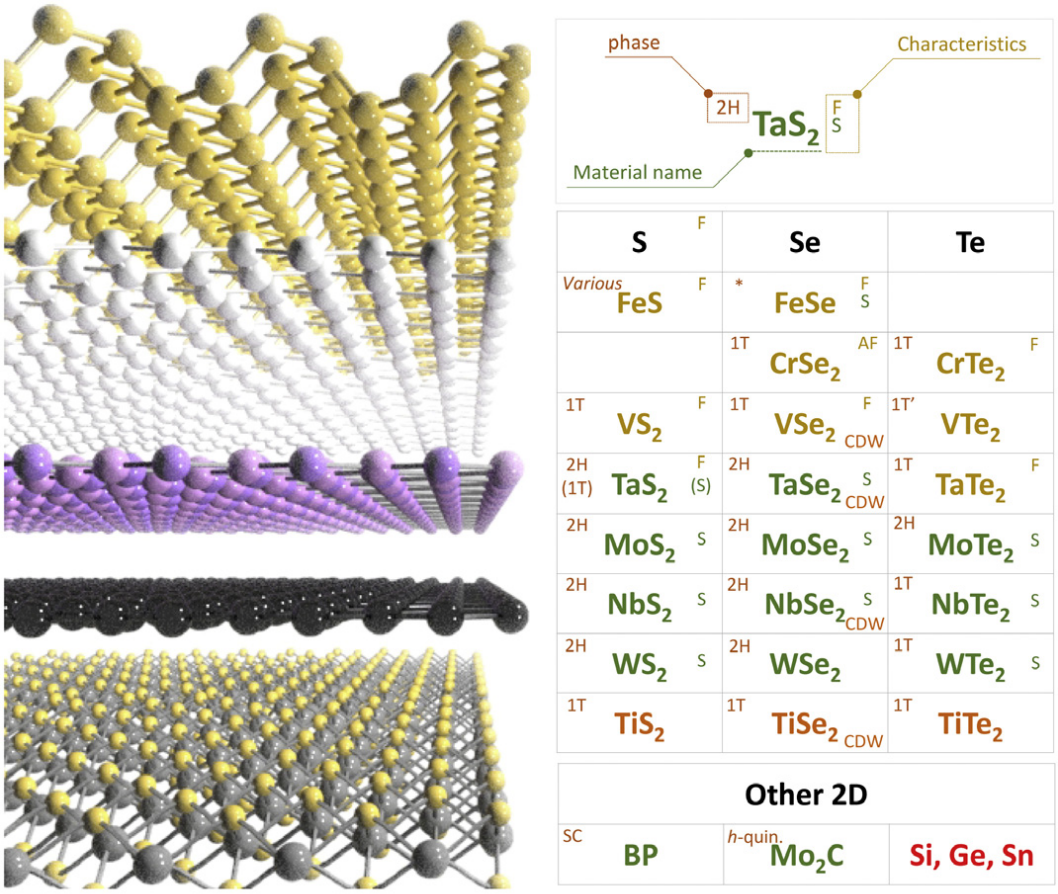

Figure 1.2.Table of various 2D TMDs and other 2D materials exhibiting physical properties: ferromagnetism (F), superconductivity (S), charge density wave (CDW), crystal structures (1H, 2T)[45].

At last the most complex behaving materials, as they could be characterized, are the graphene analogs, like the Germanane and Silane. These materials theoretically, by DFT calculations[11-12], share the same structure as the graphene, terminated with high amount of hydrogen. However it is extremely difficult to isolate a single layer from these bulk forms. As highly hydrogenated materials, they can quite easy change, thermodynamically through big possible energy absorption. That characteristic doesn't allow the fluent spectroscopic study, not even the pure isolation of a monolayer from the bulk form, due to the non steady form by the population of hydrogen that occurred.

1.2. Crystal and Electronic Structure of WSe_2

Monolayers of TMDs have only two polymorphs, one trigonal prismatic (2H type) and octahedral phase (1T type). TMDs have the chemical formula MX_2. The M presents a transition metal like the tungsten (W) or Molybdenum (M) and the X stands for a chalcogen. The crystal structure of a TMD monolayer usually consists of a hexagonally packed metal atoms stacked between two planes of chalcogens. The interlayer bond M-X is predominately covalent and the triplet of layers is developing weak van der Waals forces that allow the stacking of excess layers in the progress. Usually the M metal atom can provide four electrons for the repletion of the valence states, where the chalcogen needs only two. Initially the oxidation states are for M +4 and for X -2 respectively[53].The lone pair electrons of the chalcogen atoms terminate the surfaces of the layers and the absence of dangling bonds renders those layers stable against the reactions with environmental chemical sources. The specific bond M-M varies between 3.15 Å and 4.03 Å in length, depending on the size of the M and X ions.

The monolayer poly-types 2H and 1T belong to the D_{3h} point group and the D_{3d} point group respectively. These crystal phases can be differentiated using techniques such the high-resolution scanning transmission electron microscopy in annular dark field mode [53]. The electronic structure of a TMD depends strongly on the coordination environment of the transition metal M and its d-electron count. This count is responsible for many possible electronic or magnetic properties. Both in 2H and 1T phases, the non-bonding bands d are located within the gap between the anti-bonding σ^* and bonding σ orbits of M-X bond. Octahedrally coordinated transition metal centers (D_{3d}) of TMDs form degenerate $d_{z^2,x^2-y^2}(e_g)$ and $d_{yz,xz,xy}$ (t_{2g}) orbitals that can together accommodate the TMDs' d electrons [53].On the other hand, the d orbitals of transition metals with trigonal prismatic coordination (D_{3h}) split into three groups, $d_{z^2}(a_1)$, $d_{x^2-y^2,xy}(e)$, and $d_{xz,yz}(e')$, with a sizeable gap (~1 eV) between the first two groups of orbitals. The diverse electronic properties of TMDs arise from the progressive filling of the non-bonding d bands from group 4 to group 10 species. The structure of monolayer is recognized by the low thickness on about 6-10 Å [40]. The first triplet of planes forms the first layer of formatted material of TMD. The whole expansion of a

common monolayer constructs thicker forms of material until reaching a descent thickness to be considered pure bulk.

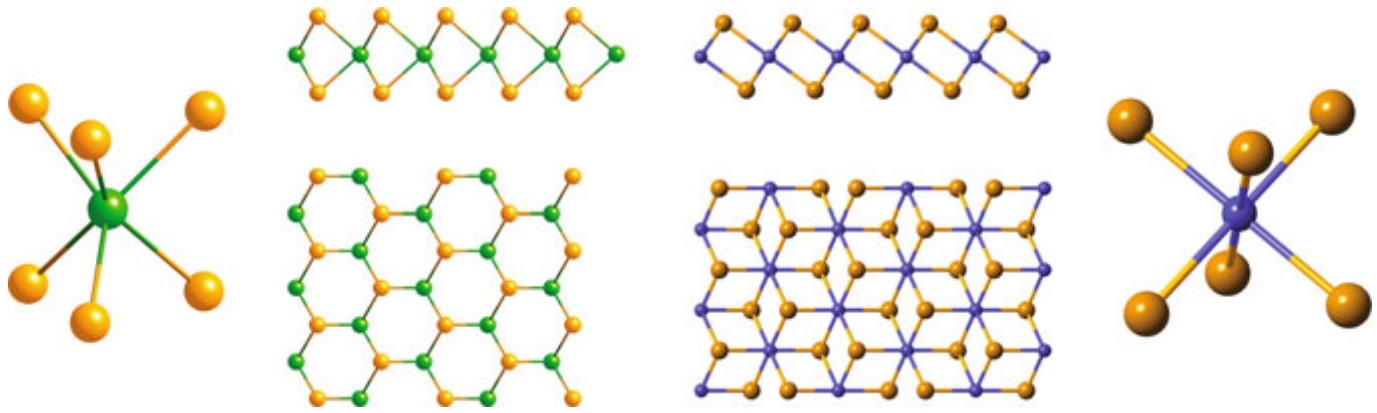

Figure 1.3.2H type trigonal prismatic structure of TMDs (left) and 1T type octahedral structure (right)[40].

The formation of monolayer WSe_2 is arranged by a hexagonal Brillouin zone. The single building unit stacked as a trigonal prismatic poly-type (2H type) with one centered atom of tungsten (W) to be bonded with six identical atoms of selenium. The formation to the first monolayer is approached by a hexagonal crystalline lattice with a repetition of the common unit cell with the minimum height. Both bulk and 2D forms are sharing the same lattice structure. Performing an XRD experiment is feasible to identify the lattice constants of the bulk form by the recognition of the crystalline planes that are waged by the final spectrum, as the Bragg-Laue law suggests. In a nutshell, this method typically induces X-Rays to the material with specific angle, while it is really slowly rotating, until it covers a given range of angles. The X-Rays that induced statistically are scattered by also a specific angle which equals the induced one and eventually crash to the photodetector.

From these results the lattice constants a, b and c are determined; it is well known by the DFT calculations of the WSe_2 and its hexagonal structure, the a constant is equal to b. Thus within XRD the distance d between two parallel planes of a crystalline lattice such the WSe_2 are set to confirm or counter the theoretical studies. Distance d shows eventually the specific distance between two crystalline planes of WSe_2. The usual constants for the bulk form are a = b = 3.32 Å and c = 15.06 Å [50]. On the other hand

the same constants for the monolayer form is a = b = 3.29 Å and c = 12.95 Å. Both of them share also the same angle rates as a = b = 60° and γ = 120° by the common geometrical unit cell of the 2H type.

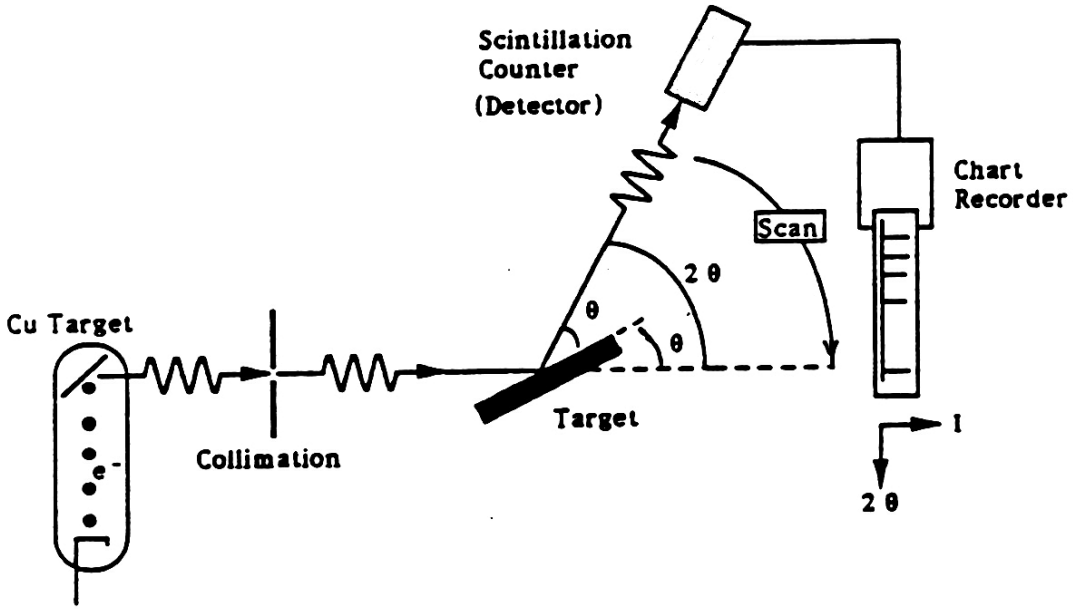

Figure 1.4. XRD building apparatus with Cu anode material[52].

The XRD method unfortunately does not apply to a monolayer. That's because of the pretty low thickness of the monolayer. The induced X-Ray needs some Angstroms in length in order to be diffracted and scattered according to Bragg law. This case makes the scattering of X-Ray almost impossible for monolayer. The induced X-Ray will automatically pass through the material as it has not the length and the time to be scattered on the specific angle as it is supposed to and it will induced after to the chosen substrate. As it is expected the scattering will be driven by the substrates lattice formation. So the final signal on XRD spectrum will include the signal peaks of the chosen substrate as well. In some cases when X-Ray wavelength is small enough like the monolayer thickness (1-10 Å) might be possible but still not pure to acquire some signal from the monolayer on the spectrum, along with the substrate signal. The corresponding set up for this X-Ray emission requires anode materials with Ka and Kb emissions on this range of wavelength.

However there is also a risk of damaging the studied material in such operation. The smaller induced wavelength the higher the energy, which can damage the studied material. In higher energy concentration the system can break, due to the high amount of energy absorbed from the material itself. Small wavelength X-Rays can overcome the chemical bond energy threshold and cut it.

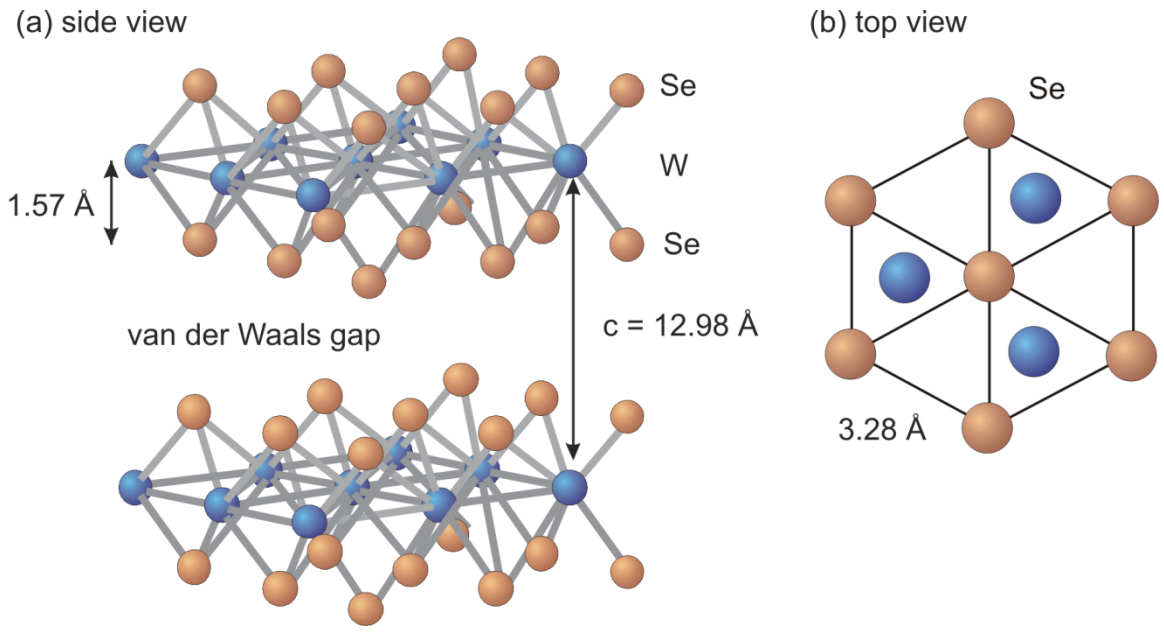

Figure 1.5 a) Side view of WSe_2 lattice (2H type) b) top view of the lattice. Blue represents W atoms while brown are the Se atoms [49].

According to the 2H type of lattice formation, the typical range of van der Waals forces is about the same length as the c lattice constant on 12.98 A. The empty space between these lengths is populated by the van der Waals interactions which are considered as attractive forces, capable of keeping two or more layers stacked for the final formation of the bulk form. So they can be described as interlayer forces. The hexagonal lattice has three fold symmetries and can permit mirror plane symmetry and inversion symmetry [51]. In the bulk form, until a few layers form, the crystalline structure has an inversion center. In the case of a monolayer that inversion center may be occurred or not.

In the bulk form of WSe_2 the electronic band gap is located in the center of the Brillouin zone and presented as indirect gap, while the monolayer form has a direct gap which is located on K points. This change of electronic structure is a characteristic of monolayer forms, as they shift the energy gap to direct [50].The indirect to direct gap transition arises from quantum confinements effects. The transition is manifested as enhanced photoluminescence in WSe_2 monolayer whereas only weak emission is observed in multi-layer forms.

The electronic band structure with direct band gap energy, where both conduction and valence band edges are located at the non-equivalent K points (K+ and K-) of the 2D hexagonal Brillouin zone, is characterized by broken inversion symmetry [54]. The inter-band transitions in the vicinity of the K+ and the K- point are coupled to right or left circular photon polarized states. These valley dependent optical selection rules are waged from the break of the inversion symmetry. That phenomenon provides a convenient method to address specific valley states (K+ and K-) by circular polarized light. A valley quantum number is a property of an electron inside a crystal that is associated with an electron's momentum. Broken inversion symmetry and spin-orbit coupling are properties of monolayer of group 6, which allow access to the valley degrees of freedom with circular polarized light. There are two inequivalent momentum valleys (K+ and K-) among the six it can be found in the hexagonal Brillouin zone of the monolayer. The ability to achieve controlled Valley polarization and its detection gives the permission to expand the electrical and optical properties for various innovated technologies.

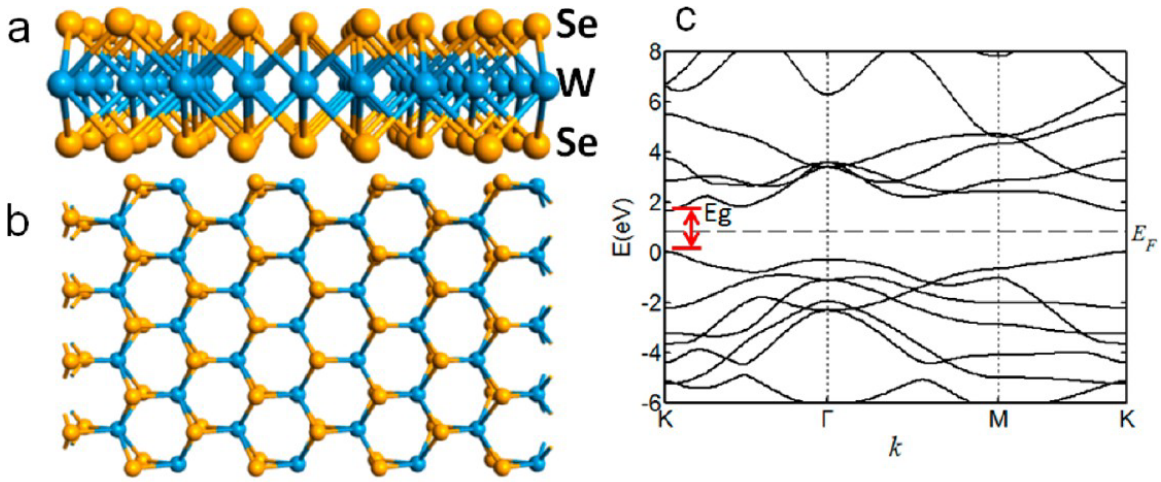

d

Crystal structure	Lattice parameter	Molecular weight	Air stability	Density
Hexagonal	a: 3.29 Å c: 12.95 Å	341.78	350 °C	9 g/cm^3

Figure 1.6. a)Schematic of a WSe_2crystalline structure-monolayer, b) top-down view of structure, c) electronic map of bands within the finite momentum of Brillouin zone shows direct gap app. to 1.6 eV, d) physical properties of monolayer[49].

1.3. Vibrational Modes – Group Theory

Vibrational modes are called the emerged oscillations (initial or collective) of the matter's molecules throughout a given energy excitation. In crystalline solids like the WSe_2 the vibrational modes also called frequently as phonons. More specific the oscillation of the crystalline ions are forming a whole oscillation of a local lattice or whole lattice collective oscillation. Phonons usually represent an excited state in the quantum mechanical quantization of the modes of vibrations of elastic structures of interacting particles. In classical mechanics a phonon designates a normal mode of vibration with a single given frequency. Normal modes allow the consideration of any excess-arbitrary lattice vibrations to be described as a superposition of the normal vibrations, using Fourier analysis. In quantum approach the phonons have wave-particle duality nature. Thus, it can be mathematically written as wave or particle as well, at will. Debye law of solids suggests that in every distinct energy-frequency quantum state of ions are existing two initial phonons. Eventually two different types of phonons are observed inside a crystal, the acoustic and the optical phonons.

Phonons can be detected by various spectroscopic methods like FT-IR and Raman. The basic principle of these methods is the energy exchange between the light source and the studied material. Especially the IR methods due to the low energy carrying light that induced in the material, it is easy to present vibrational modes (phonons) via light absorption processes. The absorbed energy is not enough to excite the whole carriers' distribution of the molecules and allow the light emission. However the energy amount is big enough to raise the molecules into virtual energy states that vibrations are occurred. Vibrations, is a mechanical process of energy consumption after the energy absorption. Raman works quite similar like IR but also has some pointed differences that make it even more accurate method for diagnosis of the phonon dispersion inside a crystal.

According to the Group Theory each molecule belongs to a symmetry group and holds many types of symmetry. In crystallography, a point group is a set of symmetry groups that includes rotation and reflection symmetries. The point groups are named according to their component symmetries. For the TMDs 2H type, the active symmetry point group is the D_n (D stands for dihedral) and indicates a n fold

rotation axis plus n two-fold axes perpendicular to that axis. D_{nh} group has, in addition, a mirror plane perpendicular to the n fold axis, while the D_{nd} group has, in addition, mirror planes parallel to the n fold axis. The 2H polytype can predict two forms of symmetric stacking: 2Ha and 2Hc. The primitive unit cell of the 2Ha or the 2Hc polytypes comprise six atoms, two transition metal atoms and four chalcogen s (Z=2, where Z is the number of structural MX_2 units required to form the primitive cell) in the trigonal prismatic coordination. In the 2Ha stacking, one transition metal atom is always on the top of another transition metal atom of the next layer. In the 2Hc stacking, any transition metal atom is sitting on top of two chalcogen atoms of the subsequent layer. 2Ha polytype is occurred in TMDs like TaS_2 or $TaSe_2$, while the 2Hc is occurred in compounds like the WS_2 and WSe_2 [56].

Each vibration belongs to a specific symmetry group. If a crystal has n atoms per unit cell then the degrees of freedom based on the vibrational modes are 3n-3 of optical vibrations. The basic bulk form of a common TMD is 2H-$MX_2$with 6 atoms per unit cell and it has 18 different vibrational modes, 15 optical phonons and 3 acoustic phonons, as long as it belongs to the D_{6h} point symmetry group. The lattice vibrations around the Γpoint of the Brillouin zone must be expressed according to the D_{6h} point symmetry, as follows[41,58]:

$$\boldsymbol{\Gamma_w = A_{2u} + B_{2g} + E_{1u} + E_{2u}} \text{for the W atom} \quad \textbf{(1.1)}$$

$$\boldsymbol{\Gamma_{Se} = A_{1g} + A_{2u} + B_{2g} + B_{1u} + E_{1g} + E_{1u} + E_{2g} + E_{2u}} \text{for Se atom} \quad \textbf{(1.2)}$$

$$\boldsymbol{\Gamma = A_{1g} + 2A_{2u} + B_{1u} + 2B_{2g} + E_{1g} + 2E_{1u} + E_{2u} + 2E_{2g}} \quad \textbf{(1.3)}$$

In a few layers material FL-$MX_2$and monolayers 1L-MX_2 the vibrational modes are changing due to the difference in topology that is occurred. The symmetry is reduced via the absence of the transitional symmetry on the z axis. Thus the symmetry groups are functioned to the number of layers the materials in consisted of. Such structural materials are belonging to D_{3h}. Thus the symmetry group is changing and so do the summary of the vibrational modes. Despite the number of the vibrational types, the symmetry also

changes, as the number of layers affects the topology of lattice and behaves in different quantum potential distribution. Especially in the monolayer case, there are no interlayer van der Waals interactions and the quantum electrostatically potential V is purified only by the initial formation of the lattice. The unit cell of a monolayer in TMDs is composed of three atoms giving rise to 9 phonon modes at the Γpoint:

$$\boldsymbol{\Gamma_{1L-W} = A_2'' + E'} \text{ for the W atom } \mathbf{(1.4)}$$

$$\boldsymbol{\Gamma_{1L-Se} = A_1' + E' + A_2'' + E''} \text{for the Se atom} \mathbf{(1.5)}$$

$$\boldsymbol{\Gamma = 2A_2'' + A_1' + 2E' + E''} \ \mathbf{(1.6)}$$

where the A_2'' and E′ are acoustic, A_1' and E″ are Raman active. For the specific WSe_2 material the summery for the vibrational modes in the bulk type are presented as well in figure (1.7):

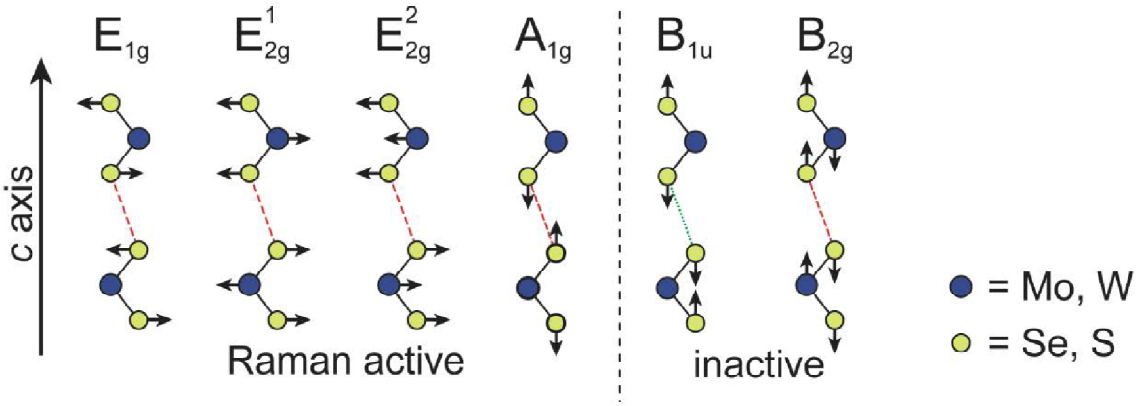

Figure 1.7.Vibrational modes on Raman, of different bulk TMDs Raman active (left) and inactive (right)[41].

In solids, the phonon dispersion of a crystal expressed as a relationship of frequency of the phonons as a functions to the wave vector. Considering that in the monolayer, there are existing six optical and three acoustical phonon branches separated by a descent frequency gap, as long as the phonons dispersion is determined by the Bose-Einstein distribution and Debye phonon law. Considering the figure 1.8a the phonon braches between optical and acoustic are separated by approximately 30 cm^{-1} of frequency. The

acoustic branches include two in-plane modes LA and TA with higher frequencies than the ZA phonons. There are also six branches of optical phonons; two in-plane longitudinal modes LO_1 and LO_2, two in-plane transverse modes of TO_1 and TO_2 and also two out-of plane modes ZO_1 and ZO_2.

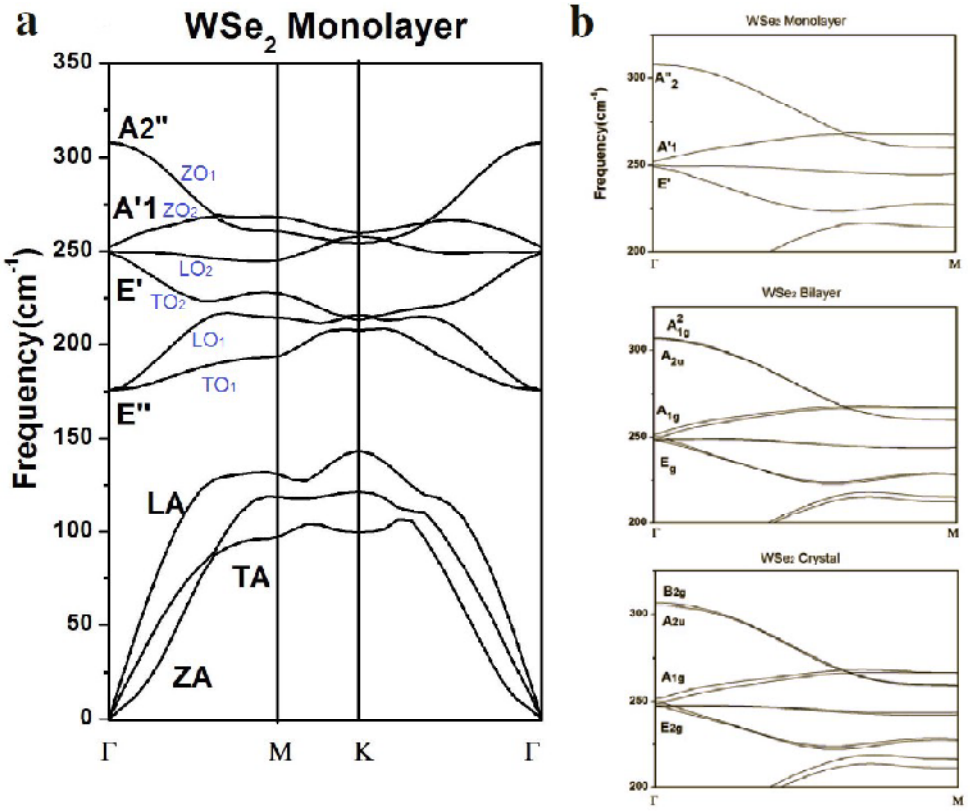

Figure 1.8.Phonon dispersion of different types of WSe_2. a) monolayer, b) monolayer upper phonons (top), WSe_2 phonons of bilayer (mid), WSe_2 crystal phonons (down).

In the case of a bilayer and bulk WSe_2, the full nine branches are splitting in two instead. That splitting results eventually into eighteen phonon branches. The frequency difference is too low because of the van der Waals interlayer forces that are pretty weak. Thus it is observed similar phonon dispersion between 1L, 2L and bulk. TMDs have similar phonon dispersion with the one of WSe_2. The main differences are the frequency shifts that are presented due to the change of the chemical elements and the physical mass.

For example the dispersion of WSe_2 differs from $MoSe_2$ in the frequency levels due to the larger-heavier atom that tungsten (W) is in comparison to the Molybdenum (Mo).

Experimental processes on Raman suggest that the studied monolayer of TMDs must be placed upon a substrate material with some van der Waals forces but not chemical sensitivity to perform a chemical reaction with the monolayer. Most of times it is used the common silicon substrate SiO_2/Si, which it has an oxidized thin region above the crystalline pure silicon. The oxide region helps the optical contrast under a microscope. The final formation of the sample in measurement is presented in the following figure (1.9):

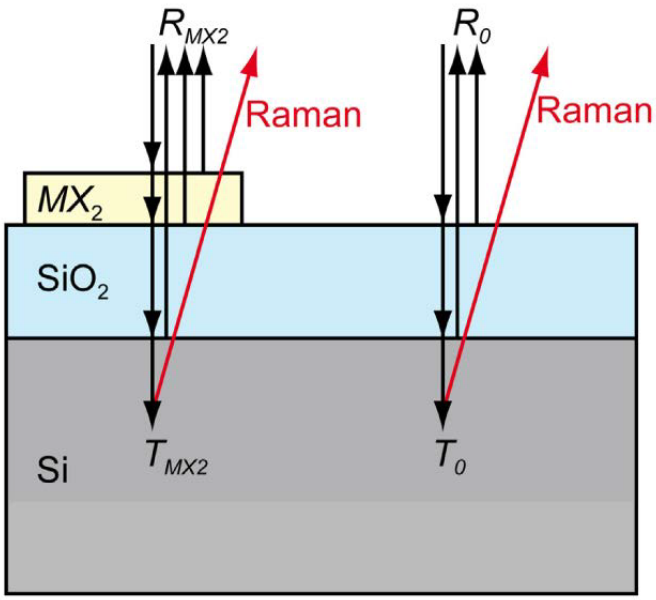

Figure 1.9. Raman scattering via TMDs monolayer and silicon substrate [41].

1.4 Optical Properties of WSe_2

As it has been already pointed out, the TDMs have the unique characteristic to shift the type of the electronic band gap as function of their thickness. The monolayer presents a direct gap, while the pure bulk has an in-direct gap on its own. Thus, the PL signal of 1L is way stronger in intensity than the one of bulk. TMDs electronic bang gap lies in the visible and near IR range, something that makes them incredible useful for optoelectronic devices and solar cells [57].

WSe_2 as a material is attractive enough for enabling strong coupling regimes of light matter interaction. The direct gap of WSe_2 monolayer is about 1.6 eV [41,57].In the PL, typical excitonic transitions observed are the neutral (X_A) and the charged excitons (X_A^-)associated with the A-exciton transition. The exciton's lifetime has a signature in the exciton's spectral linewidth. The coherence time also defines the average time in which an exciton remembers the state of the excitation field like the polarization. In a monolayer the coherence lifetime is usually less than the pure exciton's and proposes various applications on valleytronics and quantum optical devices.

Typically a monolayer can absorb up to 10-20% of the incident light beam, which is really promising for such thin material. The reduced dielectric screening and the quantum size effect, in very thin mediums, contribute to the increase of the binding energy of excitons (in the order of hundreds of meV), make them much stronger than the typical semiconductors such as GaAs. Because of the spin orbit splitting of the valence band, other type of excitons (like the B exciton) could also be observed. The series of excitons, like C or D excitons, that may be exist inside a crystal are forming in a similar way. In WSe_2, it is easy to capture the A and B excitons in a differential reflectivity measurement [41].

In the TMDs, the atoms are heavy and the outer electronic states are from the d orbitals that are having a strong spin-orbit coupling. This coupling removes the spin degeneracy in both conduction and valence band and introduces a strong energy splitting between spin up and spin down states. For the most TMD crystals there is no inversion symmetry as long as there is not an inversion center. The K valleys of 2D hexagonal Brillouin zone are not equivalent. So there are two kinds of k valleys, K+ and K-. That allows an energy degeneracy of different spin states in valence band. The crystal symmetry leads to valley depended

optical selection rules. One, a right circular polarized photon (σ+) captures a carrier in valley K+ and also a left circular polarized photon (σ-) that is shown by a carrier in the valley K-[59]. Within these two properties of valley-spin coupling and optical selection rules, it is possible for a laser beam in a specific polarized propagation and energy amount, to identify and control the valley states K+ and K- and also the spin states, up (+) or down (-).

The states around the valence band maxima are at large built of M-orbitals with an angular momentum (d_{+-2}), thus they are displaying large spin-orbit (SO) splitting ($\Delta_{SO,VB}$) on about 450 meV in WSe_2 monolayer. Respectively, the states around the minima of the conduction band (CB), are built of d_0 M-orbitals and they specify a smaller SO splitting ($\Delta_{SO,CB}$) [61]. As it seems, the splitting remains to be apparent due to the second order effect of the d_0 orbitals and the p-states of chalcogen atoms. These two effects are opposite in sign to the SO splitting and give two possible cases. The first suggests a bright monolayers with aligned spin in the upper VB and lowest CB, where $\Delta_{SO,CB} > 0$,which is optical active in ground state transition. The second suggest an optically dark monolayer with anti-parallel spins in the upper VB and the lowest CB, where $\Delta_{SO,CB} < 0$.

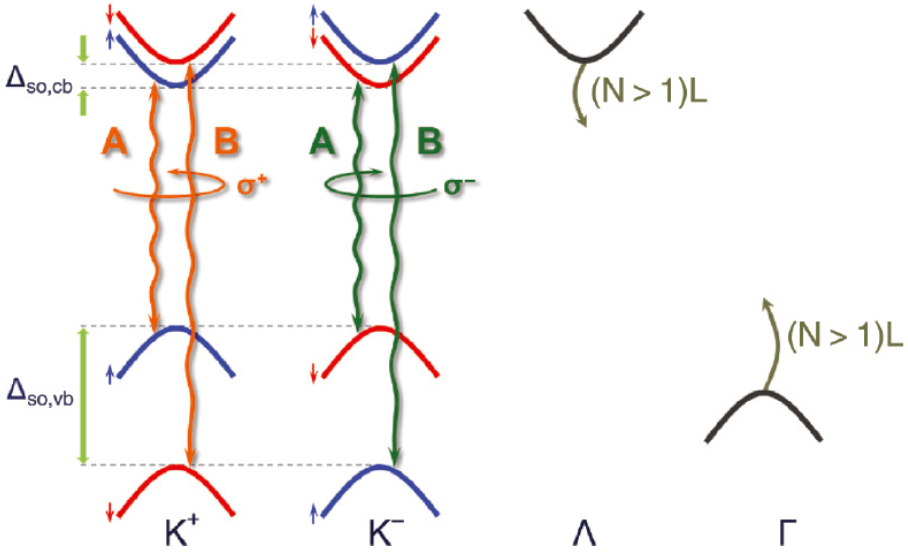

Figure 1.10. Valley SO splitting with energy gaps for valleys K+ and K- in a TDM monolayer [61].

The energy difference (positive or negative) of SO splitting between the K+ and K- valleys in the conduction band, determines the ground state transition, as bright (optically active) in positive amounts and dark (optically inactive) in negative amounts respectively. Experimentally when circular polarized light is induced to the system, both right and left helicity is initiated. Due to the broken symmetry, there is no also symmetry on polarization emission on the results. In fact it is observed a dominant circular polarized emission as PL, either right with spin up (σ+) or left with spin down (σ-) depending on the polarized light that is induced respectively. Thus when right polarized light is induced, it is expected the dominant signal to be waged out by the right also circular emission with the corresponding spin on the valley splitting. The left polarized signal with spin down it is obviously way weaker and sometimes it is not observed at all. The opposite occasion happens when left circular polarized light is induced.

The emission from the dark excitons, within the WSe_2, can be activated by mixing the spin states of dark and bright excitons via the application of an in-plane magnetic field [62]. The bright-dark excitons splitting is approximated round 50 meV for WSe_2.

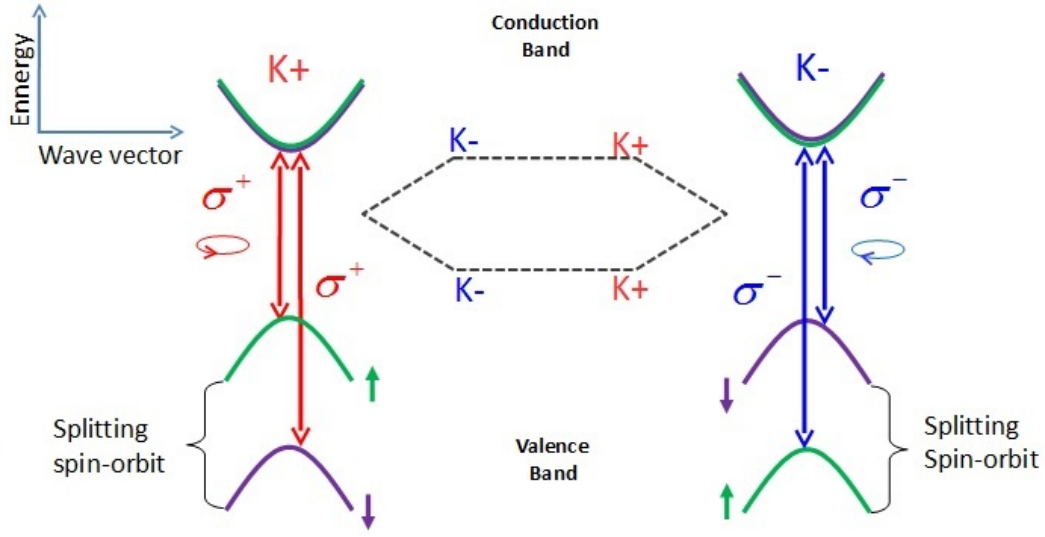

Figure 1.11. Valley Splitting of a hexagonal Brillouin zone via valence band in a TMD monolayer[60].

II. Experimental Methods

2. Experimental Processes

2.1 Raman Spectroscopy

Raman spectroscopy exists almost a century now. Depending on the unique properties of the chemical bonds that each compound has, this method has the starring role in the chemical analysis area. While many spectroscopic methods have tried to give good results in the Light-Molecule interactions via the energy absorption and emission through them, the Raman effect has the unique fundamental process to determine the nature of chemical elements by recognizing their inter-molecular bond vibrations that are resulted by the light-matter interaction. After so many attempts, beyond the first one, it is finally confirmed Raman's reliability and the expand use in many fields that related with the physical determination of physical chemistry and analysis.

Raman effect took his name from the Indian Nobel laureate Sir C.V. Raman, when he and his fellow, student Sir K.S. Krishnan, described the phenomenon, on the published scientific journal "Nature", for the first time, on March of 1928 [5]. Starting to explain the case of light scattering, when interacts with pure molecules, Raman observes a different type of scattered radiation after the original one, but not with the same purity. The original explanation suggest that keeping the same wavelength light source, as the incident beam, during the interaction it is possible to observe scattered light by the molecules. Most of those scattered photons are having the exact same wavelength and frequency as the incident beam and can be described as ordinary scattering. However, there are really low chances, to be accompanied by a modified scattered radiation with degraded frequencies [5].

In light-matter interactions, the incident photons have various possibilities to be absorbed, emitted, transmitted or even scattered by the medium they interact with. In case of Raman the starring event is the light scattering that lies beneath its interaction with the chosen medium. When the scattered radiation

consist of the same frequency, as the incident beam, it consider as elastic scattering. Whenever the scattered light shows another frequency level during the process, than the original one, the scattering is inelastic instead. The basic principle of Raman scattering is the analysis of the degraded frequencies that produced by the molecular vibrations in the light-matter interactions.

Much simple is to assume that, when the incoming light interacts with the studied medium, it can easily excite the medium's molecules. With this excitation, the molecules, act with another behavior than the rested one, and is possible to vibrate [6]. The vibration is a result of energy transfer from the light to the molecule. In fact the light can be absorbed from the molecule target and transfer its energy to it. Since the first presentations of the effect, many tried to describe the phenomenon theoretically by using the classical and quantum theory as well [6-7].

Starting with the classical theory of light, the Raman effect can be explained, if light can be considered as an electromagnetic continuous wave. Thus the energy of the electric field oscillation has a time dependency as follows the equation (2.1):

$$\boldsymbol{E = E_0 \cos\left(2\pi f t\right)} \textbf{ (2.1)}$$

Where E_0 is the amplitude of the electric field and f is the light transition frequency that a light source like the laser has. When this field radiate a molecule it is possible to create an instant electric dipole moment p that directed by the electric field itself. This dipole moment is written by the equation (2.2):

$$\boldsymbol{p = a * E} \textbf{ (2.2)}$$

This constant α is the polarizability of the molecule [6-7]. More analytically the polarizability is the ability of creating an instantaneous dipole. Furthermore it shows how easy is for a molecule to become instant a dipole as well. Technically it measures how efficient is the deformation of the electron cloud, round the nuclei and the breaking of the starting charged distribution of the molecule, when the electric field passes through. As a mathematically description is represented as a tensor, due to the unique nature of

molecules to polarized directly on some directions, depending on their shape. The equation (2.2), in fact, works only for isotropic mediums. To describe anisotropic mediums, it can be written as a rank two tensor, like a 3x3 matrix.

The chemical bond can be described as an oscillator. Like two spheres that represent the atoms, the bond is represented by a motive between them[8-9]. So it easy to imagine that the simplest vibration is just a harmonic oscillator, that shares the same properties. An oscillator is related close to the restoring constant k, which determine the force and furthermore the energy that must be collected to complete a fully oscillation, round the resting point. Respectively a chemical bond can be described with the exact same way. Consider that the atomic mass of each atom is like the mass of two opposite bodies and the energy of the bond is the restoring constant of the motive, the vibration have been described mathematically [8-10] by using the mechanical analog of the pure harmonic oscillator.

The normal function Q of the molecule has been described as well as:

$$\boldsymbol{Q = Q_0 \cos(2\pi f_v t + \varphi)} \textbf{(2.3)}$$

If Q_0 is the maximum vibrational amplitude, then the f_v is the frequency just like a transition function. The φis the phase angle and points the starting phase of the snapshot that the function's study has started. If the amplitude of the vibration is small, αcan be written down as a linear series function[6-8] as follows:

$$\boldsymbol{a = a_0 + \sum_k \left(\frac{\partial a}{\partial Q_k}\right)_0 Q_k + \frac{1}{2}\sum_{k,l}\left(\frac{\partial^2 a}{\partial Q_k \partial Q_k}\right)_0 Q_k Q_l + \cdots} \textbf{(2.4)}$$

Where the α is obviously the polarizability and the Q_k and Q_l represent the normal coordinates corresponding with frequencies f_k and f_l at the vibrations k and l. Thus in the long time vibration, where a v vibration occurs, the final form of the function is like:

$$\boldsymbol{a = a_0 + \sum_k \left(\frac{\partial a}{\partial Q_k}\right)_0 Q_k = a_0 + a'_v * Q_v} \textbf{(2.5)}$$

Now by the (2.4) and (2.5) we have:

$$a_v = a_0 + a'_v * Q_0 cos(2\pi f_v t + \varphi) \textbf{(2.6)}$$

So the final formation of the moment p, by the combination of (2.1), (2.2) and (2.6) will be considered as:

$$p = a_0 * E_0 cos(2\pi f_0 t) + a'_v Q_0 E_0 cos(2\pi f_v t + \varphi) cos(2\pi f_0 t) \textbf{ (2.7)}$$

Having in mind the formula of the cos function:

$$cosA\ cosB = \frac{1}{2}\ (\cos(A + B) + \cos(A - B)) \textbf{(2.8)}$$

The p equation now is written again as:

$$p = a_0 E_0 \cos(2\pi f_0 t) + \frac{1}{2} a'_v Q_0 E_0 \cos[2\pi(f_0 - f_v)t - \varphi] + \frac{1}{2} a'_v Q_0 E_0 \cos[2\pi(f_0 + f_v)t + \varphi]$$

(2.9)

The molecule's dipole moment is described by three terms as a result from classical theory. Using the frequency domain, the function of dipole moment should be written as well:

$$\begin{aligned} p(f) = {} & p_1(f_0) \\ & + p_2(f_0 - f_v) \\ & + p_3(f_0 + f_v) \end{aligned}$$

(2.10)

According to the equations (2.10) the first term confirms the elastic scattering, as we see that the frequency is steady. This kind of radiation scattering, described by Raman as "ordinary" [5], is also called Rayleigh scattering. In case of Rayleigh scattering the energy levels, between the original and the final, stay the same. This means that the excited molecule scatters the light in the exact same energy level that had been excited. The second and third term describe two different moments with also different rate of frequency. The different rate of frequency, during the scattering, signals the existence of Raman scattering. This form of scattering gives two different solutions accompanied by two results of energy output.

In order to understand this phenomenon, it is quite easy to consider first the fact that, the existence of the vibrational virtual states in a population of molecules inside a chemical compound, it is well defined and many molecules have different energy states in the start. During the excitation, it is possible to observe scattered light, having higher or lower frequency rate than the molecule's vibration frequency. If the scattered frequency is lower than the original one, then the scattering is called Stokes. The energy loss gap shows that the molecule can rest after the vibration in higher energy states than the original one. In cases, while the opposite process is observed, the frequency levels are bigger and there is an energy gain gap between the starting and the finally, resting, energy level of the molecule. This specific scattering called Anti-Stokes. As it was shown before by the equation (2.10) the Anti-Stokes scattering has an energy gain described by the term of f_0+f_v and the Stokes has an energy loss instead, described also by the second term, f_0-f_v.

Just to avoid any misunderstanding, let's make clear now that the vibrational energy level of each molecule, it is unique and depended by the chemical bond's properties. While the virtual energy states are considered quantum, as it will be described further later, the absorbed energy of the radiation must have the exact quantum rate that the molecule needs to start the vibration. In conclusion each molecule has its own vibrational virtual states and they are shown in another incoming frequency.

Now if the rate of the α_v' is zero, then the moment p depends only on the first term $p(f_0)$. This concludes only the conclusion by the elastic scattering of Rayleigh. In this moment, there is none of the Raman scattering and obviously no Raman signal. That gives the first big condition of Raman. Raman effect is accompanied always by the change of the polarizability of the target molecule.

According to the quantum theory the Raman explained as well, with the definition of the quantum virtual states. Each molecule, as pointed before, has its own energy states. These energy states are formed by the properties of each chemical bond, and the particle distribution, considering the stereochemistry of the molecule itself [7-9]. Quantum mechanics, in really simple words, suggested that, the molecule gain energy and shift up their energy state, while they absorb the incoming light. The exact opposite happens while the energy loss. The energy loss is expressed as an emitted light by the molecule.

Again, the process can be explained by the quantum way, considering that the excited molecules can rested on various energy levels after the emission of a photon. When the emitted photon has lower frequency than before, then the molecule rests on higher energy state, than the original one and signals the Stokes scattering. On the other hand, the Anti-Stokes scattering occurs when the emitted photon has higher frequency and the molecule rests on lower state than before. If it rested on the ground state the emitted photon has the maximum frequency also energy that this molecule can give. The excited states have short life time, about some pico to nano seconds maximum and have quite the same time of reaching the excitation level. So this process is an endless cycle as long as the beam source keeps firing photons. The schematic figure that follows, the Jablonski diagram, shows the process on different types of scattering.

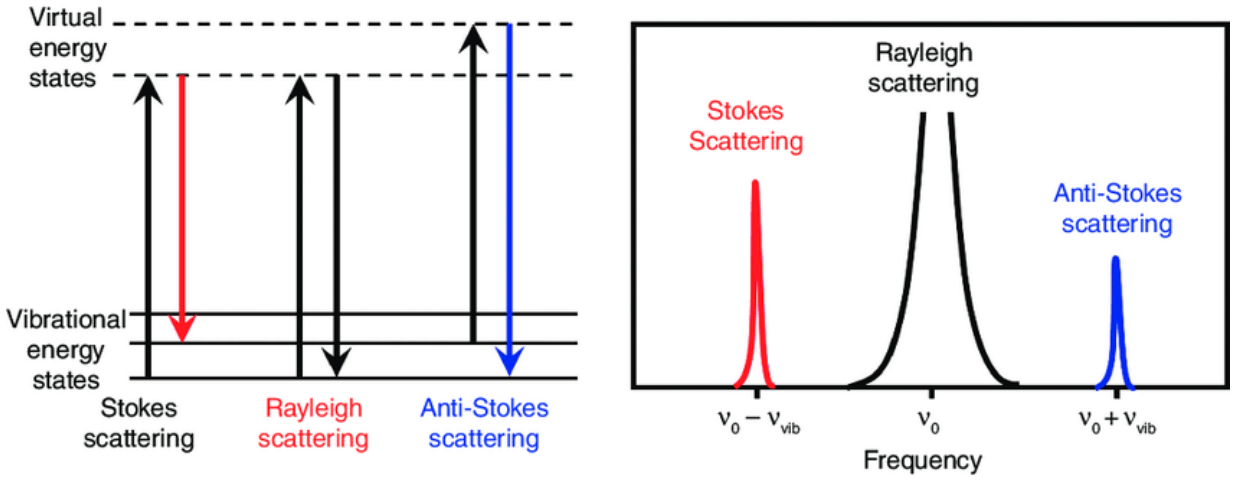

Figure.2.1 Jablonski diagram for Rayleigh and Raman scattering [7-8]

In a typical Raman spectrum after an experiment, we only focus on the Stokes peaks since the anti-Stokes lines are extremely weak. Following the Maxwell distribution, the lower energy states are more easily populated on thermodynamically equilibrium than the higher ones, cause of the molecule's potential to rest.

Compared to the Rayleigh scattering, the Raman scattering is a much weaker process, as only 1 in 10^7 photons can be inelastically scattered. The intensity of the Raman can be calculated by the following equation [6-7, 11]:

$$\boldsymbol{I = K * a^2 * P * \frac{1}{\lambda^4}} \textbf{(2.11)}$$

Where K is proportionality constant, α is the polarizability, P is the laser power and λ is the wavelength of incident photons. It seems obvious that only the laser power and wavelength are tunable and determined by the user before the experimental process.

2.1.1 Acoustic Phonons

Acoustic Phonons are oscillations of atoms of the lattice out of their equilibrium positions [64]. If the displacement is in the direction of the propagation direction, then there will be a random distance between the atoms throughout the whole collective movement. If the displacement of the acoustic phonons tends to infinity, then the oscillation expands to the whole lattice and this process costs zero rate of deformation energy. The relationship between frequency and wavelength for big wavelengths tends to be linear and for big enough wavelengths the frequency tends to zero. Longitudinal and transverse acoustic phonons usually are marked as LA and TA respectively.

2.1.2 Optical Phonons

Optical Phonons are out of phase movements of the atoms within the lattice[11,64]. Two atoms can move identically in the opposite directions. This is a way of understanding the variety of different type of atoms, the lattice is consisted of. The optical phonons are actually ions of crystals that are having response of light excitation after the infrared radiation (IR). Optical phonons have non-zero rat of frequency in the center of the Brillouin zone and don't show dispersion on long wavelength limit. The mode of vibration, whereas positive and negative ions are moving against each other is creating a time-varying electric dipole. The optical phonons that behave like this are called "infrared active". There are also optical phonons that are "Raman active", which are observed in Raman scattering. Like acoustical, the optical phonons can be divided as LO and TO optical phonons according to the longitudinal and transverse modes. The splitting between the LO and TO frequencies can be described accurate by the LST relations.

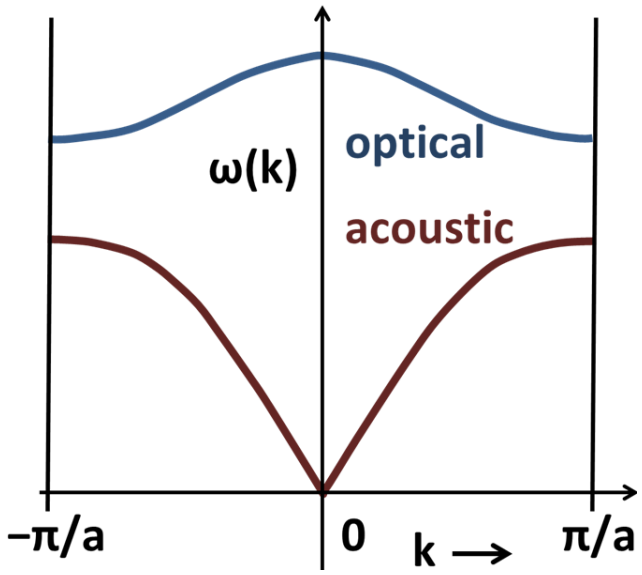

Figure 2.2. LST distribution for optical and acoustic phonons via the Brillouin zone.

2.1.3 Crystal vs Amorphous Material - Raman

As it is well known the crystalline materials have strong determined structure, which is characterized by a repetition of a unit cell and a periodic potential energy. The final form of crystal shows a whole lattice of unit cells combined together. Thus, a crystalline material is dominated by a well determined spatial order, throughout the whole lattice formation[63]. The high order defines specific distances and angles between the placements of the structured atoms and so are the chemical bonds. In this case there is an average distance between the atoms, which is approximated some Angstroms in distance, just like the length of a common chemical bond. The symmetry points allow the symmetric displacements of the vibrations and the movement (oscillations) of the chemical bonds, with some frequency. In most of crystals that frequency is about some THz high[64]. The oscillation is spatial falls via a factor of potential energy between the atoms of the lattice, until it reaches the resting point and stop moving. While the vibrations of the crystalline formation are well determined, they are almost always recognized in the Raman spectrum as sharp tall peaks [6-8,40,41].

The sharp peaks are the result of strict vibration around a resting point, as a characteristic of a point symmetry that lies within the crystal. A specific overlapping is possible by really close shifts of sharp peaks, while two atomic displacements are allowed by the crystalline point symmetry. Otherwise the vibrations are separated in different Raman shifts with specific intensity. Due to the degrees of freedom within the lattice, the atomic resonance displacements are gaining in intensity. If a vibration is spread following the lattice formation, as vibration propagation suggests, then two results are mostly possible.

One possible result is the enhancement of the signal and the higher intensity. That phenomenon is well understood, because in many cases the same vibration can happen for many unit cells identical, in progress. That combination suggests a whole lattice displacement as a fully line vibration, which scatters eventually bigger population of photons. The expression is a higher intensity at one Raman shift. The second result is the interference between two or more vibrational types that may occur during the process. This allows mechanical wave propagation to every possible direction of the lattice. Thus, it is possible for a local point of the lattice to form constructive or destructive interferences in a node of involved waves.

The destructive interference stops the atomic displacement and the whole vibrational modes at that point. Thus by this none scattering can be set on and none photon population can hit the detector. The detected photons are coming from, only by the constructive interferences, but that suggests a low intensity in general, on the final printed spectrum.

Amorphous solids, although it may be considered by similar chemical form as the crystal, are formed by a non-order expansion. In this case there is no specific periodicity or building order throughout the structure. Such solids are considered the oxides, like the silicon dioxide[68]. There is no order to the arrangement in space. Thus, no average length or specific angle between the structured atoms is allowed. In case of atom displacement, that doesn't prohibit the wave formation (vibration), but hardens the propagation into neighbor atoms. This restriction of the mechanical propagation of the vibrational modes is responded when there is not an average distance between the atoms and the electrical quantum potential is not periodic and stable. The distribution of the atomic placements and interactions is non-Gaussian. That explains the anisotropic formation of the whole structure, whereas the atoms density and packing are completely random and fluctuates point by point in local regiments.

Experimentally the amorphous structure is presented as, some hundreds wave-numbers k, broad peaks with non-determined intensity. In process, there is an accumulation of vibrations around the amorphous close packing which is completely anisotropic as well. Due to the quickly dumping oscillations and the destructive interference that mostly are presented, there is a huge overlapping of small vibrations that occurred really close one to another and form a final broad peak with medium or small intensity. For example the common substrate SiO_2/Si has an oxidized layer that interfaces the crystalline silicon structure. In a Raman spectrum is possible to observe both oxidized and crystalline region of the sample and it can be identify by the specific Stokes peaks that are presented. A long sharp peak is referring to the crystalline silicon part while a broad small curve on a different Raman shift is presenting the oxidized part of the studied sample.

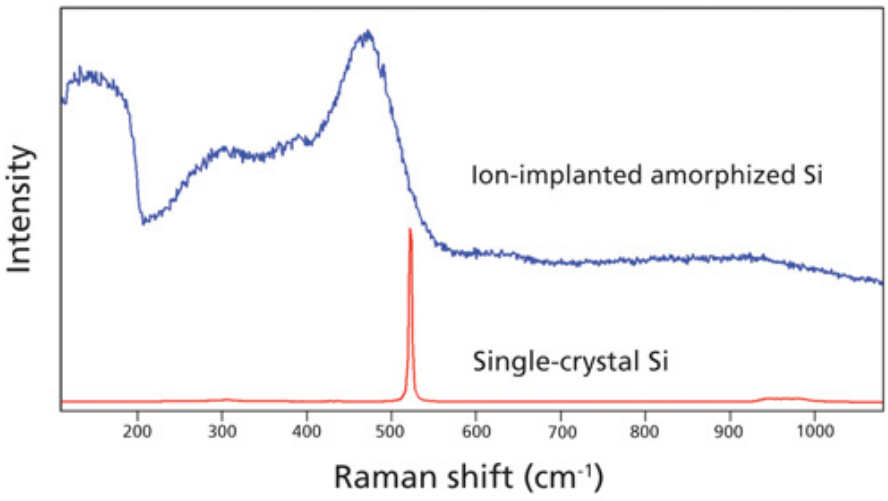

Figure 2.3.Raman Spectra of crystalline silica (red) and ion-amorphous silica (blue) [63].

The Raman spectrum of single-crystal silicon, as it is shown by the figure 2.3, consists of one triply degenerate optical phonon at 520 cm^{-1} along with much weaker second order transverse acoustic and optical modes that appear at 305 cm^{-1} and 975 cm^{-1} respectively. The band of 520 cm^{-1} is very narrow with average width at half maximum on about 4 wavenumbers[63]. The amorphous silicon spectrum is presented by broad peaks and high density of "noise" as backup baseline signal.

2.1.4 In-plane and out of plane Raman modes

The main difference between the plane-depended displacement modes is the direction of the oscillation around the symmetry point during the vibration. There are two specific types of modes that are the most commonly observed in a vibrational spectroscopy like Raman. The Eg type and the Ag type of vibration. The E type is recognized as in-plane mode of vibration and the A type as out of plane vibration [64,65]. The vibration modes are enhanced or dumped instead, according to the topology that inhabits the material's structure. Along with the point and the group of symmetry, the vibrational modes can be characterized, excess in topology of the vibration. The main principle is that every vibration in Raman active modes is an oscillation around a resting point which is activated by point symmetry.

The group of mostly solid TMDs is the D_{3h} and D_{6h}, which is a point symmetry group in a hexagonal lattice, unit cell formation (h), depending on the number of neighbor-atoms the centered atom-point of symmetry it has. Between each symmetric point that a centered atom is placed, it is formed a topological plane that includes also the main neighbor-atoms of the center. In this plane the vibration is presented with specific movement and direction on the 3D space[40,41,64,65]. The movement's direction characterizes the vibration as in or out of plane displacement. The in-plane vibration Eg is resulted when the direction of the vibration doesn't excess the determined plane's limits. Respectively the out of plane modes Ag are resulted while the vibration outspreads the plane's limits[66]. Thus the displacement of the atoms is extended vertically from the plane.

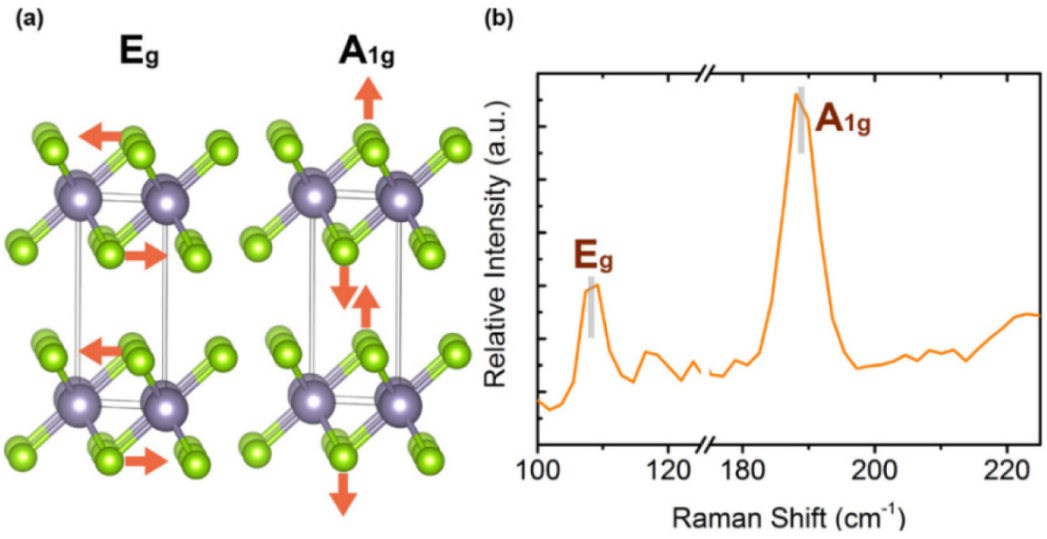

Figure 2.4. a) Vibrational modes on Raman, the in-plane modes (Eg) and the out of plane modes (Ag), b) random Raman spectrum of shows Eg and Ag common modes in different Raman shifts [66].

As it is shown by the figure 2.4b, is spotted a gap, on the Raman shift, between the two active modes of E_g and A_{1g}, that it can be presented in most of achieved Raman spectra. Due to the point symmetry the E_g vibration is a bending and the A_{1g} vibration is a stretching respectively. According to the mechanical behavior of an oscillation, the stretching mode requests bigger amount of energy to perform, while the bending itself is much easier to achieve [10]. In a bending vibration of a three atoms plane, the only energy that is required is presented via a torque with center rotary point the middle atom. The centered atom creates two bonds, one for each of the other two atoms. The whole plane confirms a specific angle between the centered atom and the other opposite two. In the same plane system the stretching vibration is required excess energy to be generated. Symmetric stretching, that is widely active on Raman, is chancing the bond's length individually for both bonded atoms with the centered one. The symmetry on the stretching needs higher levels of absorbed energy, due to the fact that two initially and symmetric oscillations are need twice the energy than the one only. This difference is resulted via the degrees of freedom of each movement in each molecule.

The bending vibration can be observed in many different types of modes. The most common types of bending vibration are the following ones: scissoring, rocking, wagging and twisting[67]. On the other hand, stretching has only two types of modes: the symmetric, where the bonds are changing equal with the same phase, like parallel oscillations and the none-symmetric bonds, where the same oscillations are out of phase. In that case the in-plane modes are generated within lower energy absorption than the out of plane modes. As long as the bending needs lower energy level to be triggered than the stretching, the incoming wavelength is bigger and the frequency lower instead. Thus the expected Raman shift in wavenumbers is obviously smaller for the bending than for the stretching. The summary of vibrational modes on Raman of a solid crystal, it is shown in the next figure (2.5).

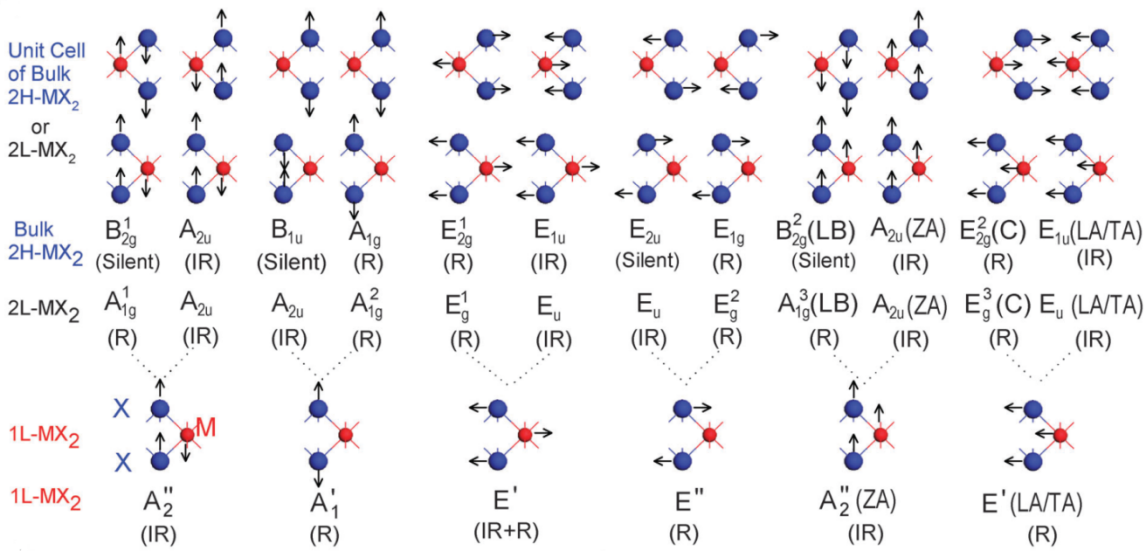

Figure.2.5. Vibrational modes of different thickness on TMDs. Modes are characterized as Raman active (R), IR active (IR) or silent [55]. In-plane modes (Eg) and out of plane modes (Ag) types are occurred only in the monolayer case.

2.2 Photoluminescence Spectroscopy

Like Raman, PL can also use the laser as the main light source. The main reason of the PL advance is the understanding of the emission behavior of the chemical compounds and the physical elements, like the optical and structural properties. PL has a huge contribution on the materials science and it is an easy experiment to perform.

The physical description of PL lies in the ability that the electrons absorb and emit light, while they change their quantum energy level. As the French physicist Louis De Broglie once confirmed the wave form of the electrons, it also pointed that electrons can change their quantum energy inside the atom by exchange energy with the environment, in the form of light. If an electron can change its energy state by using an outside energy packet, then it must absorb or emit an electromagnetic wave (photon) with a given energy. The energy gaps that an electron must overcomes, are degenerated, as the atomic energy levels are defined by the quantum realm and require specific energy to be captured.

It is possible in the light matter interaction an electron to get excited or rested and exchange light, with the environment, at will. It is known, that kind of energy exchange exists by discrete photon packets and makes possible the efficient study of the light-matter interactions. Rather than the common experiments that involved the gas and liquid form of materials, now the next step is the study of solid systems.

As one of the fundamentals form of matter, solids have shown groundbreaking properties and a great number of own applications. Most of solid systems are by nature crystals. Crystalline solids have the unique property to build up their structure by continuous, repeated-periodic motives. Starting by the common unit cell, the whole structure of each solid expands to a complete crystal lattice that confirms the final form. They are separated to insulators, semiconductors or conductors, according to their energy electronic band structure. Density Functional Theory (DFT) makes the first theoretically calculations in mapping the band structure in most of solids[11-12]. The DFT method offers a forecast for the band structure, using some fundamental elements of solids, like the Fermi's electron energy levels distribution, Debye's phonon dispersion and the Brillouin zone structure of crystals. Although, including such

mathematical components, it is not always accurate in some elements of calculation and that sometimes confuses the experimental sector.

The most of the interest rests in the semiconductors area, where the electronic band structure is characterized by a decent energy gap[11,13,14](Eg) between the valence and the conduction band. The PL principle there depends on the spontaneous emission of light, by exited atom carries like the electron, which is defined by the energy gap. While a rested electron on the valence band (VB) can get excited by an outside energy excitation, most of times via absorbed radiation or heat, it is possible to overcome this energy gap and transferred to the conduction band (CB). This particular electron, enters an unstable thermodynamically phase, a quasi-thermal equilibrium state which endures only for some picoseconds, the relaxation process, which allows it to reach the lowest limit of the CB. Finally it is possible to return in the VB emitting a photon with specific energy that depends on the energy band gap. On the next figure (figure 2.6) it is shown the PL process as it is described.

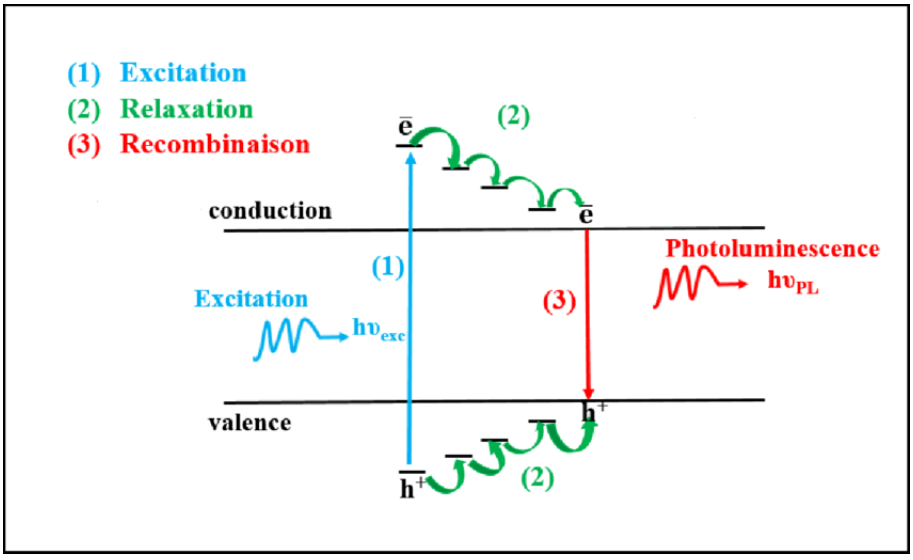

Figure 2.6.Theoretically schematic for PL process via electronic bands. E represents electrons while the h is the hole[11].

2.2.1 Photo-excitation

When the incoming light is absorbed (microscopic polarization), electrons and holes are separated with finite momentum k in the CB and in the VB respectively. In general there are three different excitations: the resonance, quasi-resonance and non-resonance.

The resonance excitation demands the central energy of the light source (monochromatic laser radiation) to correspond to the lowest exciton resonance ,$E_g = E_f$. Any excess energy amount is injected to the carrier system, although that excess is almost negligible. Coherent processes contribute to the spontaneous emission of the carriers. The continuous recycling decay of the polarizations creates instant excitons. The detection of the resonance PL is challenging, as there is no easy discrimination of the light contributions that exist on the process. The overlapping between the radiated energy and the spectral emission energy prevents a reliable diagnosis on the material's spectrum.

The opposite non-resonance case, demands the excess energy amount of excitation. This is the most common PL case. The emitted radiation can be separated using a descent spectrometer and some optical filters. In many cases the laser output is higher enough than the demanded energy, capable to be stunt by an optical filter, to avoid any interference or overlapping with the true emission spectrum of material.

$$E_f = E_g + hf \quad \textbf{(2.12)}$$

In the condition of the quasi-resonance, the energy of the excitation is tuned above the ground state but still below the barrier absorption state. The polarization decay this time is way faster than the resonance case and the coherent contributions in the quantum well emission are almost zero. The carriers hold higher temperature than the lattice itself due to the surplus energy that injected. In the end only the hole-electron plasma is created, by the high increasing of temperature. Following the thermal cooling of the system the excitons are enable formatted.

2.2.2 Relaxation process

The dephasing of the polarization leads to creation of populations of electrons and holes in the two electronic bands. The lifetime of the carrier populations is limited by radiative and non-radiative recombination that called Auger recombination. During that time it is possible for some electrons and holes to form instant excitons. The formation rate depends strongly on the environmental and experimental conditions as well as the materials properties like the Coulomb interactions potential and the excitons binding energy.

Right after the excitation the carrier distribution is determined by the spectral width of the excitation radiation. The distribution usually presents a Gaussian form, centered at a finite momentum. In the first femto-seconds the carriers are scattered by phonons, or by other related carriers via Coulomb interaction. Soon the system will relax following the Fermi-Dirac and Bose-Einstein distributions within picoseconds. The last part presents the emission of photons. The whole process can take maximum some nanoseconds according to the material's properties.

The contribution of phonons in the previous process changes the energy pathways and the final optical result. It is possible in some progress, to observe the emission of the optical phonons within the decrease of the temperature (heat loss). This loss is almost always observed in various rates due to the flat dispersion of the phonons, which increasing the chance of carriers-phonons collision in a wide range via the lattice's potential threshold. In lower temperatures the dominant dispersion comes from the acoustic phonons. Temperature continued to lower slowly, as long as the remaining energy rests on the acoustic phonons-carriers interaction. The more the hot carriers are involved in relaxation, the higher rate of optical phonons is generated and prevents the distribution of acoustic phonons instead. Over population of the optical phonons causes the high potential of their re-absorption by the charged carriers and suppress the cooling mechanism. So a system cools slower, if the carries' density is kept increasing.

2.2.3 Radiative recombination

The emission is recognized as a Gaussian distribution with specific peak and width, on the printed spectrum. If the carries are emitting right after the excitation, then the spectrum is mostly wide. Thus it is labeled as a broad PL peak. A sharper peak is hopefully printed when the system is already relaxed and cooled down and the emission is more specific without the big interference of optical phonons. Thinner peaks have accurate energy shifts and present better the optical emission of the exciton ground state. With the decreasing of the width is mostly possible to observed smalls shifts on the emission energy. In the broad peaks the population of the hot carriers that emit is high, so spontaneous are emitted multi-shifts of energy photons, in the valley close to the edge of the CB. The over-population is detected in hotter samples and recognized by such broad peaks on PL spectra. The multi-shifts emitted photons can be theoretically considered individually as side by side sharp peaks that evolve a whole wide overlapping between them. By this overlapping the final broad peak is formed.

The width of the Gaussian PL distribution shows fundamentals elements about the electronic behavior of the studied sample. Additional peaks from higher sub-band transitions appear as the carrier density or the lattice temperature is increasing as these stages can get more populated. An increasing of the PL peak width signals the excitation-induced dephasing[42] and the emission peak suffers from a small energy shift.

2.2.4 Exciton

When an electron overcomes the energy band gap and populates the CB, an empty space in VB is resulted by the missing electron. This empty space is called hole and it is considered as a positive charge. The couple of an excited electron and its corresponding hole is called exciton (X)[14-16]and within the recombination of an electron and its hole, light with specific wavelength is emitted as the existence of the exciton is terminated. Each electron can be mathematically described by a wave-vector k on the Brillouin zone and its hole with the opposite –k. The PL mechanics differs according to the kind of gab that each semiconductor has.

Energy band gap can be recognized as direct or indirect. In the direct gapthe two local limits of CB and VB, with energies Ec and Ev, are in the same wave-vector k in the Brillouin zone, while indirect gap case sets the two limits topological independent, having different k vector. In the following schematic (figure 2.8), it is shown the PL process on each type of energy bandgaps.

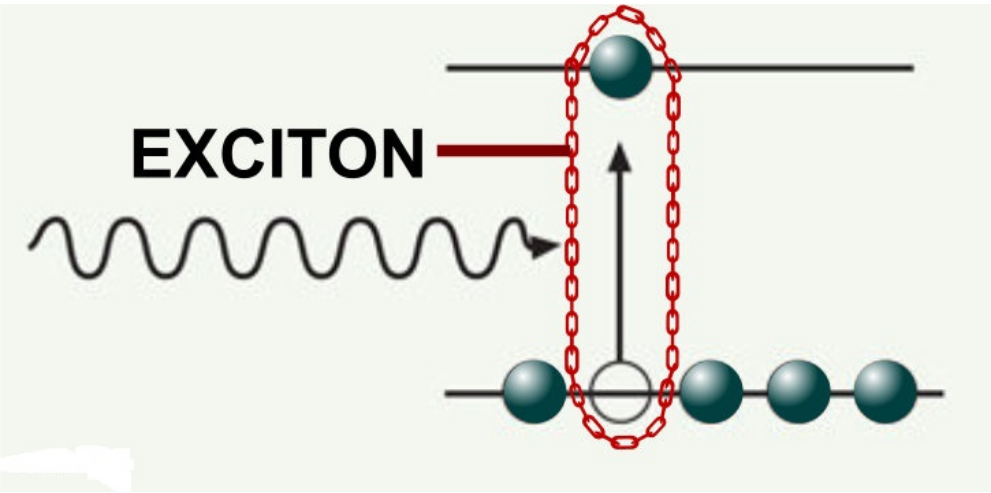

Figure.2.7.Theoretical schematics of the exciton. Blue spheres present electrons.

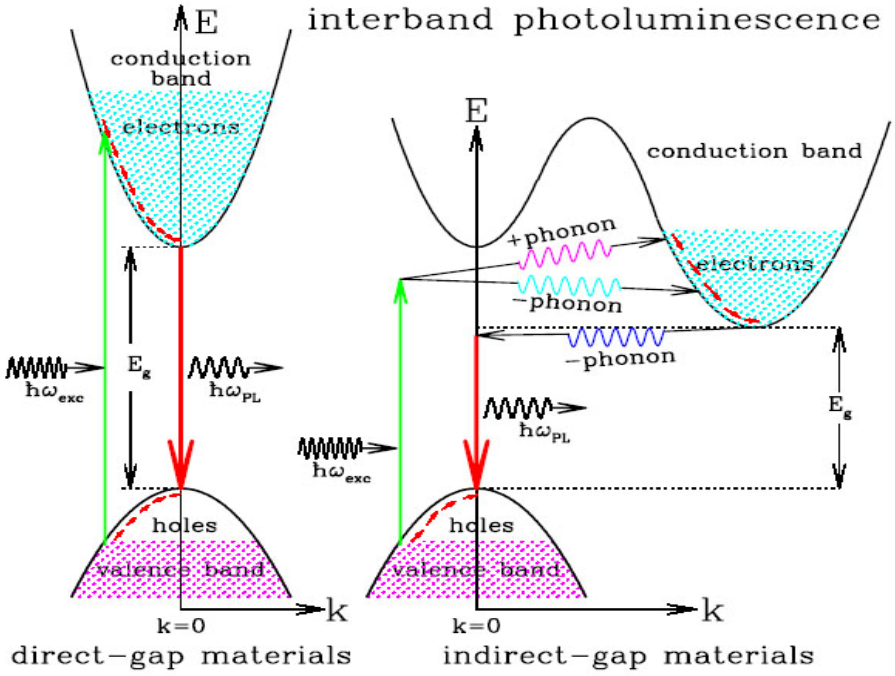

Figure2.8.Population Inversion and PL mechanics via different types of energy band gap inside a crystal[11-13].

Considering a thermodynamically process, obviously it may be occurred some energy losses, throughout the PL mechanism. For example, when the process is taken over into a direct gap then the thermal losses via the phonon-carrier interactions, which generated by the collisions of the carrier with the lattice, are limited and the most of the emitted energy of cooled electrons is approximated by the energy gap. However there are some extended elements that confirm that the emitted energy defers by the energy band gap.

There are chances a photon to contain enough energy to create an exciton but not enough to completely separate an electron from the hole. This difficulty of separation exists as a result of a binding energy that an exciton has, as long as the particles attracted by opposite electrical charges, on each different band in the semiconductor. So beneath the electronic gap, there is also the binding energy[15-16] that does not contribute to light emission in the PL process. Technically an exciton represented as a quasi-particle, due to the instability that shows and the variation of its binding energy. The remaining gab, that proposes the light emission of PL, is called optical gap[14-16] and returns obviously lower amount of energy than the whole electronic gap. At last the main notions, about the formation of the energy gap, behold to the combination of an optical gap and the exciton's binding energy. The 2D character of monolayer TMDs suggests a strong enhancement of the Coulomb interaction, between the electron-hole pair. The final formation of an exciton can reveal the optical and charge-transport properties of the 2D material.

Experimental and theoretical studies have shown, so far, that the basic excitonic properties of the bulk form differ fundamentally, compare to the 2D form of the same material. The formation of an electron-hole pair in a TMD monolayer is strongly confined to the specific plane of the monolayer and experiences reduced screening, compared to the bulk form, due to the change of the dielectric environment [80]. Thus as a result, it is visible a bigger quasi-particle band gap and an increased electron-hole interaction in the monolayer form. Theoretically it is predicted that in dielectric-free environment, the exciton binding energy is toping at least 4 times higher in 2D form than in 3D bulk space. The additional reduced screening of the

monolayer form is resulted, due to the expansion of the electron-hole electric field outside of the 1L plane, and gives even bigger enhancement factor of the binding energy. This phenomenon is called “dielectric confinement” or “image charge effect” [40,80].

The direct band gap occasion on PL is pretty simple. Process follows the common mechanism and the main emission energy loss is restricted only in the binding energy gap. On the other hand, in-direct gap, PL is more complex than that. Since every exciton is hosted in a specific couple of wave-vectors, k and -k spots, it must be placed in the bands edge in order to be recombinated. The two edges are not identical opposite, so the recombination requires the presence of an acoustical phonon loss, in order to deliver the exciton into the optical gap. Speaking of the momentum, direct gaps have low phonon interactions in the relaxation process. The in-direct gap instead has significant losses by optical phonon emission, trying to transport the exciton particles on the band edges and complete the recombination. On trial to overcome the lattice’s electrical potential threshold, the carriers need extended energy that is lost in progress and expressed as heat. Thus the productive PL intensity tends to be obviously lower comparing to the direct gap.

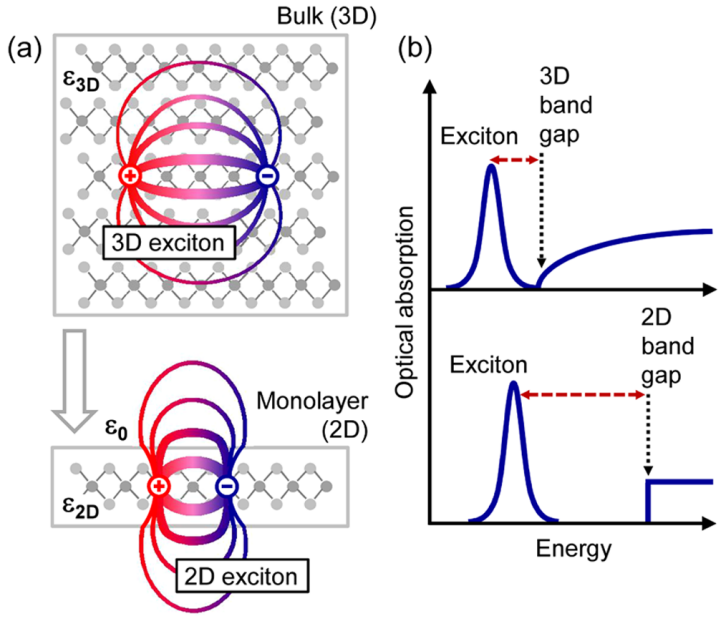

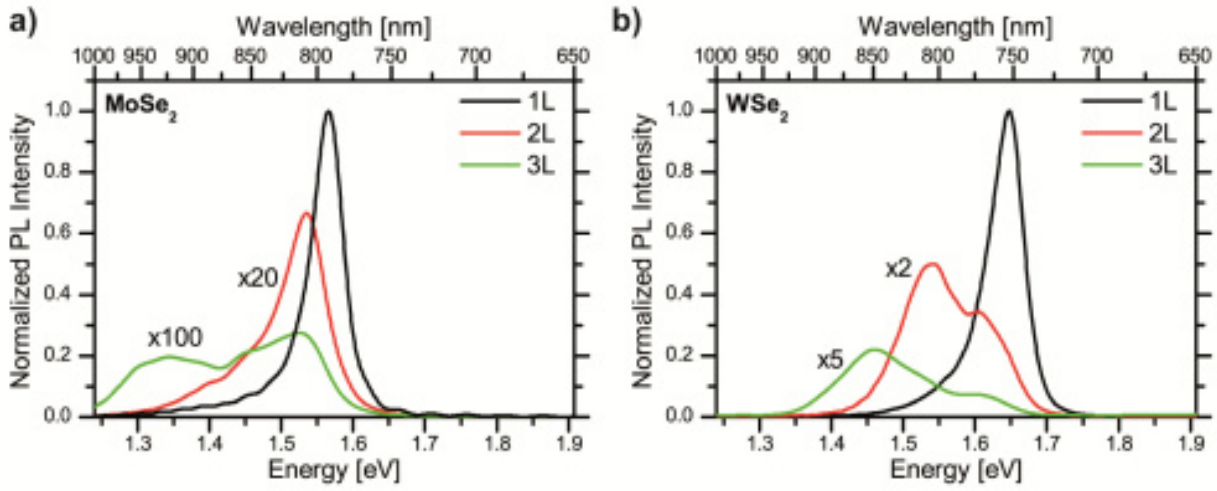

Figure 2.9. (UP) Exciton electric field in dielectric medium of 3D and 2D (a), Optical Absorption on 3D and 2D medium (b) ,(Down) PL spectra of a) $MoSe_2$ and b) WSe_2, in 1L -3L with 532nm laser source at room temperature[41,80].

Depending on the exciton radius and the strength of the Coulomb interaction between the electron and hole, excitons in solids are separated in two types. The Frenkel and Wannier excitons [40]. In a medium with small dielectric constant, like the ionic crystal, the electron and hole are tightly bound to each other within the same or the nearest neighbor unit cells. This type is the Frenkel exciton. These excitons have average binding energy in region of 0.1-1 eV. It can be found mostly not only in the ionic crystals, but also in organic crystals. In semiconductors, where the dielectric constant is typically large, the Wannier exciton type is the most efficient. The electric screening by the valence band electrons, reduces the Coulomb interaction between the electron and hole. Thus the radius of an exciton is larger than the lattice spacing. The binding energy of these excitons is in the order of some meV. In 2D TMDs, excitons have both Wannier and Frenkel character. They are radical large but also tightly bounded. For example the effective binding energy of the A exciton in the MoS_2 monolayer is 0.106 eV and the ground binding energy is leaded into 0.897 eV. Due to the large dielectric function, which allows the extended spread of the wave function to several nanometers, the large radius is explained and the poor dielectric screening explains also the big binding energy inside the 2D material.

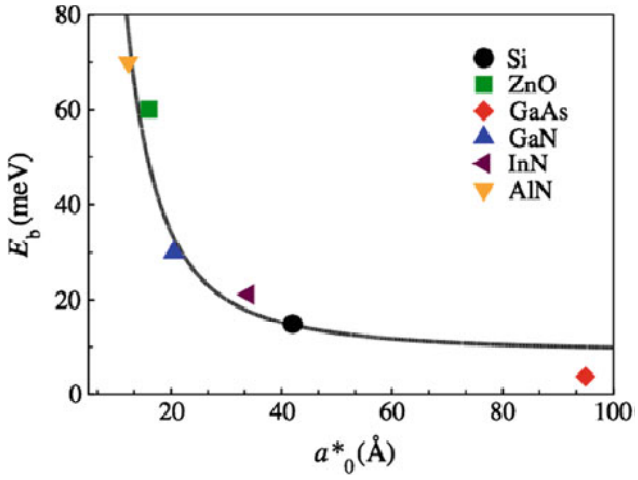

Figure 2.10.Exciton Binding energy versus exciton Bohr radius [40].

2.2.5Charged Exciton (Trion)

A trion is a charged exciton, which consist of three charged particles. Like the common exciton, the trion also is considered a quasi-particle. It can be observed as positive (X^+) or negative (X^-), according to the total charge carries. A positive trion constructed by two holes and one electron, while the negative is the exact opposite. Trion is a little more complex than the neutral exciton, having a ground state of spin being equal to ½ and an excited state of 3/2 spin[17]. The spin can also be positive or negative, knowingly the type of trion. The spin system of trion distinguishes it from the common exciton in various phenomena like the behavior of energy splitting of spins, inside an applied magnetic field. Trions are obviously more sensitive to an applied field compared to an exciton that might stay steady.

Trions can theoretically be predicted and are also presented in various optoelectronic experiments of semiconductors and even in smaller systems like quantum dots. Its first proof of existence was on carbon nanotubes[18] that confirmed the theoretical studies. Trions have at last been discovered in the 2D materials like the TMDs semiconductors. In the 2D materials like layers the interactions inside the trion

depend on the topology of each layer[19]. Thin layer materials can hold the trion longer than the bulk forms, as long as, the absent of the upper surface, especially in monolayers, does not introduce another electro-statically potential to interact with the bounded electrons or holes. Numerical results have been waged by Monte Carlo [20], especially in the 2D structures, which their topology has no further, interfering interactions between layers. As long as trions can be found in various semiconductors they make the study of the common exciton even more important and interesting; due to their unique nature and big differences they have between each other.

Specifically, trions are formed mostly on the polarized valleys inside a semiconductor and therefore it is needed a polarized light source to initiate their formation. Circular polarization [19] is a common PL experiment to confirm the trions identity. This experimental process is widely known as valley polarization PL.

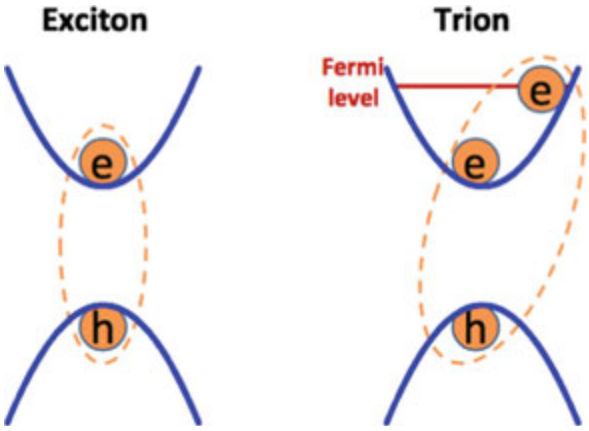

Figure.2.11.Exciton (left) and Trion (right) schematics [40].

2.2.6 Spin-Valley Polarization PL

Certain semiconductors, like the TMDs, have multiple valleys distributed within the electronic band structure. These mediums are known as multi-valley semiconductors. The attempt to control the valleys behavior and the degrees of freedom, between the local maximum and minimum of valence and conduction band, is the entry push for valleytronic technologies. In the enhanced PL form the valleytronics are performed via a similar technique, which is known as spin-valley polarization (SVP). Valleytronics and spintronics rely on the fact that the free carriers inside solid forms (electrons and holes) are carrying also spin, besides the common electric charge[69,72]. A valley is a term, that it is used to describe the region in an electronic band structure were both electrons and holes are localized, and the "valley polarization" term describes also the ratio of valley populations, which is applied as an important metric [72]. The growing fields of spintronics and valleytronics claim mostly the wide application of both spin and valley population for the electronic expansion of current and information administration within an electronic device such an electronic-logical operator.

TMDs monolayers are strongly characterized by broken inversion symmetry. At the K+ and K- valleys in momentum space, the highest and the lowest energy states on the valence and the conduction band respectively are mainly from the transition metal (M) d-orbital behavior. Due to that break in inversion symmetry some sub-orbitals of d-orbital structure, have less populated states and occupy more degrees of freedom. That increasing of freedom degrees, actually related to the absent of the QY potential of an opposite orbital d that can overlap the space between. That absent is obviously presented by the fully also absent of an upper-layer, above the monolayer. So the bilayer is keeping a sort of inversion symmetry, while the monolayer have constant break in that point of inversion. Through the broke inversion symmetry it is visible a specific energy splitting between the valence bands and another one splitting between conductive bands, which are feasible via the spin-orbit interactions. For example the spin-orbit interactions in MoS_2monolayer split the valence bands by 160 meV [69] at 293K, while the same interaction for the WS_2monolayer creates a 430 meV splitting at also room temperature [73]. Additional examples for WSe_2 and $MoSe_2$ show individual splitting on VB, of 470 meV and 190 meV respectively. The tungsten as

heavier transition metal atom is generating bigger splitting, on TMDs compounds, than the molybdenum, due to the d-orbitals behavior and the stronger Coulomb-induced dipole-dipole interaction couples [74,75]. The induced magnetic field interacts with the charged carries and their spin via the common magnetic forces of Lorentz. The separation of spin states and polarization, left (σ-) or right (σ+) is more intensive within the valleys and last as long as the applied field allows it. Thus eventually it is observed an extended exciton's lifetime and the duration of the polarization emitted signal itself. The dominant polarization on the system is determined not only by the direction of the field but also eventually the initial circular polarization of the induced light.

Excitonic states with different valley indices are energetically degenerate, related by time-reversal symmetry[71].The symmetry can be broken by optical excitation or some induced magnetic field, with the creation of pseudospin states within the valley's carriers, in radiation of some polarized light according to the spin state of the carrier. As long as it is accepted that the spin reactions affect the electro-magnetic coherence, then the intense spin separation affects also the splitting between the valence and conductive bands respectively. Experimentally it is induced an initial circularly polarized light in the studied sample. Due to the spin states that are generated via the spin-orbit coupling, the sample itself can emit also back circularly polarized light as PL signal, according to the direction of the initial light polarization. If the induced light is right or left circularly polarized then the emitted PL will also follow the same polarization instead[69].The amount of the polarized photoluminescence emission of the studied sample is expressed mathematically by the following equation (2.13).

$$\rho = \frac{I_{\sigma_+} - I_{\sigma_-}}{I_{\sigma_+} + I_{\sigma_-}} \quad \textbf{(2.13)}^{[69,74,78]}$$

Where the σ+ is the right polarized and σ- is the left polarized light with their corresponding intensity I.The induced polarized light of excitation must be on resonance with the A or B exciton energy of the monolayer in order to provide polarized PL response. The further of resonance, the less polarized PL response in intensity is observed. The time reversal symmetry and the broken inversion symmetry are resulting eventually in strong spin-valley coupling in a TMD monolayer, which is responsible for the optical selection

rules that allow the optical excitation of opposite helicity with the left (σ-) and right (σ+) polarized light to be distributed at the K- and K+ valley respectively. In the bilayer's case inversion symmetry is restored, so spin and valley are no longer coupled. Along with the time reversal symmetry, spin degeneracy of the bands is also restored at each valley separated.

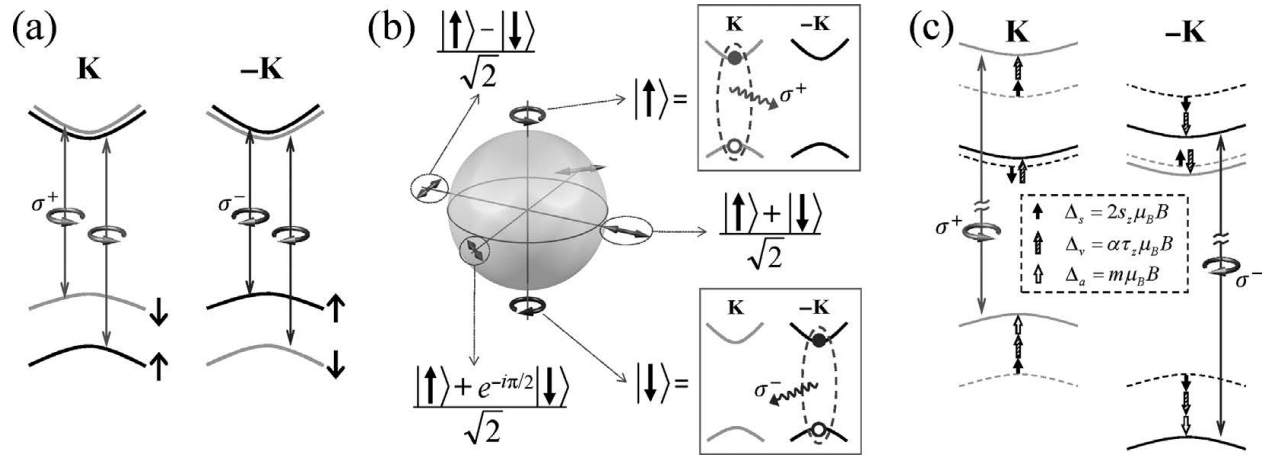

Figure 2.12. a) Valley and spin transition selection rules, b) Optical orientation of excitonic valley pseudospin, a bright exciton in the K+ valley corresponds to the spin state up (+) while the inverted bright exciton in the K- valley is responding in the spin state down (-) instead, c) Valley dependent "Zeeman" shifts of the band edge[76].

For TMDs monolayers the amount of spin-valley polarization depends strongly on temperature, it decreases as the temperature increases. At low temperatures, the number of phonons is limited through the crystalline lattice [77,78]. Thus the phonon contribution is the lowest and also the thermal energy distribution that breaks the polarization between the valleys. The inverse process is taking place after a threshold of temperature, where the phonons are dominating the inter-valley scattering and increase their inter-valley population. The conclusion suggests the corresponding decrease of the circular polarization from the system at higher temperatures. Thus the highest polarization results are achieved at very low temperature experiments [79].

In a PL experiment, the backscattering light is passing usually through a broadband of ¼ λwave plate or crystal, a beam-displacing prism to separate the beam into two beams orthogonally polarized and a

depolarizer until the final focus on the CCD camera. The light source needs to be in near-resonance with the PL emission for maximum polarization. In the case of MoS_2, for example, with specific PL emission at near energy gap, it is 1.9 eV. Thus, an appropriate light source is a He-Ne laser with 1.95 eV, with 50 meV difference and the system must be cooled down to 10K temperature[79]. For this material, it is observed that after the temperature threshold of 90K, the circular polarization gradually decreases, with temperature.

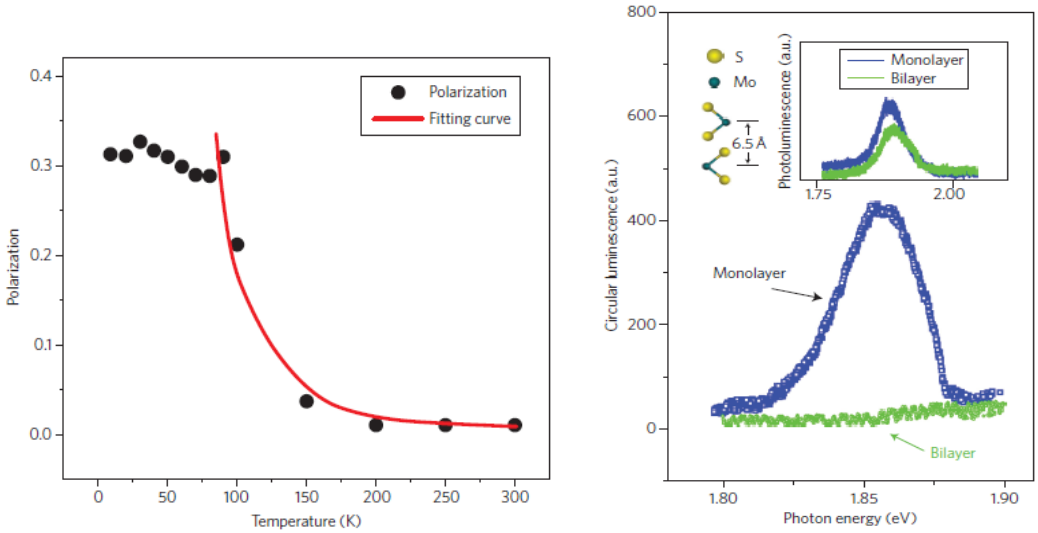

Figure 2.13. Degree of Polarization P as a function of temperature in MoS_2 monolayer (left) and optical helicity of monolayer and bilayer (right). The fitting curve (red), presents an approximation of the inter-valley scattering proportional to the phonon population [79]. Monolayer and Billayer are equally excited under the same experimental conditions.

Despite the PL difference between the 1L and bilayer, it is also visible the optical deference in circular polarization between them. As long as the monolayer has higher amount of PL emission than the bilayer, it is expected that this will also presented in the SVP. Consisted of a direct gap the monolayer also shows promising circular polarization signal as it has less phonon's population in the inter-valley. As it is eventually observed, the monolayer has way higher optical helicity than the bilayer or the bulk form of the

material. Just like the PL of thicker materials, is weaker than the first layer, the optical helicity under circular polarized, follows the exact same behavior in these materials. The degenerated valence band in each valley of the bilayer, are split by the combined spin-orbit interactions in each monolayer and their interlayer interactions, into two spin-degenerate valence bands. So an σ- excitation in resonance with the A exciton, for example, will generate excitons with e^- spin down and h^+ spin up, in both of K and K' valleys of the bilayer. There is a net spin orientation but no valley polarization. A short hole spin lifetime and small degree of PL and optical helicity is eventually observed. The physical presence of the phonon population and the temperature are the main-determined factors behind the circular polarized emission in each polarized PL process[69,74,79]. Thus the temperature decreasing or the direct gap, are resulting to a higher circular polarized emission and a corresponding higher optical helicity.

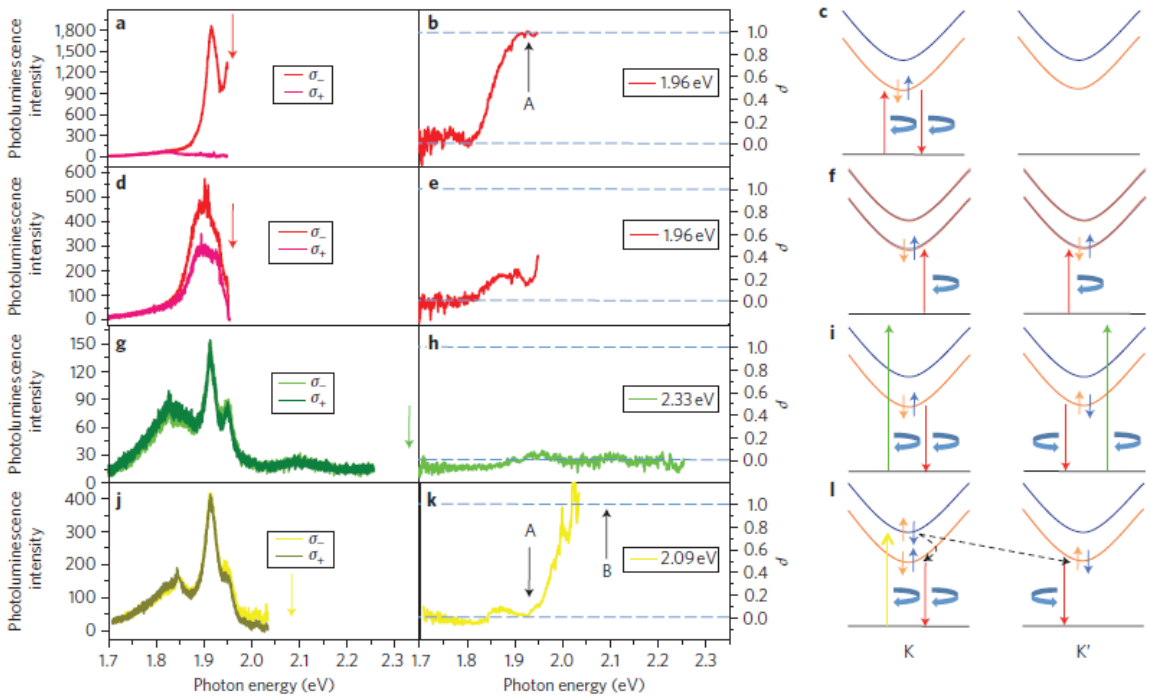

Figure 2.14. The optical control of valley-spin polarization in a MoS_2 monolayer. The optical excitation is with left circular polarized σ-. ***A-C****, Excitation of monolayer at 1.96 eV near resonance (633 nm) with A exciton.* ***D-F****, Excitation of bilayer at 1.96 eV.* ***G-I****, Excitation of monolayer with 2.33 eV (532 nm), off resonance with both A and B exciton.* ***J-I,*** *Excitation of monolayer at 2.09 eV (594 nm), in near resonance with B exciton. [69]*

From the figure 2.14 it is understood that the observed emission, under the 2.33 eV excitation is fully un-polarized, thus no spin-valley polarization is occurred. This non resonance behavior is a result of the relaxation of the optical selection rules [69,79]. The off-resonance excitation actually populates both K and K' valleys, so there is not an optical selection via spin-valley coupling. Near the B exciton resonance, 2.09 eV, only K-point valley is populated by excitons, due to the optical selection rules. There the A exciton is fully un-polarized, despite the linear polarized PL emission it can show. Thus according to the near resonance region on each exciton, the optical pump is tuned to provide the polarization PL requested results. In the case of the bilayer the polarized PL results show that there is a similar intense on polarized emission in both spin states. That confirms the existence of the inversion symmetry along with the time reversal symmetry as well. The final polarized optical helicity, in bilayer, is significant lower than in monolayer.

The used substrate also affects the resulted polarization and needs to be into account during the experimental processes. Studies have shown that the common silicon substrate SiO_2/Si, with a MoS_2 monolayer, can give an A exciton lifetime of about 5 ps, while in the h-BN substrate the same A exciton presents a ten times longer lifetime, of about 50 ps[69]. The quantum yield PL, also follows the same behavior in each substrate with the h-BN to have the highest rate of emission. The optical helicity on h-BN yields a hole the valley-spin lifetime higher of 1 ns in the monolayer. The bilayer as it is expected has much shorter exciton lifetime in-depended of the substrate. The QY PL emission is about 20 times lower, than the 1L and the exciton lifetime cannot exceed the femtoseconds region.

2.3 Differential Reflectance

Differential Reflectance spectroscopy (DR) is a technique that measures the difference in reflectance between two individual studied samples. Most of work on this spectroscopy finds application on metals and their various alloys. Modern uses suggest that it is applied also in crystal poly-structures, semiconducting mediums and even in clinical purposes [39].

In 1969 it was performed the first correct experiment of DR spectroscopy by the Soviet physicists A.A. Volfson and V.K. Subashiev[28], when they try to study two highly doped semiconductors of silicon and germanium via their reflect properties. The main plan was to measure the deference that was resulted by the reflectance spectrum of the pure sample and the doped one. The experimental set up was installed in a way so the substrate, that carried the two samples, could rotate while it was radiated by white light, which reflected as a monochromatic radiation, alternatively from the two samples. This method revealed critical features about the optoelectronic properties and the structure of a semiconductor system, as long as it can also be used for piezo- or thermo dependence reflectance measurements.

The basic principle is the reflection ability that matter has on an incident radiation. Reflectance is considered as a light-matter interaction. As long as a material is radiated by light it is possible, among the variety of interactions that have been mentioned previously, to reflect a specific light back. The concept behind the phenomenon comes from the classical and the quantum description. Incident light can be refracted or reflected instead, depending on the medium it hits. Classical explanation begins with the Huygens principle of reflection, suggesting that the reflection result is functioned to the angle the light interfaces the medium. According to the geometrical optics, light is also reflected with an equal angle of the incident one[11]. This phenomenon is observed every time light passes from a medium with given refractive index to another one. Generally a medium can refract a percentage of the incident beam while the remaining light is reflected. Knowing the equality of the angle between the two beams, it is possible to calculate the index of each medium by the reflection angle.

The calculation of the geometric angle is mathematically accurate by the Snell's law, which suggests the rate of the angle that refracted inside a passing medium. The incident beam is usually known and most always is determined by the light source. As long as the energy conservation prohibits the change of light frequency, the photon must be recapped by wavelength or velocity from one medium to another. From classical electrodynamics the light is considered as an electromagnetic wave. While this faces a medium, induces small oscillations of polarization in the individual electron cloud of medium's itself. That mechanism causes the instant radiation of a secondary electromagnetic wave in all directions, as spherical waves[32]. By the Huygens- Fresnel principle the emitted waves collectively give specular reflection and refraction. It can be explained that, changes on the electrical distribution of the medium are happened when the light automatically collides upon it. Spontaneous, the electrons will also emit light in every possible direction. This is a quasi-state of the electron cloud as exchange energy with the passing electromagnetic wave and it needs only picoseconds for that recycled interaction. The resulted reflection is the new-secondary radiated light of the electron emitters that face backwards the incident light's direction.

The quantum explanation is more complex than that. Quantum reflection is happened whenever the motion of particles is reverted against the force which acting on them. This action detonates the wave function of particles and compromise collisions of them with their interfaces [29-31]. The quantum analog of reflection is applied to any particles that interact with surfaces. In definition of surfaces, the consideration of the possible reflection can exist only in solid and liquid forms, where the meaning of surface is valid. Gases cannot present a way of surface, due to their long distances between its interacting atoms. The mathematically explanation of the quantum analog needs calculated approximations and dimensional analysis, according to quantum mechanics protocols and is way more complex than the classical one.

By continuous development of the method, the recent use has focused on advanced semiconductors such as the TMDs and other materials of high interest like the graphene analogs. The experiment requires as main light source a lamp with white light emission and not some monochromatic radiation. The white light allows the main part of light to refract the measured sample, while a specific radiation will be reflected back by it. This radiation as it was proposed previously is the secondary radiation of the electron

emitters, backwards and considered monochromatic. In the semiconductors area, this monochromatic radiation suggests a peak of energy that lies between the CB and the VB inside the band structure. If the light emission is achieved by the CB electrons' cooling, then reflection results mostly until the electron populate the CB[33].Due to the quantum energy band gap, the only passing or absorbed light is the one with the exact or higher energy than that, meaning that the reflections immediately are set on during the process as long as it lasts. If white light fires upon the sample, the lower energy range of wavelengths are reflected backwards monochromatically, while the higher range is absorbed and emitted as the common PL.

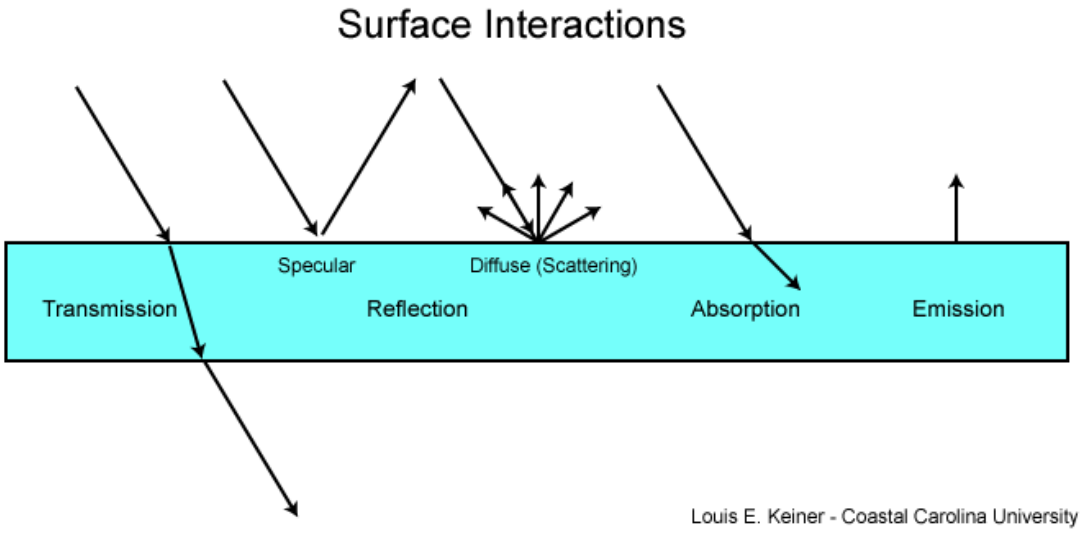

Figure.2.15.Surface interactions of light. Reflection mostly presents as diffuse, rather than the specular due to the random, in most cases, incident angle of light.

The white light use is basically more efficient by statistics. Since the frequency range that reflected is big enough, statistically the other beyond that cannot contain a bigger range. In the result spectrum, of a semiconductor, is compromised the gradual decrease of reflectance, function to the energy output that directed by the sample[34,37] and so on the biggest numerical reflectance usually is set on the lower energy photons. The reflectance spectrum often presents a continuous downstream with a slight curve cutting it

on a specific energy point. That curve signals the energy band gap and the exciton energy state[34-36]. Sometimes it may be occurred fluctuations of reflectance during the resulted spectrum, which is characteristic on the semiconductors systems, explaining the existence of lower or higher energy bands that exist on the valance and the conduction area respectively. The variety of the existing excitons also concludes the number of the curves that printed on the resulted spectrum. Despite the recognition of the basic elements by the reflectance, the results are not always pure, since the complex mechanisms that take place together during the experiment and the finite quality of the experimental set up. In order to have forthcoming results the experimental process leads to the difference of the reflectance between two individual samples that are related.

The DR process follows the same mechanism of the starting reflectance and prints two separated spectra, for the studied sample and a referenced sample for calibration. For example, in the 2D materials domain the studied sample is usually a monolayer compound and the referenced sample is a substrate, which many experiments present the SiO_2/Si bulk material. This substrate has been chosen because usually it doesn't overlaps the sample's DR. Despite the energy band gap of silicon on 1.14 eV energy the DR spectrum shows promising reflectance signal on about 3.4 to 4.3 eV photon energy, due to the optical anisotropy in lattice formation in the interface of the crystalline and the oxidized region of silicon[37,43]. The process measures with the previous way the reflection spectra of two materials. Then the final act is the difference calculation between them. The calculation uses the numerical difference between the exported data of each reflectance and prints the final spectrum of DR. The calculation formula mathematically described by the following equation (2.14):

$$\frac{\Delta R}{R}(\lambda) = \frac{R_s(\lambda)-R(\lambda)}{R_s} = \frac{|R(\lambda)-R_s(\lambda)|}{R} = \frac{4}{n_s^2-1}a(\lambda)n = -8\pi\left(\frac{d}{\lambda}\right)Im\left(\frac{1-\varepsilon_s}{1-\varepsilon_b}\right)^{[34]} \quad (2.14)$$

Where the Rs is the substrate's reflectance, n_s the given refractive index of the substrate, a(λ) the absorption coefficient that depends on the studied sample and n the index of the studied sample as well. Es and Eb present the dielectric function of surface and the thickness of the semiconductor respectively.

The numerical data of DR presents the quality result of the experimental method and they have not some accurate physical, quantified units. The experimental units are hidden by the number of reflected photons ending up to the photo-detector. Usually the photo-detector is the common CCD camera that can convert the incident photons into voltage and electrical power output units. Thus in a DR spectrum the vertically axis (y) presents the intensity by quality as a measurement of photon capacity. In that way most of cases there is no need of physical units presentation vertically, as the main interest comes in the horizontal axis (x) where the photon energy in eV units is spotted.

DR method became very famous quickly for the application on very thin films, such as 2D structures. The less the thickness the better results the method can get. That paradox depends again on the refractive law. Supposing that the incident white light, comes from a lamp source, travels through the air medium with known refraction index. Finally it hits on the studied sample, assuming a 2D monolayer that obviously has bigger index than the air. By this hypothesis, the percentage of refractive light cannot be absorbed as easy as in the bulk form, due to the small thickness of the monolayer. There is a correlation between the distance travel d and the wavelength of the incident photon λas d/λ. Using that term it is defined the quality of the reflectance spectrum by the Fresnel law on small or far distances diffractions [28,34]. In the case of DR method the d/λterm considers d the thickness of the medium as travel distance. It can predict the rate of the refractive and reflective photons through a given sample. In case the d term is pretty low like the monolayer's thickness, then the refractive-absorbed photons are close to zero rate[28,33-35]. Thus the only interaction that is occurred is the reflection. The monolayer's thickness is about some Angstroms and that requires similar incident wavelength to interact with. As long as the interacting wavelength becomes smaller, the other range of light cannot be part of any other interaction than the reflection. In that case there is an increasing of the reflected photons by the sample. That increasing occurred in the final printed spectrum as higher intensity of DR. So using the silicon substrate, in bulk form, which can refract and absorb immediately the incident photons, the DR spectrum can be even more accurate and clear.

The experimental set up has been suffered by various innovations through the years. Its development was proofed critical for the extended use in various samples, the smoothness on the protocol process and

the results output. Various advanced technologies like better light-emission devices and optical filters contribute to the best experimental output and also less financial cost. The main light source till now is delivered by a white light lamp [38]mostly or another wide wavelength range emitter, as long as, it contains the visible range emission. It's easy to understand that in semiconductors area, the band gap varieties from upper 0 to at least 4 eV energy requirements. This energy is occurred in the visible spectrum, thinking about the wavelength and frequency domain.

Although the white light source is appropriate for such spectroscopy, it is important to choose a capable lamp based on the brightness that can provide. Despite the fact that, high brightness can give more DR intensity, there are also cases, where constitutes an obstacle to the whole process. In many monolayer-substrates systems it is possible to have high amount of background noise signal, during the spectrum printing, especially when the brightness is accompanied by high power output. This couple prevents the intensity of the monochromatic reflected radiation by the studied sample and is shown in the final spectrum as noise or wide DR peaks. It is highly required to get more intense reflectance signal than any other aspect that may be part in the process. This problem is solved with the use of optical filters. Long pass or short pass filters are commonly used for such applications, in order to stunt the unnecessary radiation and leave the monochromatic to pass eventually to the photo-detector.

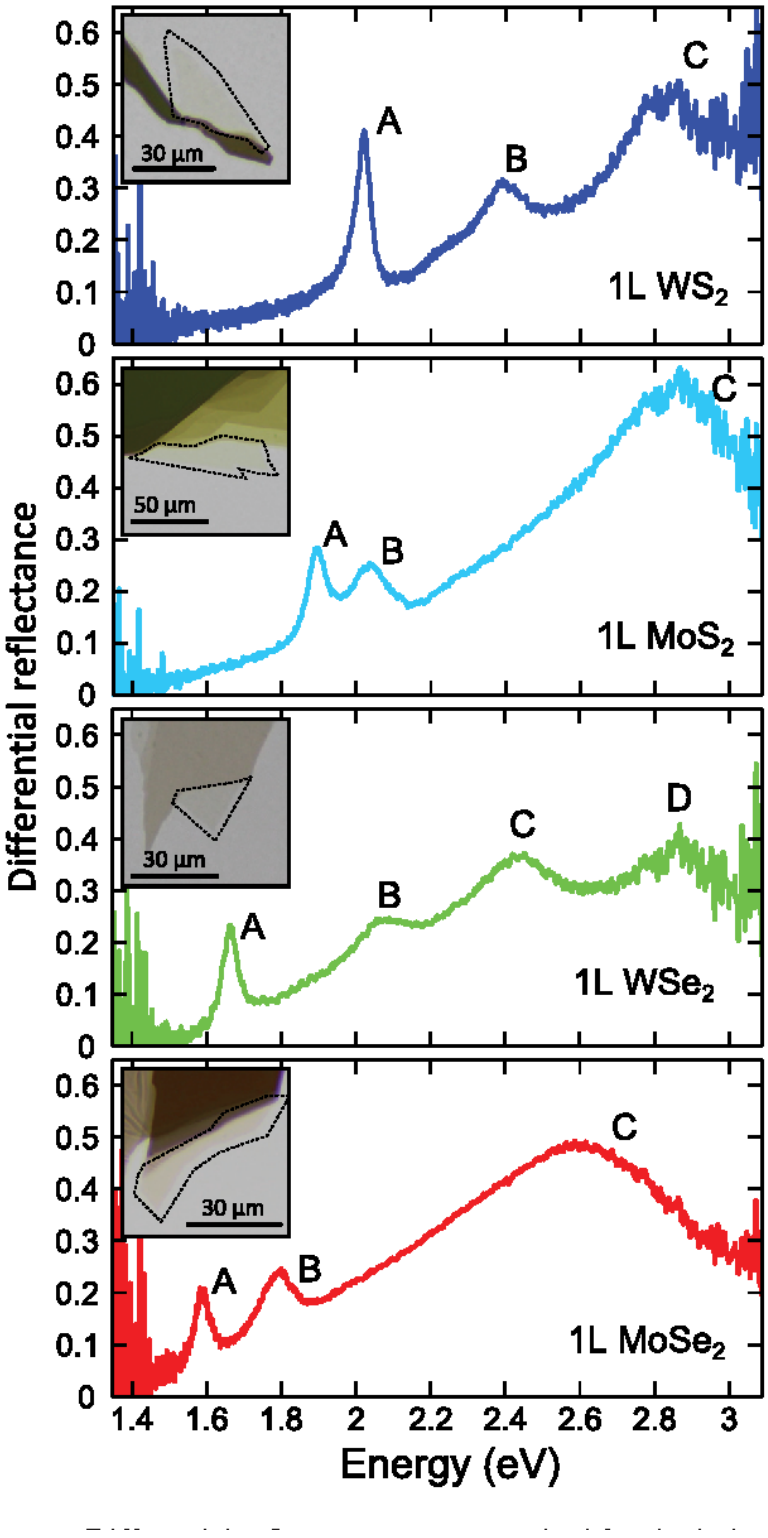

Figure.2.16. Differential Reflectance Spectra for different monolayer (1L) types. A, B and C represents the exciton states in order [44].

2.4 Mechanical Exfoliation

Mechanical exfoliation is a common experimental process of isolating parts from a proper solid bulk material. The first attempt introduced on 2D materials, was the isolation of graphene[1] in 2007 and has been expanded to various solid materials, expecting to attract thinner forms of materials and 2D structures like the monolayers.

By taking into account the van der Waals interactions that keep the crystal structure of a solid tightly bounded, the isolation needs the application of a bigger and opposite mechanical force, so thin structures can be dragged out of the bulk form. The isolation also needs a transport medium and a descent substrate to create, hopefully, a 2D structure. Although it is proofed that, this method of isolation has worked in the past, it doesn't mean that it works every time. Statistically speaking the success of the process fluctuates to 10%-20%, in an amount of hundred tries by an amateur user. Experienced users also face such difficulties, despite their huge practice on this method, because of the random results may occur. The fact that the exfoliation is really difficult yet so useful, have attract the attention of the scientific community the last 10 years, in the isolation of 2D materials.

Attempting to use this process, it is needed a transport medium, like the common scotch tape[25,26] that has strong attraction forces, bigger than the van der Waals, to part the bulk form into even thinner bulk forms. Next it is used a substrate surface to transfer the parts of material by manually forcing the tape on the substrate and quickly draw it back[26]. In this way it is possible many pieces of material be deposited through the tape to the substrate. The opposite force of the van der Waals is applied by a mechanical shear[21] from the top of the bulk material, advantaging the strong attraction forces of the tape. So, the combination of the strong attraction and the shear creates a diagonal force[21,23] that allows the exfoliation of thinner pieces of materials directly to the substrate by breaking the inter-crystal van der Waals interactions.

The selection of an appropriate substrate surface, is dealing with the contrast and the optical accuracy under the microscope. Commonly it is used the usual silicon bulk piece with a surface of its own oxide, like Si/SiO_2. Silicon oxide can accept the pieces of the exfoliated material, as long as, has its own also van der

Waals attraction forces that contribute the opposite force of the yield tape. The oxide surface has more optical reason. The oxide layer can have acceptable contrast with the pieces of studied material and that advance the optical resolution under an electronic microscope. In the real thing, the user actually observes a difference of color between the substrate and the deposed material. Silicon oxide has the characteristic pink color, while most of times the material is showed as white.

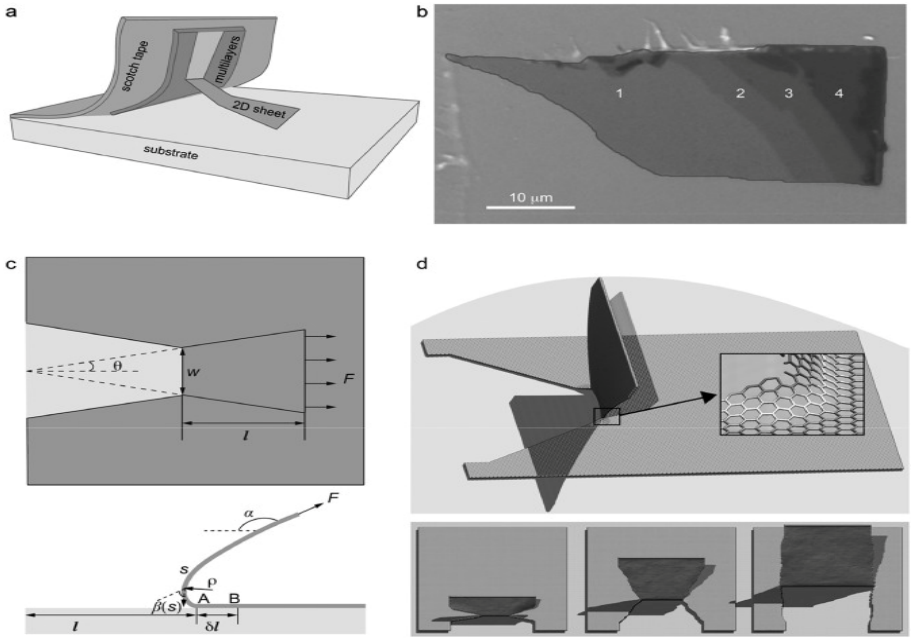

Figure 2.17. Schematic presentation of mechanical exfoliation of 2D layers[26].

The following figure (2.17) presents the exfoliation process on the graphene by graphite bulk material. In most of cases the single layer products are really difficult to be spotted even under an 100x objective lens of an electronic microscope.

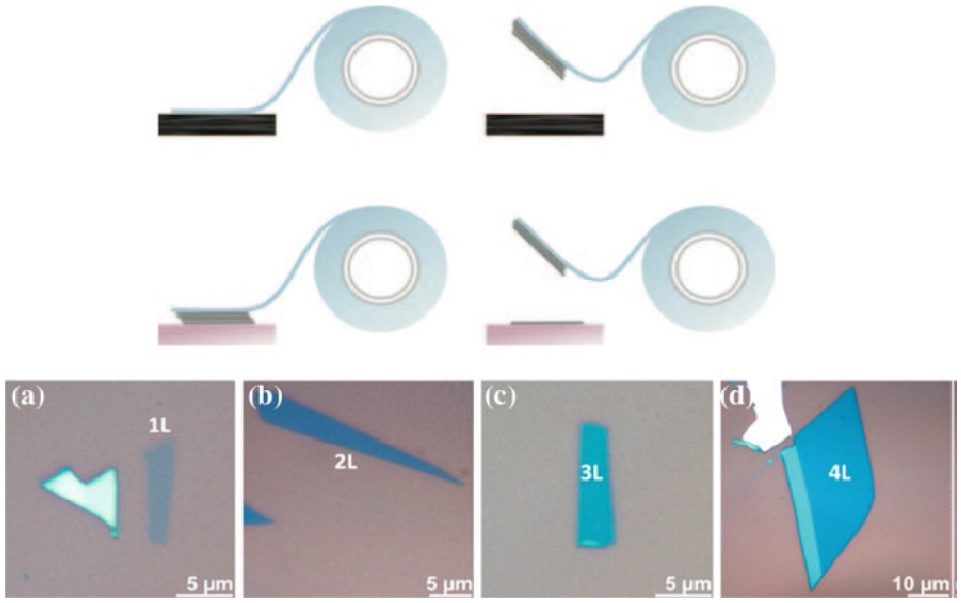

Figure.2.18.Scotch tape exfoliation process on various peeled off layers [40].

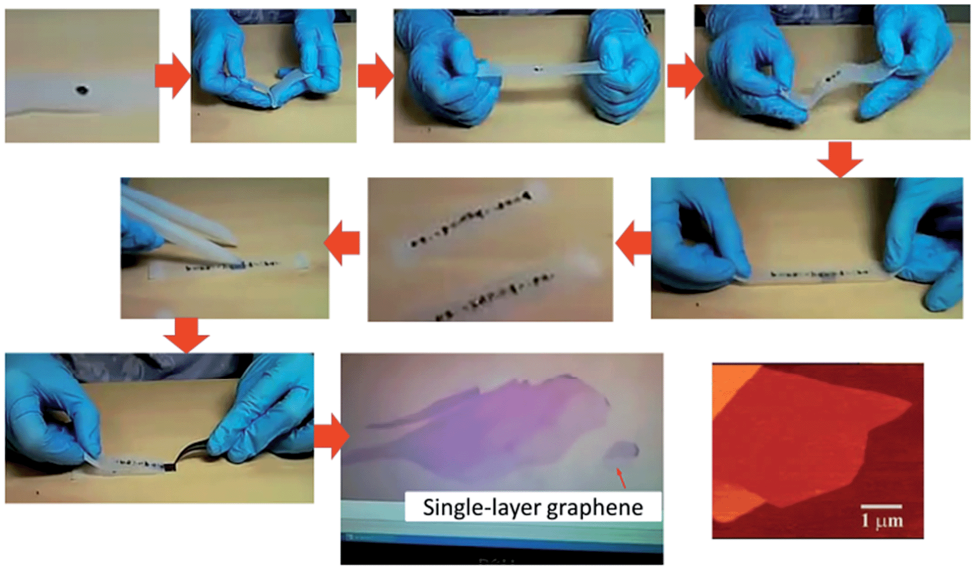

Figure. 2.19. Mechanical isolation of Graphene monolayer flake[21].

2.5.1 Mechanical Exfoliation with PDMS

Polydimethylsiloxane (PDMS) is a well known polymer that in modern uses has the role of a transport medium for the mechanical exfoliation process. While the common try is hard to achieve the isolation of a 2D structure, PDMS has been introduced recently in the process of exfoliation to more and bigger thin structures.

PDMS $(C_2H_6OSi)_n$ is originated by a group of organosilicon compounds that called silicones. It is constructed by the polymerization of repeating building units $[SiO(CH_3)_2]$, following the next chemical reaction (2.13):

$$\boldsymbol{nSi(CH_3)_2Cl_2 + (n+1)H_2O \rightarrow HO[-Si(CH_3)_2O-]_nH + 2nHCl} \quad \textbf{(2.13)}$$

Hydrolysis of the $Si(CH_3)_2Cl_2$ creates the polymer chain that terminated at last with the silanol groups. The polymerization process is developed by cross-linking bonds of the silanol groups with the next chloride group, between the chain and the next building unit. The ability of cross linking eventually can terminate the polymerization progress in the phase where the final polymer has the form of linked network. This polymer is called elastomer. The elastomer form is a gel-like phenotype material and is recognized by various levels of viscosity and elastic modulus. The mechanical properties are resulted by the polymerization process and the type of structure.

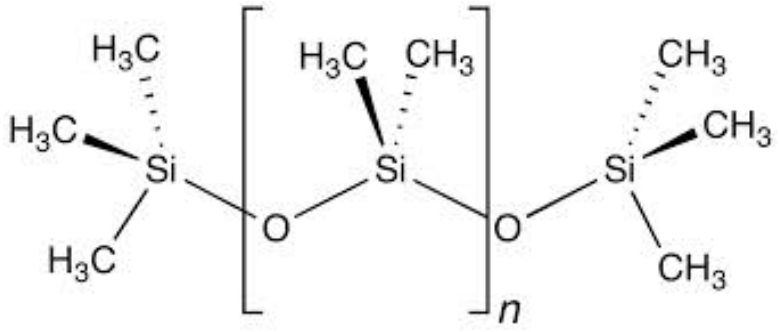

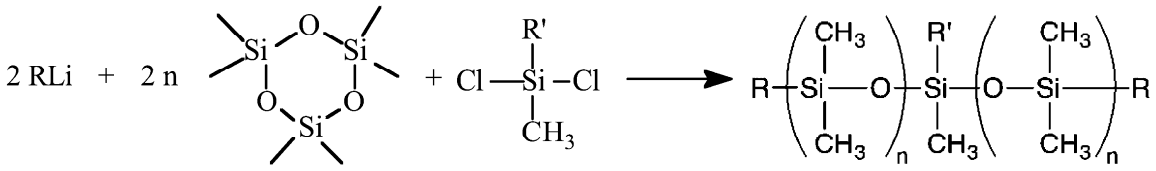

Figure.2.20.PDMS stereochemical formation and synthesis[22].

The bond of silicon oxygen is covalent and strong enough to hold the main chain steady. In the case of elastomer network, the creation of crosses between the siloxane polymer chains, via the Si-O cross linking bonds, tend to make the compound harder to strains and give an amorphous structure[22,24]. The cross-linked bonds are depended by the amount of the crosslinker and the polymerization's components. Typically the cross linker is usually a Si-O individual bond that most of times is bounded vertically between two polymer pieces. The rate of the amorphism throughout the structure expands within the continuous cross linked bonds that are created during the polymerization process. The final form of a common PDMS is a white-grey gel like elastomer.

PDMS have been proof useful enough in the mechanical exfoliation process. The unique structure it has as a siloxane gives the appropriate growth rate of van der Waals interactions with another medium like pieces of bulk material. The main reason of the use, is to keep the PDMS as a transmit medium, for the extraction of bigger pieces of materials on the substrate and a higher percentage risk to exfoliate a monolayer. The process is very common with the original one, including the PDMS contribution throughout the steps. When the scotch tape rips thinner pieces from the bulk form, the next step is to try to exfoliate even thinner pieces to the PDMS substance with the same method as before. Like the tape, thus the PDMS share similar van der Waals interactions but not with the same rate. Thus the attached PDMS-material with the silicon oxide, can store more pieces of the material over the substrate[27]. The extraction of PDMS becomes slowly and steady so the interactions can work properly and print hopefully a 2D structure on the substrate. The following steps for the mechanical exfoliation using the PDMS polymer extraction method[27] as the next figure presents:

a) Using the common tape, cut the bulk material to thinner pieces on the tape as the original method.

b) Transfer the material to the PDMS stamp (first exfoliation).

c) Second transfer from the PDMS to the selected substrate (second exfoliation) to the print of the final material piece.

d) Peeling of the PDMS slowly for the deposition of material to the substrate.

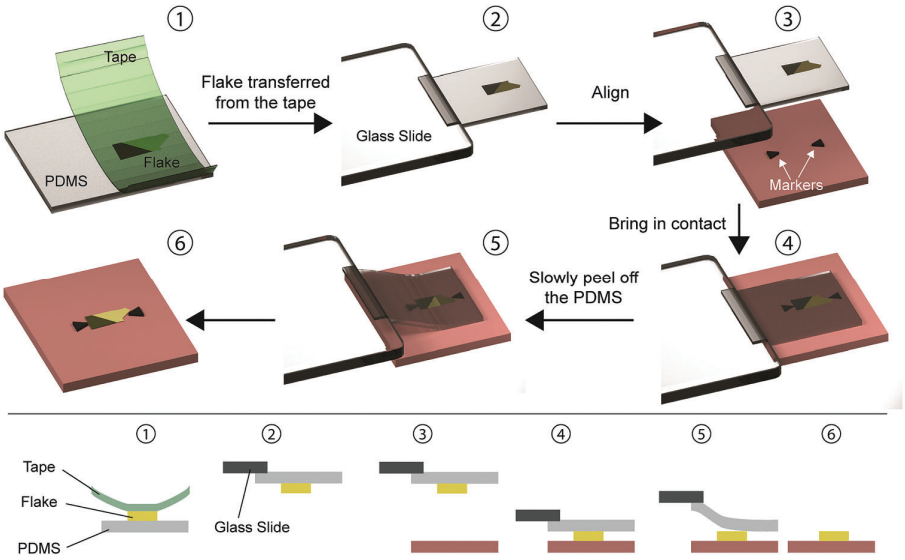

Figure 2.21.Dry transfer of 2D flake via PDMS exfoliation method[27].

III. Experimental Results

3. Experimental Set up and Results

3.1 Isolation and preparation of the studied sample

A single TMD monolayer isolation or synthesis considers one of the fundamentals basic experiments in the 2D materials study. Two dimensional TMDs can by synthesized by various experimental techniques mostly separated in two approaches. One, the top-down approach, where 2D pieces are successfully isolated from a bulk crystal and another one, the bottom-up approach like the chemical vapor deposition (CVD) or the epitaxial growth, in which 2D pieces are grown via chemical process.

In this thesis 2D pieces of samples are isolated successfully with the mechanical exfoliation process. The bulk crystal is pure WSe_2 TMD material. Commonly tiny pieces of the crystal are placed in the sticky side of an adhesive scotch tape and placed above a capable substrate. While the tape has stacked well in the substrate then it is performed a mechanical shear force, pulling the tape away. The bulk crystal then is peeled off by repeatedly stick and pull the tape to the substrate. In this way eventually small flakes of material are deposited to the substrate. The used substrate is a small plate of a silicon/silicon-oxide (Si/SiO_2) wafer. The tape with the peeled material is stacked in the oxide-area of the wafer, where van der Waals forces are dominating and can attract small pieces of the deposited material. Additional the oxide surface provides better contrast with the deposited material under microscope's light. As it is described before, a PDMS polymer piece can also used as a transition material, just like the adhesive scotch tape. It provides also van der Waals forces just like the silicon wafer but it is not so sticky like the tape. So that makes the process of exfoliation easier than the common tape.

In this thesis are successfully isolated WSe_2 monolayers with the mechanical exfoliation technique using as transferring-peeling material, a piece of PDMS polymer. The samples are used for Raman, polarized PL and reflectivity measurements for their characterization. Typically, the monolayer size ranges

from μm to tens of μm. The studied sample is shown in the following figure 3.1. The substrate was indeed the common silicon oxide wafer. The final series of experiments are performed on the same sample.

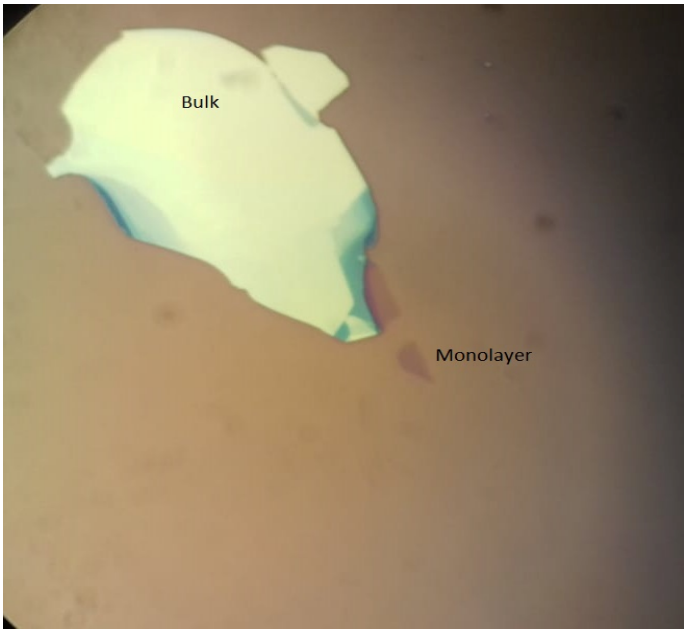

Figure 3.1. WSe_2 monolayer and bulk pieces under microscope.

3.2 Raman Spectroscopy on WSe_2 monolayer

A typical Raman set up is divided on three distinct components. One light source, in modern cases is a laser output. Second it is needed a spectrometer for the analysis and study of the collected emitted radiation from the sample. Third, a focus lens apparatus it is required to control and direct the excitation light beam, by angle and focus distance. Most experimental set ups, nowadays, on Raman are usually packed in a lab-instrument, where each company-provider of laboratory equipment can produce. Most Raman devices are providing an analyzing system of a coupled spectrometer and an optical system of microscopic lens. Thus, the microscope can be focused on a 1-10 μm spot, where the final beam target is set. External optical materials are included in each Raman spectroscopic set up to aid the optical resolution and the light separation via the experimental process.

Typically, in a Raman set the laser beam is first passing through a beam splitter. The beam splitter is performing a light separation in an orthogonal angle between them. So eventually two different beams are formed in the optical path. The one is steady, focused on the objective-microscope lens, while the second one it faces the optical path up front the spectrometer. In front of the lens, it stands a platform stage, which it can be moved by every possible dimensional shift (x,y,z axes) and it is used as a standing seat for the studied sample. The scattered radiation is emitted towards the beam splitter and is also separated by the same angle rate, as before. An optical filter usually is placed after the beam splitter in order to block the Rayleigh scattering which is equal with the laser output. The blocking is essential to avoid the overlapping with the Raman scattering and to protect also the photo-detector by the laser power. The optical filter is also determined, according to the required wavelength's region, which needs to be blocked. If Stokes scattering is to be measured in the process, then it is used a long or short pass filter, depending on the Stokes shift, close to the laser wavelength. After the specific filter, instrumental set up, usually include a pin hole with a specific aperture, on about some μm. This pin hole rejects the incoming signal that is not in the focal plane. The incoming radiation is arranged through the hole to give the best objective resolution by focus distance. Thus, the background noise-signal is mostly reduced within the aperture. The focus distance is tuned by the objective lens, of each microscopic system it is used at processing. Eventually the incoming Raman scattering is inserted in a spectrometer, where it is modified

by a diffraction grating and ends to a CCD camera. The CCD camera can convert inductively the incoming photons into voltage output and creates a digital signal to its processor and project them as data points. Thus, the final spectrum is printed to screen via the software program that is connected to the instrument.

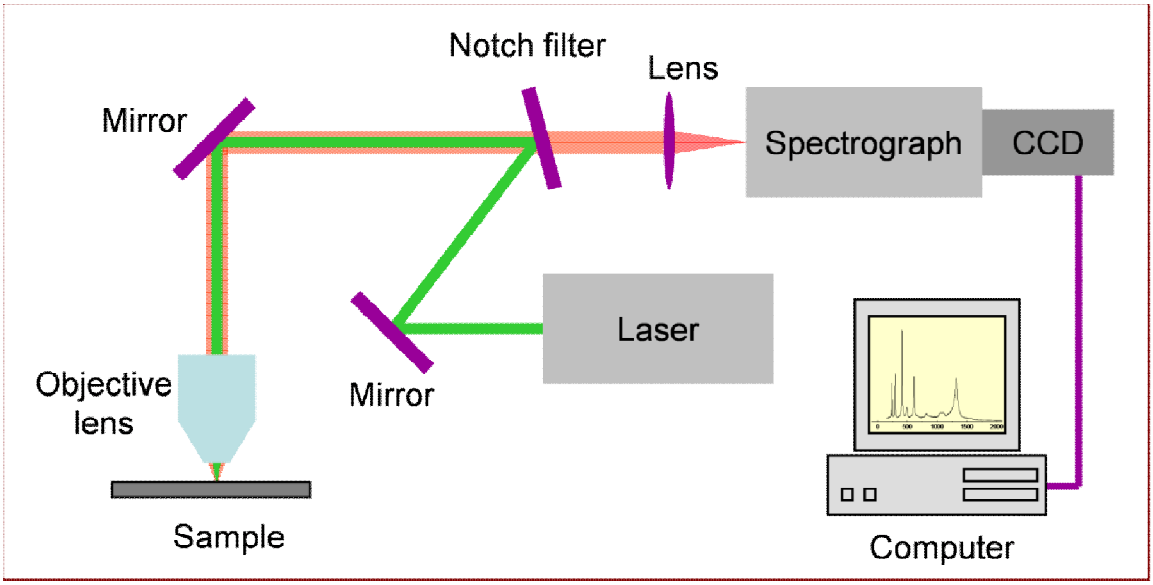

Figure 3.2. Raman experimental set up.

During this thesis, the experiments are performed, using the Raman instrument, Nicolet Almega XR, by ThermoFisher[81].This instrument provides also a micro-Raman capability in scale of nanometers. Also contains a choice of several laser lines. Most models provide two specific laser excitation lines of 780 nm (red), and a 473 nm (green) by diode pumped solid state laser (DPSS) with maximum power 50 mW. A high resolution grating of 2400 grooves/mm is used and the con-focal aperture of the pin hole is at 100 μm. The microscopic lenses are presenting available optical resolution from 10x to 100x size of the placed objectives. It is connected with its written software via its digital circuit and can be operated directly within the computer's available software interface compiler. The stage seat is motorized and the movement is controlled by the user directly, in the 3D space. The final spectrum is printed in digital form in the computer's screen after the processing, where it can be modified.

Figure 3.3.Raman Spectroscopic Instrument of ThermoFisher, Nicolet Almega XR [81-83].

The following measurements present Raman spectra for different thicknesses of an exfoliated WSe_2 crystalline sample on silicon wafer. In this thesis we only focus on the Stokes lines since the anti-Stokes are extremely weak. In this thesis are taken five different measurements of Raman in the same area of the silicon wafer which contains different thicknesses of exfoliated WSe_2 pieces ass it is shown in the figure (3.7).The excitation source that is was used, is the 473 nm laser line (blue) that is provided by the Raman instrument. The sample's exposure time was 3 seconds in 2 different accumulations.

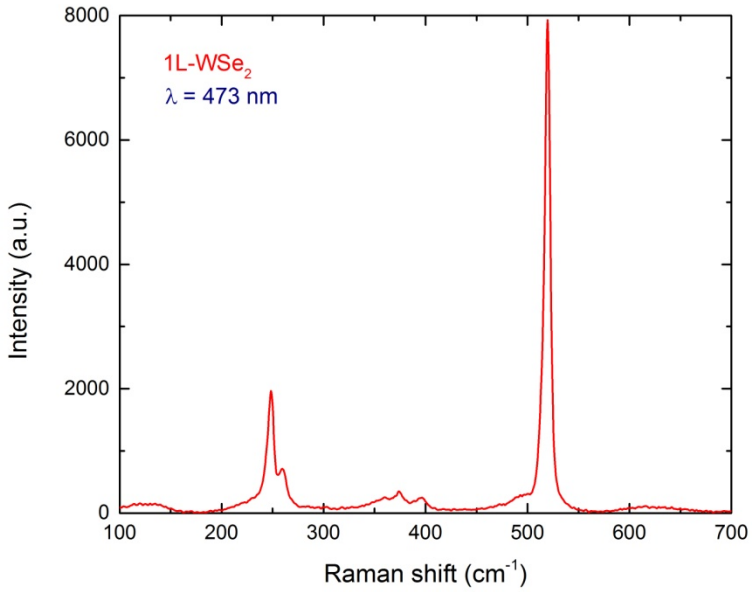

Figure 3.4. Raman Spectrum of 1L WSe_2.

According to the figure 3.4, we see two intensive peaks in the given frequency range. The first, in nearly 250 cm^{-1}, corresponds to the vibrational mode of the WSe_2. The second, highest peak at 520 cm^{-1}, corresponds to the first order optical phonon of the silicon substrate. The high intensity of silicon and the much lower of WSe_2, is evident that the measured TMD sample is dimensionally small, maybe a monolayer. Generally, the intensity of TMD's mode in Raman lowers with the dimensional reduction. Thus, the silicon peak has much higher intensity than the monolayer's peaks. In pretty low thicknesses, a major portion of the incident light passes through the sample and reaches the substrate. This condition initiates the vibrational mode of the substrate. This interaction usually creates additional peaks in the spectrum with intensity proportional to the sample's thickness. Eventually, as the thickness of the sample increases, the transmitted light decreases and thus reducing the substrate's Raman intensity. This case in presented in the bulk WSe_2(> 10 nm in thickness) Raman spectrum (Fig.3.6), where the coupled in and out of plane modes E_{2g}^1+ A_{1g} gain intensity in favor of silicon's vibration at 520 cm^{-1}. The silicon substrate also crates additional second order modes which if they are not high in frequency sector of the spectrum, will be suppressed even from the monolayer's signal.

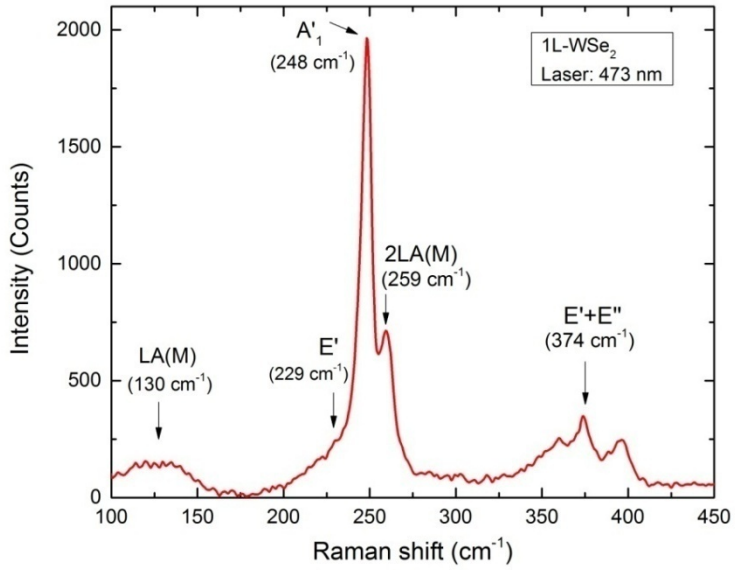

Figure 3.5. Raman Spectrum of 1L- WSe_2 with 473 nm laser.

As it is shown in the spectrum (figure 3.5), are presented multiple peaks of vibrations in various wavenumbers. The highest peak is at 250 cm^{-1}, which is the most intensive vibrational mode, the A'_1. The A'_1 mode is an out of plane mode that occurred in selenium Γpoint vibrations equation. The intensity of this peak is high enough, as the stretching is performed through the symmetric motion of the two selenium atoms round the centric atom of tungsten, in the triplet. The tungsten atoms are heavy enough to stay rested mostly in a range, while the selenium atoms are lighter enough to be stretched easily, in symmetric range around the tungsten atom.

Next to high peak of A'_1 mode is a lower intensity peak at 259 cm^{-1}. This mode, represents the longitudinal acoustic phonons, 2LA(M) at the M-point of the Brillouin zone, These two modes are expected from the phonon dispersion of WSe_2 monolayer, (figure 1.8). The LA(M) mode at 130 cm^{-1} point has also been observed. Thus, eventually with this correlation between the LA(M) and 2LA(M) confirms the identification of the two peaks at each wavenumber point respectively. The frequency difference of 11 cm^{-1} between the two main phonon modes A'_1 and 2LA(M), confirms also that the excited sample is a monolayer. At last there are also two more Raman active modes in the spectrum, the in-plane vibrational

modes E' and (E'+E''). The first E' appears in frequency of 229 cm^{-1} and is close enough in the out-of plane mode A'_1. The second in-plane mode is a summary of both E' and E'' round the M point of Brillouin zone, where the required frequency is higher according to the phonon dispersion of 1L and appears at 374 cm^{-1}.

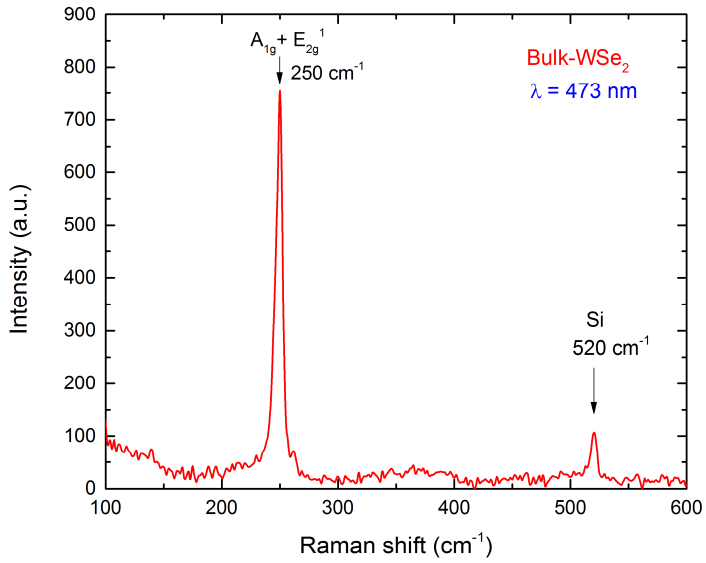

Figure 3.6. Raman of bulk WSe_2 sample.

The correlation between WSe_2 and silicon's modes is almost inversely proportional. The Si peak at the bulk WSe2 sample is much weaker than the corresponding one form the monolayer. For that reason, we have taken the spectra from several points of the sample and map the thickness at each point (Fig. 3.1).The spots are shown in the following figure 3.7. The thickness differences are visible by the color difference within the contrast under the microscope's light. The monolayer that confirmed by Raman is presented as number 1. The monolayer is barely visible under the microscope having a light purple color while other pieces can have another color hue, scattering back a wide range of light from purple color to almost white. This color difference between the different spots is a characteristic of also different dimensional size of pieces of the sample.

After five Raman measurements, with the same experimental conditions as before, it is plotted by stacking them in a single normalized spectrum (Fig. 3.7). The spectra are normalized. From this plot, it is

clearly visible the correlation between the sample's thickness and its Raman intensity. As the thickness increases the intensity increases as well (more material to scatter more photons), than the monolayer. Furthermore, the produced Raman signal of silicon wafer follows the opposite behavior, i.e the silicon Raman signal is reduced drastically as the thickness of the sample increases.

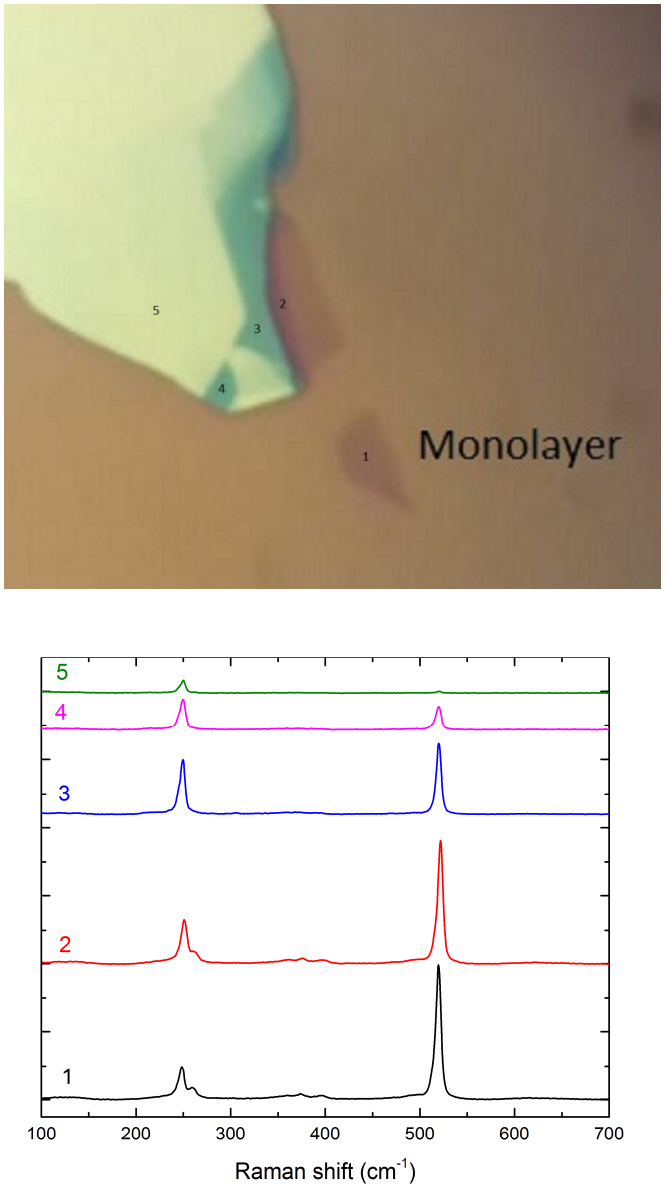

Figure 3.7. Different measurement spots of Raman on sample (up) and Raman stack spectrum in different measurements (down).

3.3 Differential Reflectance on WSe_2 monolayer

The differential reflectance method (DR) measures the difference between the two spectra of reflectance, the sample's and the silicon wafer. The sample is the deposited WSe_2 monolayer on the silicon oxide wafer. This experiment tends to confirm the exciton states and the energy band gap of the studied sample. Thus the DR method constitutes one the fundamentals and useful experiments on the opto-electronic characterization of 2D materials.

The experimental set up is similar to PL set up. This time the excitation medium is a white-light lamp. The optical path matches also with the PL path, as it is shown in the figure 3.11. The white light radiates the studied sample and the reflected light ends up in the CCD camera that prints the spectrum in computer's screen. The sample is placed inside the cryostat, which cools down and evacuates its interior from various gases like oxygen, (< 0.2 Pa) with liquid nitrogen. The nitrogen inserts in the cryostat and dropped out as gas after the cool down. The differential reflectance spectrum is resulting, using the DR formula (2.14).

During this thesis it was characterized the WSe_2 monolayer via temperature dependence differential reflectance experiment. The sample was placed into the cryostat until was cooled down to 78K. The experiment took place with the first DR measurement at this temperature. Then the process continued on higher states of temperature until the sample reaches 300K. More specific are taken six different measurements in six different temperatures respectively, in 78K, 100K, 150K, 200K, 300K.The exposure time of the sample was 3 seconds with two different accumulations.

Differential reflectance (DR) produced by the mathematical difference of the two spectra of reflectance. The DR spectrum projects the excitonic states of the studied sample. In this case the targeted sample is the known WSe_2 monolayer. The presence of the excitonic states is evident in the DR spectrum. The first excited state is the A exciton, which presents the optical gap for this excitonic state. A exciton manifested by a sharp peak at nearly 1.74 eV at 78K (Fig.8) with a very small curve next to it, nearly at 1.71 eV, which confirms the first trion state. The B exciton state rests at 2.17 eV at the same temperature. The energy

gap between the A and B exciton is 430 eV, which is matched with the theoretically WSe_2spin orbit interaction. The energy difference between the A and B exciton states constitutes a measure of the effective splitting that contains the energy splitting that occurred both of conduction and valence band. In the W based TMDs the ground state A transition to exciton is described as energy equal to $E_{opt} + \Delta_{scCB}$ and the B ground state to exciton transition, $E_{opt} + \Delta_{scVB}$. Thus the energy gap between A and B, actually presents the energy gap $\Delta_{scVB} - \Delta_{scCB}$.

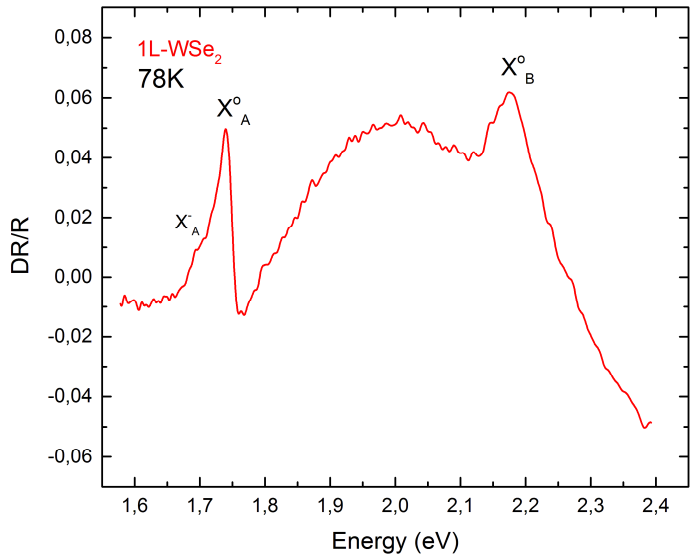

Figure 3.8. Differential Reflectance spectrum of WSe_2 monolayer at 78K.

In the case of 300K the exciton states shift energies. The presented energy is lower than the 78K and the difference in reflectance is lower, due to the domination of thermo interactions that take place in the sample and in the substrate. The thermo-interactions are a result of the increasing numbers of phonons that starting to arise as the temperature increases from 78K to higher states like the 300K. The A exciton arise in lower energy (Fig. 3.9), specifically on 1.66 eV and the B exciton on 2.08 eV. This behavior is pretty ordinary to semiconductors and resulted by two major contributions. The most important is the increasing of the phonon population in the monolayer that concludes to an increased exciton-phonon interaction [85].

The exciton interacts with multiple phonons, while it moves inside the lattice, via scattering. There two types of phonon scattering. The one is phonon absorption and the other is the phonon emission [86,87]. The phonon absorption is dominant on low temperatures where the most phonons are not active yet. The renormalization process becomes temperature independent. However in higher temperatures, especially those ones in order of Debye distribution the phonons scattering is presented by both ways, absorption and emission, with the dominant contribution to be via emission due to the high population of phonons it can emitted while the lattice is hot enough. Thus the increasing exciton-phonon interaction causes the exaction states to shift their energy state lower, in higher temperatures, like the 300K.The second contribution is the change of the average distance between the atoms of the lattice within the thermal expansion. The inter-atomic distances are increasing as the atoms gain energy in higher temperatures and shrinking the relative positions of conduction and valence band respectively. However this effect is not so strong and affects a very small range of the observed shifts sometimes is not taken into account so seriously.

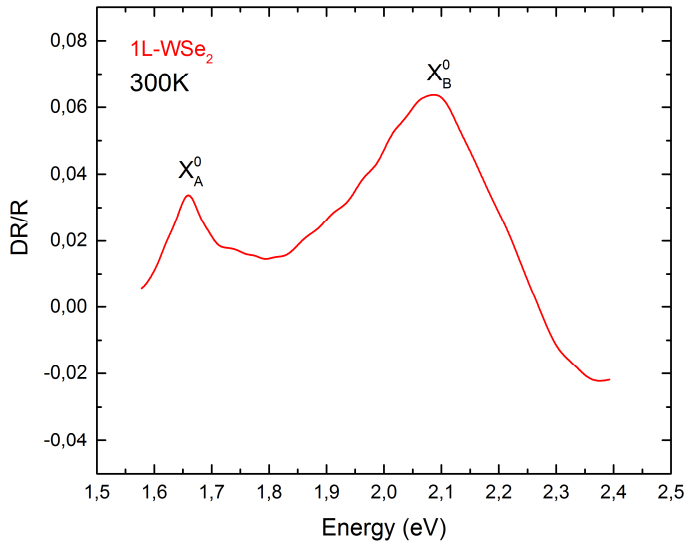

Figure 3.9. DR spectrum of WSe_2 monolayer at 300K.

More details about the temperature dependence of monolayer's DR, are given by the full spectrum of every measurement at each temperature. The five measurements have all the same experimental aspects and light power so the spectrum can be as accurate as it can. Temperature dependent reflectivity measurements prove further the progressive energy shift, at lower energy states, of A and B excitons. The energy gap between them stays the same at any temperature. Both of the excitons can arise at room temperature (300K), but the trion is no longer emitted after the 150K (Fig 3.10). The increase of temperature is the major reason on the excitons energy shifts, while taking into account the two contributed mechanisms of semiconductors, under thermal expansion, that were explained before.

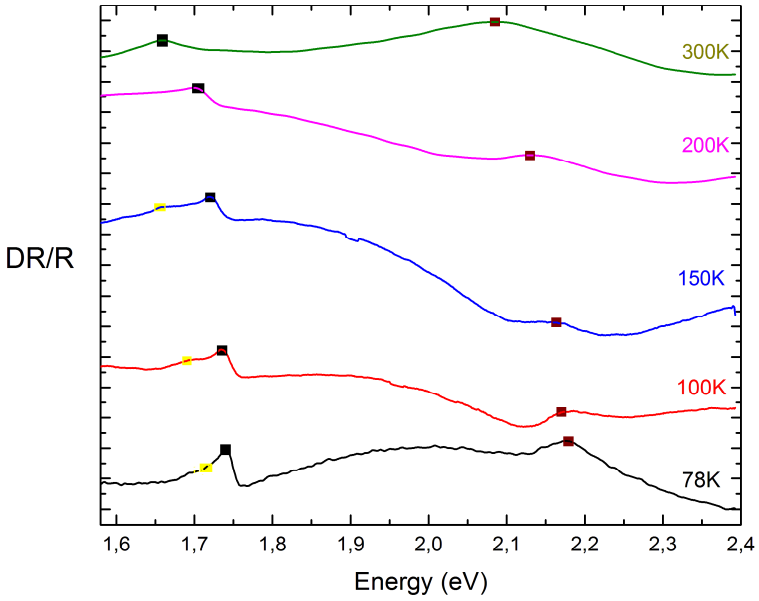

Figure 3.10. Spectrum of temperature dependent DR, of WSe_2 monolayer. Black dots show the A exciton, while the brown dots show the B exciton. Trion emission is shown with yellow spots until the 150K.

3.4 Spin Valley Polarization PL on WSe_2 monolayer

In the Spin Valley Polarization measurements, we use the same sample of WSe_2 monolayer, as we have used in the Raman before. The experiment took place in a custom developed set up in the ULMNP lab at IESL-FORTH. The spin valley polarization process is similar to the common PL process as it was noticed before, using circular polarized light instead of linear. The specific set up uses a laser output as the light source, a spectrometer and a CCD camera, considering them the most important specs of the set up itself. The optical path is built by the usual way, consisted of a full pack of mirrors and a beam splitter as well as optical filters, such a long-short pass filter or a neutral density filter. An objective lens gives the focal plane-spot, where the light beam, will eventually meet the steady sample. The sample is mounted in a tunable stage that it is allowed to move in 3D space.

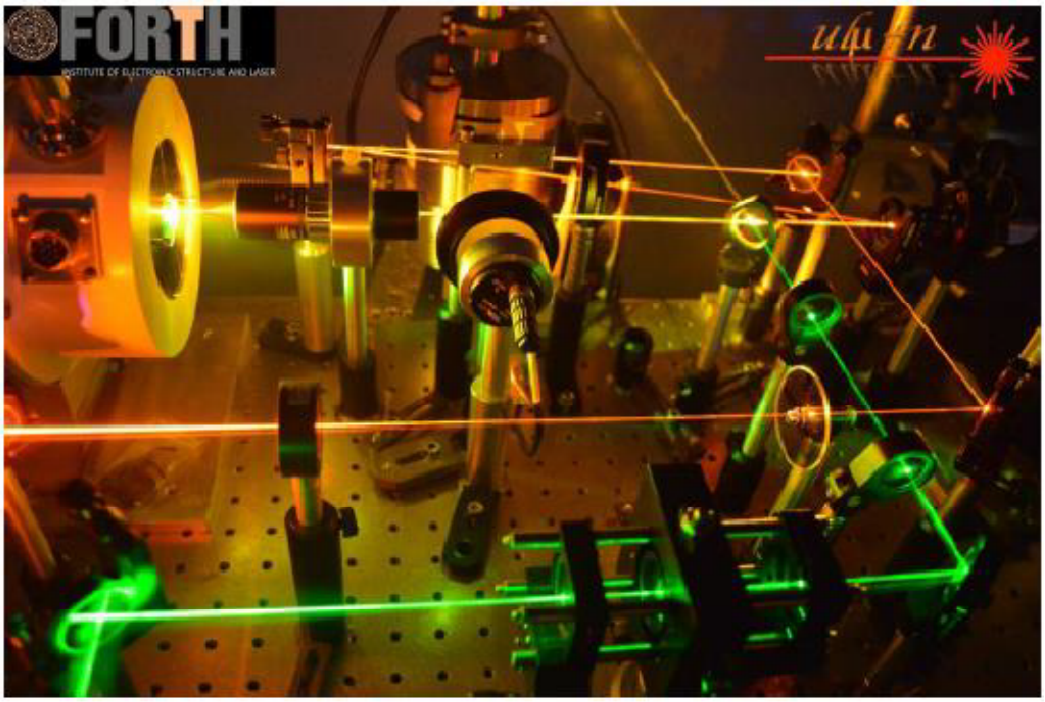

Figure 3.11. Photoluminescence Spectroscopy set up in ULMNP Lab at IELS-FORTH.

The used spectrometer is an iHR-320 (Horiba Scientific/Jobin Yvon Technology) [84]. It is automated with a 320 mm focal length and f/4.1 aperture. It can operate two different gratings on the turret. One 300g/mm and another one 1200g/mm. It has a wavelength accuracy of 0.20nm long and a scan speed160 nm/sec. The grating step is tuned on 0.002 nm and the resolution is set to 0.06 nm. The spectral dispersion is automated to 2.35nm/mm.

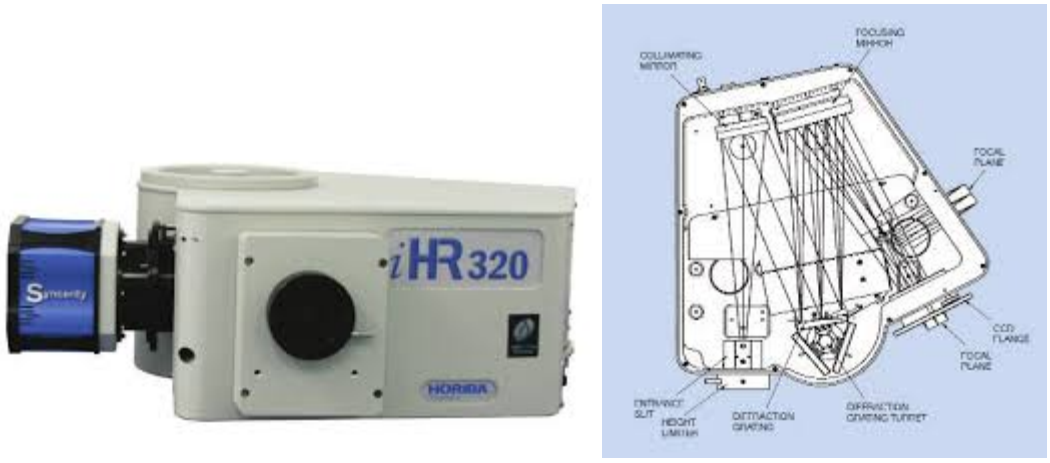

Figure 3.12. ihr320 spectrometer (left), interior design (right) [84].

The sample is mounted on a continuous flow cryostat which cools down the sample in various temperature and provides vacuum in its interior (< 0.2 Pa). A continuous-wave He-Ne laser of 632 nm (red) is used as excitation source. The beam first passes through a spatial filter and obtain the central part of its Gaussian beam. A short pass filter is placed to block radiation beneath the wavelength of the laser (< 632 nm). The power of the laser output is controlled by using a neutral density filter. The laser radiation passes also through a 50/50 beam splitter which separates in half the radiation in two different optical directions. One half is targeted to the sample and the other half is headed into a long pass filter. The long pass filter is used for blocking the unwanted radiation and allows the lower energy states of radiation to pass. The laser's radiation eventually is blocked there. The laser radiation, on the sample, is focused using a 50x long objective lens with a numerical aperture 0.42. The light spot has a 1.5μm diameter. The emitted PL is collected with the reverse scattering (back-scattering geometry) by the same microscope objective

and is headed into the entrance split of the spectrometer with 0.32 m focal plane. Before it enters the spectrometer, it passes through a ~λ/4liquid crystal, which changes the polarization of PL from linear to circular. The polarizer is tuned to give left or right circular polarization respectively, at will. After the diffraction grading analysis by the spectrometer the PL is projected in the CCD camera detector. The CCD camera converts the imported light into electrical current and prints the PL spectrum in the computer screen.

The Photoluminescence experiment takes place in different temperature, starting from 78K, until reaching room temperature. Spectra were collected at 78K, 100K, 150K, 200K, 250K and 300K. The sample was exposed to the laser light for 3 seconds. Two sets of measurements were taken for better statistics and the average polarization was recorded. The subtraction of the background noise is needed in order to take the true measurement of polarization. This background comes from the operation of CCD camera, which is tuned to give some additional counts of measurement by default.

The spin valley polarization strongly depends on the temperature. In this thesis only the A exciton is taken into account. The 632 nm laser that is used is not really close to resonance as since it has an energy of 1.96 eV, while the A exciton at room temperature is nearly at 1.66 eV. It is expected like the common PL of WSe_2 monolayer, an energy shift while the temperature decreases. The reverse behavior is also observed. Eventually a temperature dependent SVP is shown clearly the correlation between polarized exciton emission and thermal heating. At 78K, the energy of the A-exciton is at 1.74eV and it is co-polarized with the incident laser beam (right polarization much higher than the left one – Fig. 3.13).Two sets of polarization measurements were taken and the values that were measured were 17.6% and 16.7%. Thus, the average polarization is nearly **$P(X^0) = 17\%$**. The difference between the two measurements is of the order of 1%.The trion (X^-) peak is also visible next to the A exciton nearly at 1.71 eV, which is characteristic at low temperatures, due to the absence of thermal effects. The energy difference of 30meV from the neutral exciton, implies a trion binding energy of 30meV.

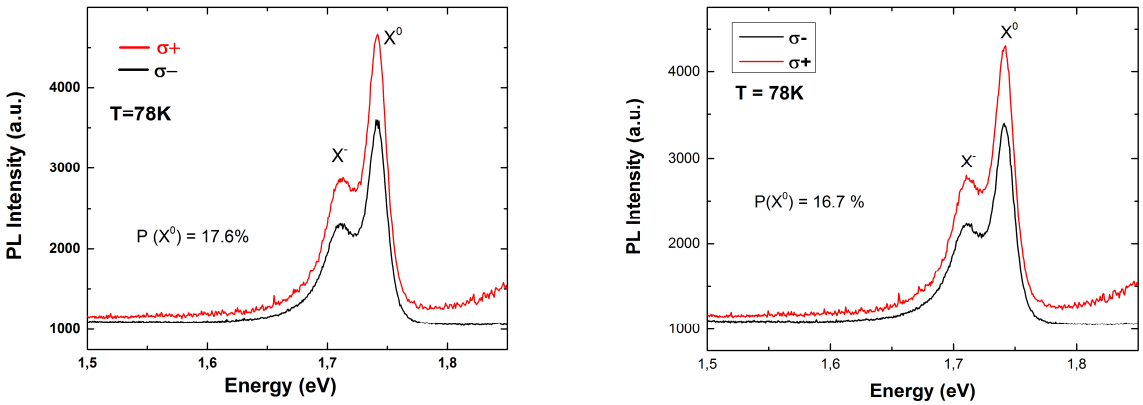

Figure. 3.13. Spin Valley Polarization PL on WSe_2 monolayer at 78K.

Right polarization σ+and left polarization σ-.

In higher temperatures, it is expected a decrease in the emitted circular polarization due to the phonon generation that leads to exciton phonon intervalley scattering mechanisms [86]. This intervalley scattering results in a reduction of the imbalanced carrier populations between the two inequivalent K-valleys. The polarization at 100K falls to $P(X^0)$ = 9.8% (9.5% in the first set of measurements and 10.2% in the second one). The A neutral exciton shifts at 1.73 eV with the trion at 1.70 eV. The difference in polarization between the two sets of measurements at 100K was 0.7%, lower than the 1% measured at 78K, evidence that the measurement was accurate.

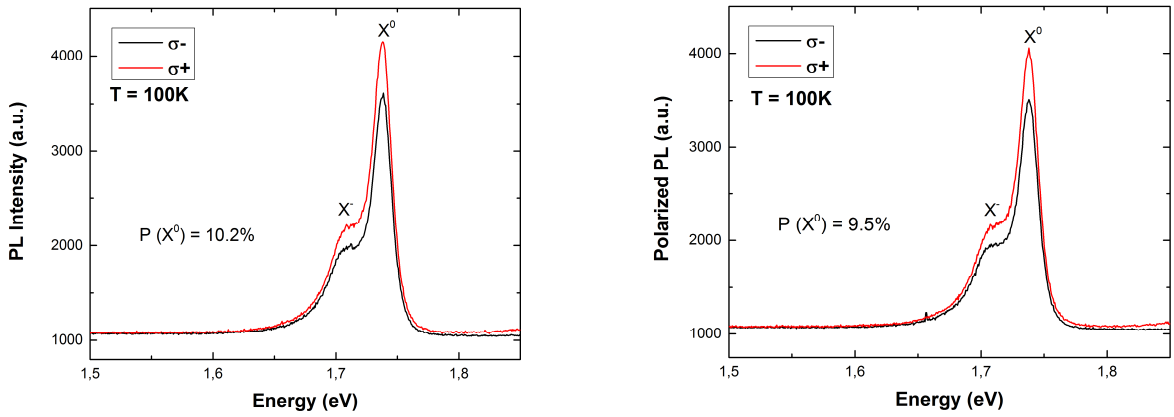

Figure 3.14. Spin Valley Polarization PL on WSe_2 monolayer at 100K.

Right polarization σ+ and left polarization σ-.

Above 100K the A-exciton shifts even more in lower energy. Specifically, as the sample warms up to 150K the neutral exciton is at 1.72 eV, while the trion at 1.69 eV. The circular polarization at this temperature is $P(X^0)$=3.8% (3.5% and 4.1% for the two sets of measurements). The trion is much weaker in 150K than the last two temperatures. This is expected since the thermal dissociation starts to play a key role above 150K. The measurements are considered accurate as the percentage gap between them is 1.4%.

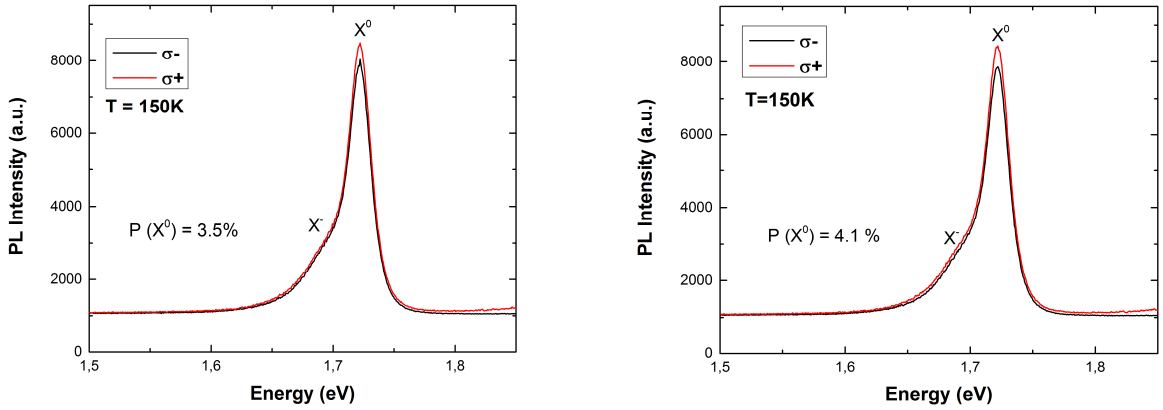

Figure 3.15. Spin Valley Polarization PL on WSe_2 at 150K.

Right polarization σ+ and left polarization σ-.

The neutral exciton continues to red-shift in energy and at 200K is at 1.70 eV. The circular polarization drops even further at 1.6%. At this temperature, there is no emission from the trion state at all. The same behavior is observed also at 250 K and 300K with polarizations of 1.9% and 0.5% respectively.

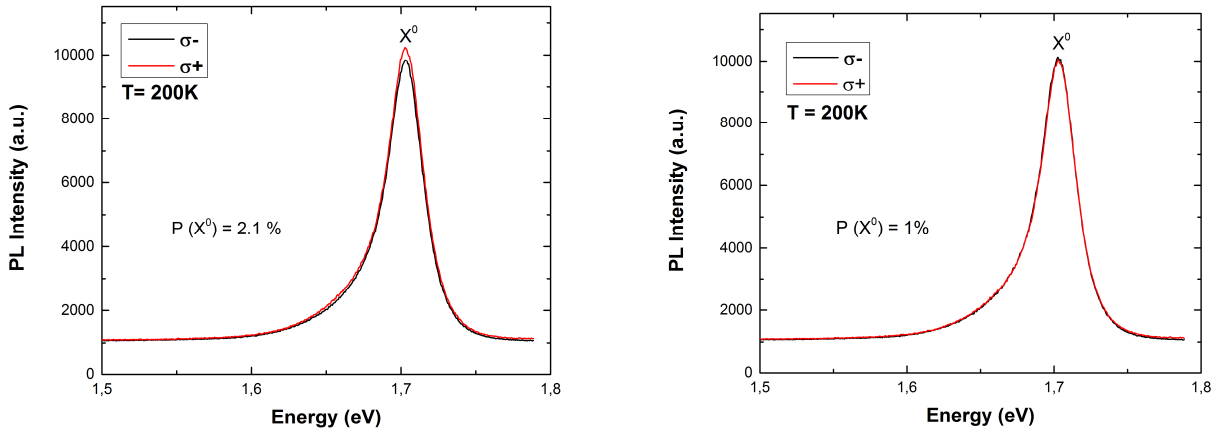

Figure 3.16. Spin Valley Polarization on WSe_2 monolayer at 200K.

Right polarization σ+ and left polarization σ-.

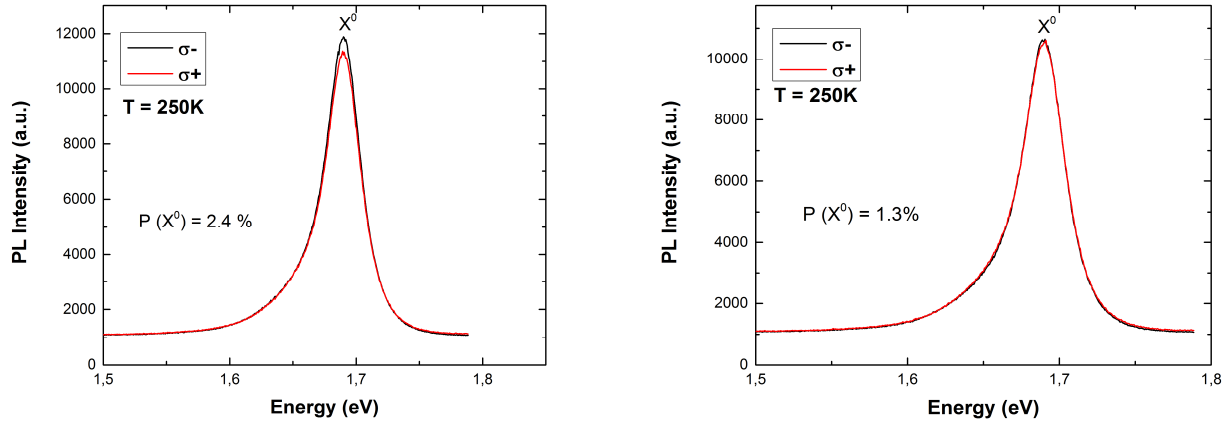

Figure 3.17. Spin Valley Polarization PL on WSe_2 monolayer at 250K.

Right Polarization σ+ and leftpolarization σ-.

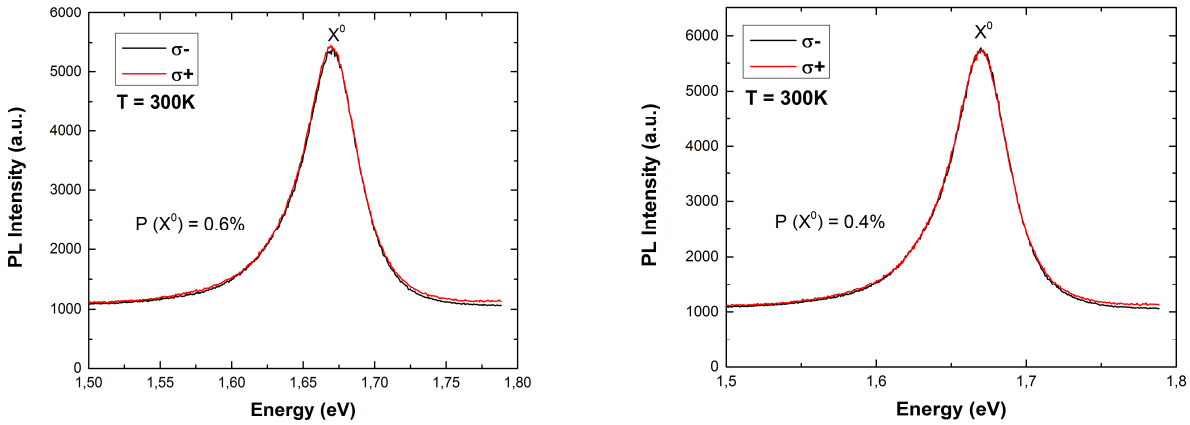

Figure 3.18. Spin Valley Polarization on WSe_2 monolayer at 300K.

Right polarization σ+ and left polarization σ-.

Therefore, the polarized PL is strongly temperature-dependent. In continuous heating the sample presents bigger population of phonons starting with the lowest at 78K, having almost only acoustical phonons. In progress the population arises more phonons from thermal heating that are mostly optical, due to the higher energy state. The highest polarization that was achieved at 78K was 17% and the lowest 0.5% at room temperature. The results are summarized in the following table (Tab. 3.1) were we show the two sets of polarization measurements together with the average value and plotted in Fig.3.19).

Temperature (K)	Polarization 1 (%)	Polarization 2 (%)	$P(X^0)$ (%)
78	17.6	16.7	17
100	10.2	9.5	9.8
150	4.1	3.5	3.8
200	2.1	1.0	1.6
250	2.4	1.3	1.9
300	0.6	0.4	0.5

Table 3.1. Temperature dependent polarization measurements.

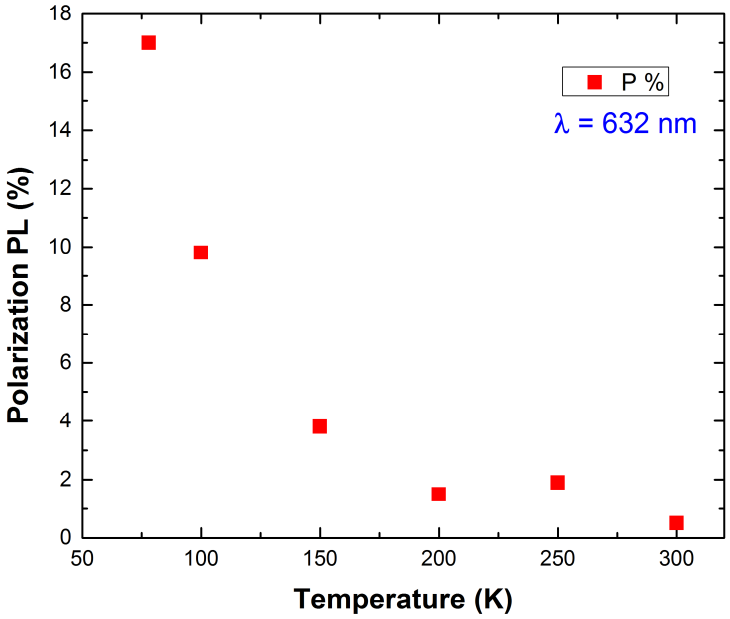

Figure 3.19. Temperature dependent spin valley polarization PL of WSe_2 monolayer.

This T-dependent polarization behavior is explained in the literature using two models. One deals with intervalley scattering through phonons [89] and the other one follows the electron-hole exchange model [90]. The excited WSe_2 with light of particular helicity will only populate a single valley (K or K') and the emitted light should exhibit the same helicity unless there is some intervalley scattering. As the pumping energy increases the intervalley scattering becomes important. Optical phonon assisted intervalley scattering becomes possible only with higher pumping energies. However the scattering cannot by itself account for any decrease of the polarization because emission of the B exciton in the same valley has the same circular polarization. The decrease in polarization requires intervalley scattering. The intervalley scattering channel requires participation of the in plane longitudinal phonons at the K points of the Brillouin zone. These phonons are determined by the phonon dispersion. The induced pumped energy must exceeds the $E_p > E_A + TA(K)$ for the outbreak of the intervalley scattering.

Varshni proposes a semi-empirical relation for the variation of the energy band gap with temperature (Fig. 3.20). Eg(0) is the gab at 0 K temperature, a and b are fitting parameters, which related to electron-

phonon interaction and Debye temperature, respectively. The gap is obviously changing slightly between the 0 and 78K temperatures. The results are quite similar to those of previous studies on WSe_2 [88]. The numerical differences are related to the experimental errors, which occurred within many reasons that can take place in the experimental process. In higher temperatures the parameters are very small compare to the temperature number. Thus the relation of Varshni acquires linear profile.

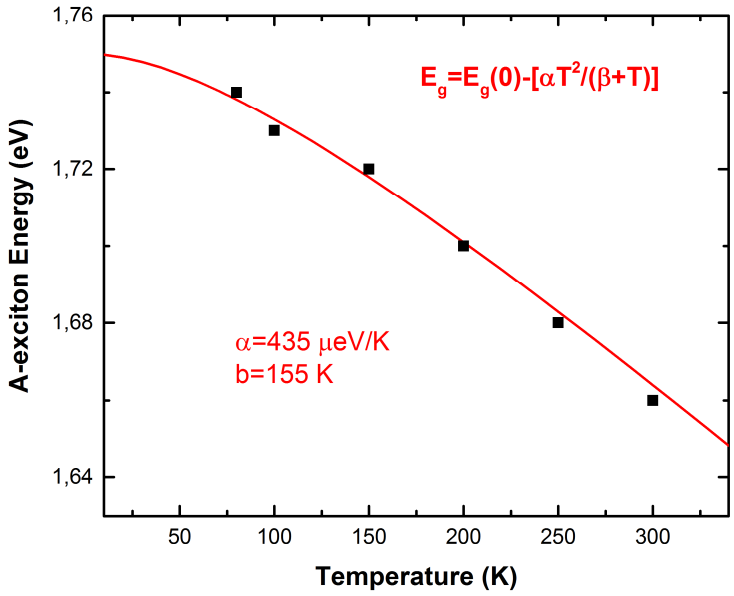

Figure. 3.20. Varshni plotted curve on experimental result about the A exciton.

IV. References

[1]. The rise of Graphene, A. K. GEIM AND K. S. NOVOSELOV, **Nature Materials**, vol 6, March 2007

[2]. Electric field effect in atomically thin carbon films, K. S. Novoselov,A. K. Geim, S. V. Morozov,D. Jiang,Y. Zhang,S. V. Dubonos,I. V. Grigorieva,A. A. Firsov, **Science**, vol 306, October 2004

[3]. Atomically thin MoS_2, Kin Fai Mak, Changgu Lee, James Hone, Jie Shan, and Tony F. Heinz, **Physical Review Letters**, PRL 105, September 2010

[4].Emerging Photoluminescence in monolayer MoS_2, Andrea Splendiani, Liang Sun, Yuanbo Zhang, Tianshu Li, Jonghwan Kim, Chi-Yung Chim, Giulia Galli, Feng Wang, **ACS Nano Lett. 10**, March 2010

[5]. A new type of secondary radiation, C.V. Raman, K.S. Krishnan, **Nature 501**, March 31, 1928

[6].Introductory Raman Spectroscopy, J. R. Ferraro, K. Nakamoto and C. W. Brown, Elsevier, 2003(Second Edition)

[7]. Modern Raman Spectroscopy, Ewen Smith, Geoffrey Dent, John Wiley and Sons Ltd., 2005

[8].Infrared and Raman spectra of inorganic and coordination compounds, Nakamoto, K., Part A (5th ed.) New York: Wiley, (1997)

[9].Physical Chemistry, Atkins, P. W. Paula, J. de, New York: W. H. Freeman. (8th ed.), (2006)

[10].Mechanical Vibration and Damping, Hayek, Sabih I., **Encyclopedia of Applied Physics**, WILEY-VCH Verlag GmbH & Co KGaA, (15 Apr 2003)

[11].Optical Properties of Solids, Mark Fox, OXFORD University Press, 2007

[12].Band-structure calculations for semiconductors within generalized-density-functional theory, I. N. Remediakis and Efthimios Kaxiras, **Physical Review B**, vol. 51, February 1999

[13].Fundamentals of Semiconductors: Physics and Materials Properties, S P. Yu, M. Cardona, pringer,4th edition, 2010

[14]. Principles of Electronic Materials and Devices, S.O.Kasap, McGraw-Hill Education 3rd Edition, 2005

[15].Excitons, Physics Education, Liang, W Y, 1970

[16]. Semiconductor Quantum Optics, Kira, M.; Koch, S. W., Cambridge University Press, 2011

[17]. Bose-Einstein condensation of excitons and biexcitons: and coherent nonlinear optics with excitons, S. A. Moskalenko, Cambridge University Press, 2000

[18].Observation of Charged Excitons in Hole-doped Carbon Nanotubes Using Photoluminescence and Absorption Spectroscopy. Matsunaga R., Matsuda K., Kanemitsu Y., **Physics Review Letters106**, 2011

[19].Tightly bound trions in monolayer MoS_2, Mak, K.F.,**Nature Materials, 12**: 207–211, 2013

[20].Diffusion Quantum Monte Carlo, Reynolds Peter J., Tobochnik Jan, Gould Harvey, **Computers in Physics**, **4**, 1990

[21]. A review on mechanical exfoliation for the scalable production of graphene, Min Yi and Zhigang Shen, **Materials Chemistry**, 2015

[22]. Living polymerization routes to siloxane macromers and higher order silicone structures, Jonathan Goff, Edward Kimble, Barry Arkles, In progress in silicones and silicone-modified materials, chapter 5, Washington 2013

[23]. Elastic properties of suspended multilayer WSe_2, Rui Zhang, Vasileios Koutsos, Rebecca Cheung, **AppliedPhysics Letters**, 108, 2016

[24].Structural and Thermoanalytical characterization of 3D porous PDMS foam materials: The effect of impurities derived from a sugar templating process, Jose Gonzales Rivera, Rossella Iglio, Giuseppe Barillaro, Celia Duce, Maria Rosaria Tine, **Polymers**, 10, May 2018

[25]. Adhesive tape exfoliation: why it works for Graphene, Jakob Bohr, **EPL DTU library**, 2015

[26]. Mechanical exfoliation of two dimensional materials, Enlai Gao, Shao-Zhen Lin, Zhao Qin, Markus J. Buehler, Xi-Qiao Feng, Zhiping Xu, **Journal of Mechanics and Physics of Solids,** March 2018

[27].Recent progress in the assembly of nanodevices and van der Waals heterostructures by deterministic placement of 2D materials, Riccardo Frisenda, Efren Navarro-Moratalla, Patricia Gant, David Perez De Lara, Pablo Jarillo-Herrero, Roman V. Gorbachen, Andres Castellanos-Gomez, **Chem. Soc. Rev**. 47, 2018

[28]. Differential Reflection Spectra of Heavily doped Silicon and Germanium in the Ultraviolet Spectral Region, A. A. Volfson, V. K. Subashiev, **Physica Status Solidi**, 1969

[29]. Quantum Reflection, workshop Cambridge, MassachusettsUSA, October 22–24, 2007

[30]. Quantum reflection of Heon silicon, H.Oberst, Y.Tashiro, K.Shimizu, F.Shimizu, *Physical Review A*., **71** (5): 052901,2005

[31]. Effective-range theory for quantum reflection amplitudes, F.Arnecke, H.Friedrich, J.Madroñero, *Physical Review A*. **74** (6): 062702, 2006

[32]. Huygens' Principle, MathPages, 2017-10-03

[33]. G. B. Dubrovskii and V. K. Subashiev, Fiz. tverd. Tela 6, 1104, 1963

[34]. Differential Reflection spectroscopy of very thin films, J.D.E. McIntyre, D.E. Aspens, **Bell Telephone Laboratories, Surface Science,** vol 24, 1971

[35]. Differential Reflectance spectroscopy of Semiconductors, M. Gal, C. Shwe, J. Tann, P. McMillan, M. Gross, R. Shi, **SPIE,** vol 1286, Modulation Spectroscopy, 1990

[36]. Reflectance Spectroscopy: Principles, Methods, Applications, Gustav Kortum, Springer-Verlag New York Inc. 1969

[37]. Differential Reflectance and second-harmonic generation of the Si/SiO_2 interface from first principles, V. I. Gavrilenko, **Physical Review,** B 77, 2008

[38]. Optical differential reflectance spectroscopy for photochromic molecules on solid surfaces, Fabian Nickel, Matthias Bernier, Uwe Lipowski, Wolfgang Kuch, **Review of scientific instruments**, vol 89, 2018

[39]. Reflectance Spectroscopy, Michael B. Wallace, Adam Wax, David N. Roberts, Robert N. Graf, National Cancer Center, 2009

[40]. Two-Dimensional Transition-Metal Dichalcogenides, Alexander V. Kolobov, Junji Tominaga, National Institute of Advanced Industrial Science and Technology, **Springer Series in Materials Science**, 239, 2016

[41]. Photoluminescence emission and Raman response of monolayer MoS_2, $MoSe_2$ and WSe_2, Philipp Tonndorf, Robert Schmidt, Philipp Böttger, Xiao Zhang, Janna Börner, Andreas Liebig, Manfred Albrecht, Christian Kloc, Ovidiu Gordan, Dietrich R. T. Zahn, Steffen Michaelis de Vasconcellos, Rudolf Bratschitsch, **OPTICS EXPRESS**, Vol 21, No.4, 2013

[42]. Transient nonlinear optical response from excitation induced dephasing in GaAs, Wang Hailin, Ferrio Kyle, Steel Duncan, Hu Y., Binder R., Koch S. W., **Physical Review Letters**, vol **71**, 1993

[43]. Understanding the optical anisotropy of oxidized Si (001) surfaces, F. Fuchs, W. G. Schmidt, F. Bechstedt, **Physical Review** B 72, 2005

[44]. Micro-reflectance and transmittance spectroscopy: a versatile and powerful tool to characterize 2D materials, Riccardo Frisenda, Yue Niu, Patricia Gant, Aday J Molina-Mendoza, Robert Schmidt, Rudolf Bratschitsch, Jinxin Liu, Lei Fu, Dumitru Dumcenco, Andras Kis, David Perez De Lara, Andres Castellanos-Gomez, **J. Phys. D: Appl. Phys. 50,** 2017

[45]. Recent development of two dimensional transition metal dichalcogenides and their applications, Wonbong Choi, Nitin Choudhary, Gang Hee Han, Juhong Park, Deji Akinwade, Young Hee Lee, **Materials Today,** Volume 20, Issue 3, April 2017

[46]. Tunnel Field-Effect Transistors in 2-D Transition Metal Dichalcognides Materials, HESAMEDDIN ILATIKHAMENEH, YAOHUA TAN, BOZIDAR NOVAKOVIC, GERHARD KLIMECK, RAJIB RAHMAN, AND JOERG APPENZELLER, **IEEE** Journal on Exploratory Solid-State Computational Devices and Circuits, July 2015

[47]. Recent Trends in Transition Metal Dichalcogenides Based Supercapacitors Electrodes, Jayesh Cherusseri, Nitin Choudhary, Kowsik Sambath Kumar, Yeonwoong Jung, and Jayan Thomasa, **Nanoscale Horizons**, 2019

[48]. Two-Dimensional Nanomaterials for Biomedical Applications: Emerging Trends and Future prospects, David Chimene, Daniel L. Alge, and Akhilesh K. Gaharwar, **Advanced Materials**, 2015

[49]. Role of Metal Contacts in Designing High-Performance Monolayer n-Type WSe_2 Field Effect Transistors, Wei Liu, Jiahao Kang, Deblina Sarkar, Yasin Khatami, Debdeep Jena, Kaustav Banerjee, **Nano Letters**, vol 13, March 2013

[50]. Materials project, WSe_2, https://materialsproject.org/materials/mp-1821/#

[51]. Stacking, strain, and twist in 2D materials quantified by 3D electron diffraction, Sung S.H, Schnitzer N, Brown L, Park J, Hovden R., **Physical Review Materials,** 3(6), 2019

[52]. XRD, http://www.cas.miamioh.edu/~marcumsd/p293/lab3/lab3.htm

[53]. The chemistry of two-dimensional layered transition metal dichalcogenides nanosheets, Manish Chhowalla, Hyeon Suk Shin, Goki Eda, Lain-Jong Li, Kian Ping Lohand Hua Zhang, **Nature Chemistry**, March 2013

[54]. Optical Generation of Excitonic Valley Coherence in Monolayer WSe_2, A. M. Jones, H. Yu, N. J. Ghimire, S. Wu, G. Aivazian, J.S. Ross , B. Zhao, J. Yan, D. G. Mandrus, D. Xiao, W. Yao, X. Xu, **Nature Nanotechnology**, vol 8, 2013

[55]. Phonon and Raman scattering of two dimensional transition metal dichalcogenides from monolayer, multilayer to bulk, Xin Zhang, Xiao-Fen Qiao, Wei Shi, Jiang-Bin Wu, De-Sheng Jiang, Ping-Heng Tan, **Chem. Soc. Rev**., August 2014

[56]. Group theory analysis of phonons in two-dimensional transition metal dichalcogenides, J. Riberio-Soares, R. M. Almeida, E. B. Barros, P. T. Araujo, M. S. Dresselhaus, L. G. Cancado , A. Jorio, **Physical Review**, B 90 115438, 2014

[57]. Nanophotonics with 2D transition metal dichalcogenides, Alex Krasnok, Sergey Lepeshov, Andrea Alu, **Optics Express**, Vol 26, No 12, 2018

[58]. Molecular Vibration Theoretical Analysis of Two-Dimensional Photoelectric Conversion Material WSe_2, Zhang Rui, Li Hongbo, Hao Guoqiang, Liu Wenbo, Ye Xiaojun, Li Zhenghong, Yuan Xiao, Liu Cui, **Key engineering Materials**, Vol. 765, 2018

[59]. Valley-selective circular dichroism of monolayer molybdenum disulphide, Ting Cao, Gang Wang, Wenpeng Han, Huiqi Ye, Chuanrui Zhu, Junren Shi, Qian Niu, Pingheng Tan, Enge Wang, Baoli Liu, Ji Feng**, Nature Communications,** Article 887, 2012

[60]. Three-band tight-binding model for monolayers of group-VIB transition metal dichalcogenides, Gui-Bin Liu, Wen-Yu Shan, Yugui Yao, Di Xiao, **Physical Review B**, Vol. 88, 2013

[61]. Optical properties of atomically thin transition metal dichalcogenides: observations and puzzles, Maciej R. Molas, Maciej Koperski, Ashish Arora, Karol Nogajewski, Artur O. Slobodeniuk, Clement Faugeras, Marek Potemski, **Nanophotonics**, Vol 6, issue 6, 2017

[62]. Magnetic brightening and control of dark excitons in monolayer WSe_2, Xiao-Xiao Zhang, Ting Cao, Zhengguang Lu, Yu-Chuan Lin, Fan Zhang, Ying Wang, Zhiqiang Li, James C. Hone, Joshua A. Robinson, Dmitry Smirnov, Steven G. Louie, Tony F. Heinz, **Nature Nanotechnology**, Vol. 12 (9), 2016

[63]. Spectroscopy, solutions for materials analysis: http://www.spectroscopyonline.com/why-are-raman-spectra-crystalline-and-amorphous-solids-different

[64]. Solid state Physics- Introduction to Theory, James Patterson, Bernard C. Bailey, **Springer** 2018 ed.

[65]. Observation of the out-of-plane mode in the Raman scattering from the graphite edge plane, Yasushi Kawashima, Gen Katagiri, **Physical Review B**, Vol. 59, No. 1, 1998

[66]. Tin diselenide as a new saturable absorber for generation of laser pulses at 1μm, Chen Cheng, Ziqi Li, Ningning Dong, Jun Wang, Feng Chen, **Optics express**, Vol. 25, No.6, 2017

[67].SocraticQ&A,https://socratic.org/questions/what-are-the-differences-between-stretching-vibration-and-bending-vibrations

[68].Chemistry,Libre-Texts™, https://chem.libretexts.org/Bookshelves/General_Chemistry/Book%3A_ChemPRIME_(Moore_et_al.)/08Properties_of_Organic_Compounds_.../8.21%3A_Silicon_Dioxide

[69]. Control of valley polarization in monolayer MoS_2 by optical helicity, Kin Fai Mak, Keliang He, Jie Shan, Tony F. Heinz, **Nature Nanotechnology**, June 2012

[70]. Giant valley splitting in monolayer WS_2 by magnetic proximity effect, Tenzin Norden, Chuan Zhao, Peiyao Zhang, Renat Sabirianov, Athos Petrou, Hao Zeng, **Nature Communications**, Vol. 10, 2019

[71]. Excitonic valley effects in monolayer WS_2 under magnetic fields, Gerd Plechinger, Philipp Nagler, Ashish Arora, Andres Granados del Aguila, Marianna V. Ballottin, Tobias Frank, Philipp Steileitner, Martin Gmitra, Jaroslav Fabian, Peter C.M. Christianen, Rudolf Bratschitsch, Christian Schuller, Tobias Korn, **Nano Letters**, November 2013

[72]. NRL Clarifies Valley polarization for Electronic and Optoelectronic Technologies, Daniel Parry, **U.S. Naval Research Laboratory**, October 19, 2017

[73]. Band offsets and heterostructures of two dimensional semiconductors, Jun Kang, Sefaattin Tongay, Jian Zhou, Jingbo Li, Junqiao Wu, **Applied Physics Letters**, 102, 012111, 2013

[74]. Inverted valley polarization in optically excited transition metal dichalcogenides, Gunnar Berghauser, Ivan Bernal-Villamil, Robert Schmidt, Robert Schneider, Iris Niehues, Paul Erhart, Steffen Michaelis de Vasconcellos, Rudolf Bratschitsch, Andreas Knorr, Ermin Malic, **Nature Communications**, 9:971, 2018

[75]. Spin-orbit coupling in the band structure of monolayer WSe_2, Duy Le, Alexei Barinov, Edwin Preciado, Miguel Isarraraz, Iori Tanabe, Takashi Komesu, Conrad Troha, Ludwig Bartels, Talat S Rahman, Peter A. Dowben, **Journal of Physics: Consisted Matter,** Vol. 27,2015

[76]. Valley-spin physics in 2D Semiconducting Transition Metal Dichalcogenides, Hongyi Yu, Wang Yao, **Columbia University Libraries**, August 2017

[77]. Valley-polarized exciton dynamics in a 2D semiconductor heterostructure, Pasqual Rivera, Kyle L. Seyler, Hongyi Yu, John R. Schaibley, Jiaqiang Yan, David G. Mandrus, Wang Yao, Xiaodong Xu, **Science Journals AAAS**, Valleytronics, Reaserch reports, Vol. 351, 2016

[78]. Probing the origin of excitonic states in monolayer WSe_2, Jiani Huang, Thang B. Hoang, Maiken H. Mikkelsen, **Scientific Reports**, 6:22414, 2016

[79]. Valley polarization in MoS_2 monolayers by optical pumping, Hualing Zeng, Junfeng Dai, Wang Yao, Di Xiao, Xiaodong Cui, **Nature Nanotechnology**, Vol. 7, 2012

[80]. Exciton Binding Energy and Nonhydrogenic Rydberg Series in monolayer WS_2, Alexey Chernikov, Timothy C. Berkelbach, Heather M. Hill, Albert Rigosi, Yilei Li, Ozgur Burak Aslan, David R. Reichman, Mark S. Hybertsen, Tony F. Heinz, **Physical Review Letters**, PRL 113, 2014

[81].Raman Instrument – Nicolet Almega XR, http://anff-q.org.au/wp-content/uploads/2016/07/Vibrational-Spectroscopy-Suite-Nicolet-Almega-XR-dispersive-Raman-microscope-brochure.pdf

[82]. https://www.ifj.edu.pl/dept/no5/nz53/Raman.htm

[83]. https://cmrf.research.uiowa.edu/thermo-nicolet-almega-xr-raman

[84]. Horiba Spectrometer iHR320, https://www.horiba.com/us/en/scientific/products/optical-spectroscopy/spectrometers-monochromators/ihr/ihr320-imaging-spectrometer-198/

[85]. Temperature dependence of the energy gap in semiconductors, Y.P. Varshni, **Physica 34**, Issue 1, p. 149-154, 1967

[86]. Temperature dependence of the energy gap in semiconductor band gaps, K.P. O' Donnell, X. Chen, **Appl. Phys. Lett.,** 58, 2924, 1991

[87]. Origin of Indirect Optical transitions in Few-Layers MoS_2, WS_2 and WSe_2, W. Zhao, R.M. Ribeiro, M. Toh, A. Carvalho, C. Kloc, A.H. Castro Neto, G. Eda, **Nano Lett**., 13 (11), 2013

[88]. Excitonic resonances in thin films of WSe_2: from monolayer to bulk material, A. Arora, M. Koperski, K. Nogajewski, J. Marcus, C. Faugeras, M. Potemski, **Nanoscale**, vol 7, 2015

[89]. Valley Polarization and intervalley scattering in monolayer MoS_2, G. Kioseoglou, A. T. Hanbicki, M. Currie, A. L. Friedman, D. Gunlycke, B. T. Jonker, **Appl. Phys. Lett.**, vol 101, 2012

[90]. Spin and Valley dynamics of excitons in transition metal dichalcogenides monolayers, M. M. Glasov, **Physica Status Solid**, 252, No.11, 2015